Groundwater Modeling Assessments of Remediation Alternatives at the Stratford Army Engine Plant (SAEP) – Fate and Transport Modeling of Chlorinated Solvents and Chromium

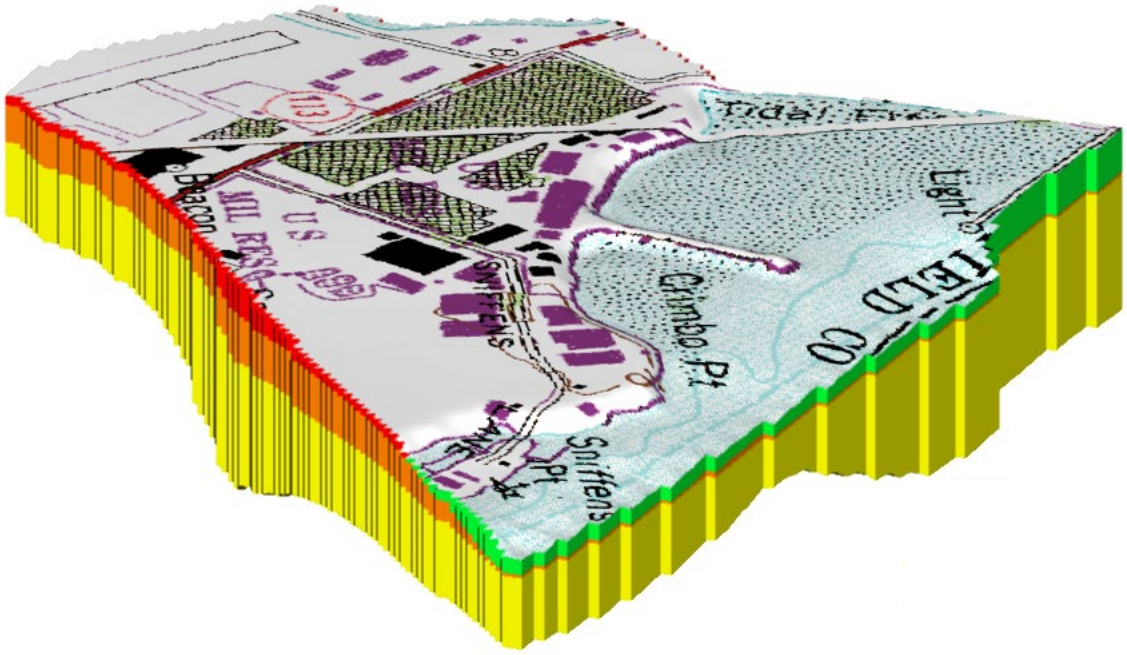

29 January 2002

Prepared by:
Christian J. McGrath[1], P.G.,
Mansour Zakikhani[1], Ph.D., and
Cary Talbot[2], P.E.

[1]Environmental Laboratory
[2]Coastal & Hydraulics Laboratory
US Army Engineer Research & Development Center
3909 Halls Ferry Road
Vicksburg, Mississippi 39180-6199

0.1 SUMMARY

This document describes the application of groundwater flow and reactive transport models in the quantitative assessment of several remediation alternatives proposed for the Stratford Army Engine Plant (SAEP). The contaminants of primary concern are chlorinated solvents (PCE, TCE, TCA and their transformation products) and hexavalent chromium. The SAEP is located on the west side of the Housatonic River, near it's terminus at Long Island Sound.

Groundwater flow simulations indicate low flow velocities beneath the SAEP site in the general direction of the Housatonic River. The low hydraulic gradient reflects the low topographic relief and low elevation of the area. The groundwater model MODFLOW was utilized to simulate three-dimensional flow through four hydrostratigraphc units. A flow model using 9 layers and 40x40 foot cells was developed for use in Tasks 2 and 3. The grid was refined for Task-1 (11 layers, 20x20 foot cells) to support requisite spatial resolution in shallower media.

Assessment of the impact of SAEP building removal on groundwater flow indicates that only minor, localized changes would be affected. The flow and transport model FEMWATER was utilized in this assessment.

Assessment of the long-range efficacy of a stripping of the three "hot spots" (**Task-1**) indicates that stripping the entire lateral and vertical extent of the contaminant plumes to an elevation of –30 to –40 feet is necessary to minimize the likelihood of VOC rebound and re-contamination at the water table. Stripping to any significantly shallower depth increases the risk of recontamination of the treatment zone by upward contaminant migration. Any residual contaminant halo upgradient of the treated zone will migrate laterally into that zone. Thus, accurate delineation of the lateral and vertical extent of the contaminant plumes and full treatment of that area is required for the application of this remediation alternative.

Assessment of natural attenuation of the solvents (**Task-2**) suggests that transport rates are sufficiently slow to provide the time needed to affect the natural attenuation of TCA- and PCE/TCE-related contaminants before seepage into the Housatonic. The possible presence of a DNAPL (dense non-aqueous phase liquid) extends the longevity of the contamination plume, but has little effect on the lateral extent of the plume. The presence of strongly reducing mudflat sediments between the solvent plumes and the river may serve as a natural reactive barrier for solvent dehalogenation and biodegradation. Since the groundwater flow rate is slow and the contaminant transport rates are suppressed further by retardation (adsorption), any contaminant flux to the Housatonic likely would be quite small. The presence of DNAPL is indicated by the elevated concentrations of solvent observed at several locations. Determination of the mass and distribution of any DNAPL should be a high priority, not only as input to long-term predictions of contaminant fate, but as input to the efficient design of any engineered remediation.

Assessment of the natural attenuation of hexavalent chromium (**Task 3**) suggests that adsorption combined with the low rates of advective transport will retard the migration of chromium toward the Housatonic River. The strongly anaerobic mudflat facies located between the plume and the river may act as a natural permeable reactive barrier to induce chemical reduction to trivalent

chromium and precipitation of sparingly soluble mineral phases, effectively immobilizing chromium. Though this hypothesis requires more field documentation and feasibility analysis, the modeling conducted here suggests no impediment to its potential success.

All predictions are conditioned on the available water quality data from SAEP. The solvent degradation rates are not well validated for site-specific conditions due to data limitations. The results of a new, thorough sampling round planned for the near future are expected to provide data to support more thorough model calibration/validation.

0.2 PROBLEM OVERVIEW

The chlorinated solvents PCE, TCE, and TCA and hexavalent chromium (Cr[VI]) have been detected in groundwater at the Stratford Army Engine Plant (SAEP) in excess of their respective MCLs. Solvent transformation products (*e.g.*, 1,1-DCE, VC) also have been detected above MCL. The contaminant plumes appear to be moving very slowly toward the Housatonic River, due in part to regional groundwater gradients that are very low. High VOC concentrations at a few locations suggest the presence of DNAPL, though none has been recovered to date.

The most immediate concern is the potential health risk posed by impacted air quality in several SAEP buildings in which elevated levels of VOCs have been detected. Dissolved and adsorbed VOCs, and possibly residual DNAPL, in the shallow subsurface are the presumed sources. Treatment of at least the shallow portions of VOC "hot spots" by thermally-enhanced soil vapor extraction (SVE), *e.g.*, steam injection or electrical heating, has been proposed to resolve the indoor air issue. Concern has been expressed that the long-term efficacy of these potentially costly solutions might be compromised if the treated zones are recontaminated by migration of residual contaminants from proximal untreated media.

Removal of some or all SAEP buildings and conversion of the site to outdoor recreational use also have been proposed. This action would resolve issues regarding indoor air quality. However, concerns have been raised that the resulting altered groundwater recharge pattern may accelerate contaminant transport and increase any environmental risk posed by contaminant seepage to the Housatonic River.

Monitored natural attenuation (MNA) may be an attractive, cost-effective, cleanup alternative for both solvents and chromium at SAEP. Chlorinated solvents are susceptible to natural, abiotic and microbially-mediated, reductive dehalogenation reactions that can yield innocuous products susceptible to subsequent mineralization. Under mildly reducing conditions, hexavalent chromium (Cr[VI]) may be reduced to the trivalent form (Cr[III]), which tends to precipitate as a stable, sparingly-soluble, solids (*e.g.*, $Cr(OH)_3$). Given the slow rate of transport and the presence strongly reducing conditions in the tidal mudflat sediments flanking the Housatonic (see **Figures 0.1** and **0.2**), it is hypothesized that MNA may be a viable alternative that can be evaluated with reactive transport models. The affect of active cleanup of solvent and chromium hot spots, which is under consideration, can also be evaluated.

Figure 0.1. Photograph of SAEP (left) showing the causeway extending toward the Housatonic River (right). (Photograph by Durgin on 9/24/01).

0.3 PURPOSE

The purpose of this investigation is to evaluate the efficacy of proposed cleanup actions and provide on-site decision makers with estimates of long-range impacts. Through the application of contaminant transport models, ineffective and costly cleanup alternatives can be identified and avoided.

0.4 GENERAL APPROACH

Any proposed remediation plan that relies on natural or engineered processes can benefit from the rigorous, quantitative evaluation that advanced, remediation simulators provide. Three, broad, modeling tasks were defined and conducted as follows in terms of the cleanup concern to be address:

Task 1. Assess long-term effectiveness of SVE treatment.
Task 2. Assess natural attenuation for solvents.
Task 3. Assess natural attenuation for Cr[VI]

Each task involves specific questions posed by parties involved in SAEP cleanup decisions. These questions and concerns, mentioned in section 0.2, are summarized below. The specific modeling assumptions, parameter selections, and approaches adopted to address these questions

are discussed in separate sections by task. Discussion of the common issues of hydrogeologic conceptualization and flow modeling are described in a following section.

Task 1. Assess Long-Term Effectiveness of SVE Treatment.
Thermally-enhanced SVE has been proposed for cleanup of the three, fairly distinct, VOC hot spots at SAEP. Several fundamental questions should be addressed before proceeding with SVE applied to any portion of the plume. First, since 100% removal of any contaminant source is unlikely, what transport processes are active locally that may reintroduce contaminants to the treated zone? If extraction is a cost-effective option, to what depth and lateral extent is cleanup required to avoid the eventual return of VOCs at the water table and subsequently into the buildings? Cleanup of the hot spot cores would leave in place a halo of the lower concentration portions of the plumes, that could continue to impact indoor air quality. The stripped zone could be re-contaminated, albeit at lower concentrations, by subsequent lateral plume migration and any upward transport by advection or diffusion. If rebound is significant, the threat to air quality returns, and costly cleanup efforts would have to be repeated. If SVE is determined to be cost effective, modeling will also be useful in the design and operation phases. Though the DoD Groundwater Modeling System (GMS) includes models developed specifically for the design of thermally-enhanced VOC recovery, such a modeling effort would be premature and was not conducted as part of this study.

Upward transport mechanisms in the saturated zone include advective-dispersive transport and molecular diffusion. Previous, regional flow modeling with FEMWATER – a 3D, variably-saturated flow and transport model – indicated very low flow velocities under the current hydrologic conditions. The upward component of flow vectors is significant locally. The potential for upward advection in the vicinity of what would be the "roots" of the dented or decapitated VOC plumes is the focus of this task. In order to pose a risk, the upward component of advective transport must be sufficient to reach the water table before lateral transport removes it from beneath the building of concern. Upward transport will be retarded by both adsorption and natural attenuation processes, which are considered.

The VOC stripping process is not modeled explicitly. The stripping of the solvents and their transformation products within the treatment zones were affected by manually editing the initial conditions to a much lower concentration. The lateral extent of the treatment zone was delineated by initial concentrations above a critical threshold (20 ppm of TCE).

For the purpose of this analysis, VOC concentration at the water table beneath SAEP buildings is the target prediction. These values will be used as input to other models to estimate indoor air quality. We are assuming that any rebound effect in the groundwater will be the critical or rate-limiting step, *i.e.*, that mass transfer through the thin vadose zone (~4 feet) and into the building would be rapid by comparison. The precise relationship between VOCs at the water table, flux into the vadose zone, and penetration into overlying buildings is uncertain. Developing this relationship will be conducted as an independent effort, to which we will provide support. Indoor air quality is being reassessed.

The reactive transport model RT3D is employed for this task. Only the sequential degradation

package for PCE-TCE-DCE-VC is applied. The results of this analysis are assumed to be equally valid for TCA-associated contaminants. Low reaction rates, of the same order of magnitude as those determined in Task 2, are assumed.

Task 2. Assess MNA for solvents.
Two sub-tasks are included under Task 2: (a) PCE/TCE predictions, and (b) TCA predictions. These sub-tasks are modeled independently. Within each sub-task are four, so-called "end-member" scenarios, referring to two conditions of recharge distribution and either the presence or absence of a DNAPL.

The presence of DNAPL, though not yet confirmed by direct recovery, is indicated by the very high concentrations observed for primary solvents (PCE, TCE, TCA). Obviously, model estimates of how long it would take to clean the site by natural processes will be strongly influenced by the mass and distribution of any DNAPL. In the absence of data that quantitatively delineates a DNAPL (or demonstrates its absence), a conservative treatment of the DNAPL source is adopted. The effect of a DNAPL is approximated by imposing a constant-concentration condition at one or more grid blocks within the existing hot spots.

The highly industrialized condition of the site – buildings, paved parking lots and roads – minimizes the amount of direct surface recharge. Removal of buildings and parking lots and conversion of the property for use as a park or athletic fields has been proposed. Such a major alteration of the surface recharge distribution could have significant influence on the rate of advective transport of groundwater contaminants. The initial scope of work included analysis of two end-member flow fields on contaminant transport. However, as will be demonstrated below, flow simulations indicated only minor and isolated changes in flow velocities. Thus, evaluation of variable recharge on contaminant transport is not considered.

In support of MNA at SAEP, the following arguments may be made: (1) the presence of transformation products, such as DCE and VC, suggests that attenuation processes are active; (2) the slow rates of advective transport under the current hydrologic conditions – minimal recharge – may provide sufficient time for MNA; (3) reducing conditions in the mudflat sediments located between the sources and the river may act as a natural, permeable reactive barrier (PRB) to both solvents and chromium; (4) there are no human receptors in the path of the plume. Conversely, MNA may not be a viable alternative: (1) if natural degradation rates are too slow to attain acceptably low levels before discharge near the Housatonic; (2) if it is deemed economically beneficial in the long term to address the building air quality issues with partial or full VOC removal. Even if some level of source removal is conducted, MNA will be involved in the cleanup of residual contamination. The key products of Task 2 are long-range, site-specific, predictions of solvent transport.

One of the standard RT3D-GMS reaction packages for the sequential dehalogenation of solvents was used in the assessment of MNA for PCE, TCE, DCE, and VC. Predictions for TCA required the application of a new RT3D module developed recently by Dr. Zakikhani. Each module requires a first-order decay constant for each step in the degradation process.

Task 3. Assess MNA for Cr[VI]
Only one major hot spot of hexavalent chromium (typically present as chromate CrO_4^{-2}) has been delineated at SAEP. There are reports of minor, isolated detections of Cr elsewhere at SAEP, but the focus is on the major plume. Regional flow suggests slow advective transport toward the Housatonic River. The presence of strongly reducing mudflat sediments between the current plume location and the river suggests that even if Cr were to be approach the river it might be immobilized in the mudflat. The immobilization process would involve chemically reduction and precipitation as a sparingly soluble solid phase.

The end-member scenarios conducted for the Cr simulations include assessing fate and transport with and without partial plume recovery. The effect of source depletion was imposed by manually editing any initial Cr concentration in excess of 5 ppm (highest 1999 observation was 950 ppm) to a concentration of 5 ppm. As mentioned previously and discussed below, the end-member recharge scenarios yield very similar flow fields, eliminating the value of considering the effect of a flow field change on Cr transport.

A relatively simple transport model (MT3DMS) involving only advection, dispersion, and adsorption was employed. The immobilization process is approximated as strong adsorption within the mudflat sediments.

Implicit in each contaminant transport task are several sub-tasks. The flow fields must be defined using MODFLOW, output from which is used to drive the reactive transport models used here. These flow simulations were conditioned on the regional, calibrated, FEMWATER simulations completed previously. Additional grid refinement and calibration of the MODFLOW model were required. A 3D conceptual model of critical reactive transport processes, conditioned on available monitoring data, was developed. Reaction rates were approximated based initially on observations at similar sites, but final predictions were adjusted to better capture trends SAEP water quality data. Though temporal data trends are discernable, the available data were determined to be inadequate for proper transport calibration. Another sampling round is planned to support a defensible calibration.

0.5 HYDROGEOLOGIC CONCEPTUALIZATION

This modeling effort builds on the hydrogeologic conceptualization and steady-state flow field developed previously by Dr. Philip Durgin (NAE) and Cary Talbot (ERDC-WES) using FEMWATER-GMS. Four hydrogeologic units are defined (Figure 1): (1) glacial outwash, (2) reworked glacial outwash, (3) fill material, and (4) estuarine, tidal flat mud (**Figure 0.2**). Crystalline bedrock underlies the site and defines an impermeable flow and transport boundary. There are minor, isolated accumulations of peat. Hydrogeologic parameters are summarized in the following table.

Table 0.1 Summary of model parameters for hydrostratigraphic units.			
Medium	Hydraulic Conductivity [ft/day]	Hydrodynamic Dispersivity [ft]	Effective Porosity [–]
Tidal Mudflat	16.	10 to 30	0.24 to 0.30
Fill	142.		
Reworked glacial	11.		
Glacial outwash	4.2		

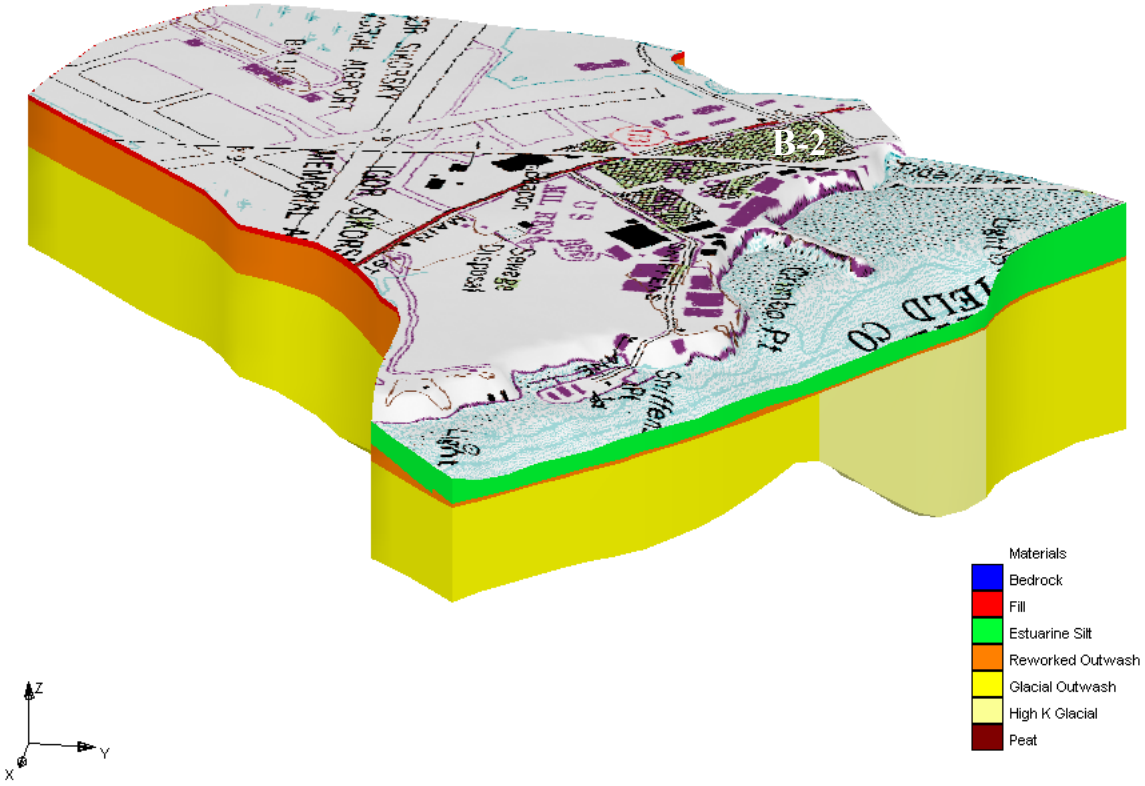

Figure 0.2. SAEP map relative to hydrogeologic conceptualization.

0.6 FLOW SIMULATIONS

A finite element mesh consisting of 18752 nodes and 31787 elements was generated from the hydrologic conceptualization described in the previous section. Two layers of mesh elements were used for each of the surface soil, reworked glacial and estuarine silt materials while three layers of elements were used to represent the glacial outwash material. Element sizes range from 50 feet in the study area to 300 feet at the southwestern boundary. Because of the unstructured nature of the finite element mesh, stratigraphic features such as the irregular bedrock surface can be honored and represented in the mesh directly. Surface features such as the dike and causeway on the eastern edge of the site are also included in the model as FEMWATER has the capability to track flows in the unsaturated zone.

Model boundaries were selected at appropriate regional locations far enough away from the site to minimize boundary influences within the groundwater-flow area of interest. In the regional FEMWATER model, boundaries were chosen at lower elevations, coinciding with either surface water bodies or locations with measured groundwater elevations. For the SAEP model the boundaries on the east and west were designed as specified head with water levels specified in relation to the mean tidal level of the Housatonic and the mean tide level in the estuary. The north-south boundaries are a combination of no flow and specified head boundaries. The assumption is made that the groundwater discharge is predominantly to the tidal flats and Housatonic on the east and to the estuary system to the west. The no flow boundaries assume that the boundaries are parallel to the groundwater flow and that there is no regional flow to or from the north or south.

Steady-State Flow Field Calibration

The regional FEMWATER model was calibrated using available groundwater elevation information gathered from local well logs, transducer measurements, and other available data sources. The model was run assuming a steady-state condition; thus, tidal fluctuations were averaged into mean values for the boundaries along the tidal flats and river. Model computed head values were compared to field data in both horizontal and vertical perspectives to ensure that the model was capturing the vertical components of flow at the site.

Calibration results indicate that the FEMWATER model is able to simulate the steady-state flow conditions at the SAEP site with a good degree of accuracy. On average the model will predict groundwater elevations within 4.4 inches. Using the more stringent Root Mean Squared (RMS) calibration statistic indicates that the model is accurate to just over 5 inches.

The groundwater flow simulations indicate low flow velocities beneath the SAEP site in the general direction of the Housatonic River. The low hydraulic gradient (**Figures 0.2 and 0.3**) reflects the low relief and low elevation of the area.

MODFLOW models

The FEMWATER modeling effort established the conditions for steady-state flow, boundary conditions, media properties, and recharge across the SAEP installation and surrounding area. The finite-difference, reactive transport models utilized here (RT3D, MD3DMS within GMS) require independent simulation of flow conditions. Within the GMS, this is most readily accomplished using output from the popular, finite-difference, flow model MODFLOW (McDonald and Harbaugh, 1988). Two MODFLOW grids were built within the area modeled by the FEMWATER model (**Figure 0.4**) at a smaller scale and finer resolution than that of the FEMWATER model, providing for more accurate modeling of the contaminant fate and transport.

A MODFLOW grid defining 9 layers of variable thickness and uniform, 40x40 foot cells was developed for use in Tasks 2 and 3. The model domain extends well beyond the SAEP boundary to include the tidal mudflat area, flanking the Housatonic River, and an upgradient groundwater divide beneath the Sikorsky Memorial Airport to the southwest of SAEP (**Figure 0.4**). The grid was refined for Task-1 both vertically (11 layers) and laterally (20x20 foot cells) and focused on the SAEP property. The refinement was required to support requisite spatial resolution in shallower media.

The MODFLOW boundary locations, conditions, and grid orientations were based on the FEMWATER flow model results. These parameters and properties were transferred readily to the two MODFLOW grids used here *via* the DoD Groundwater Modeling System (GMS). Calibrations of the MODFLOW simulations were conducted and yielded slightly better agreement with the observed data than that achieved with the FEMWATER flow model. This is due to the smaller scale and higher resolution of computational cells in the MODFLOW models.

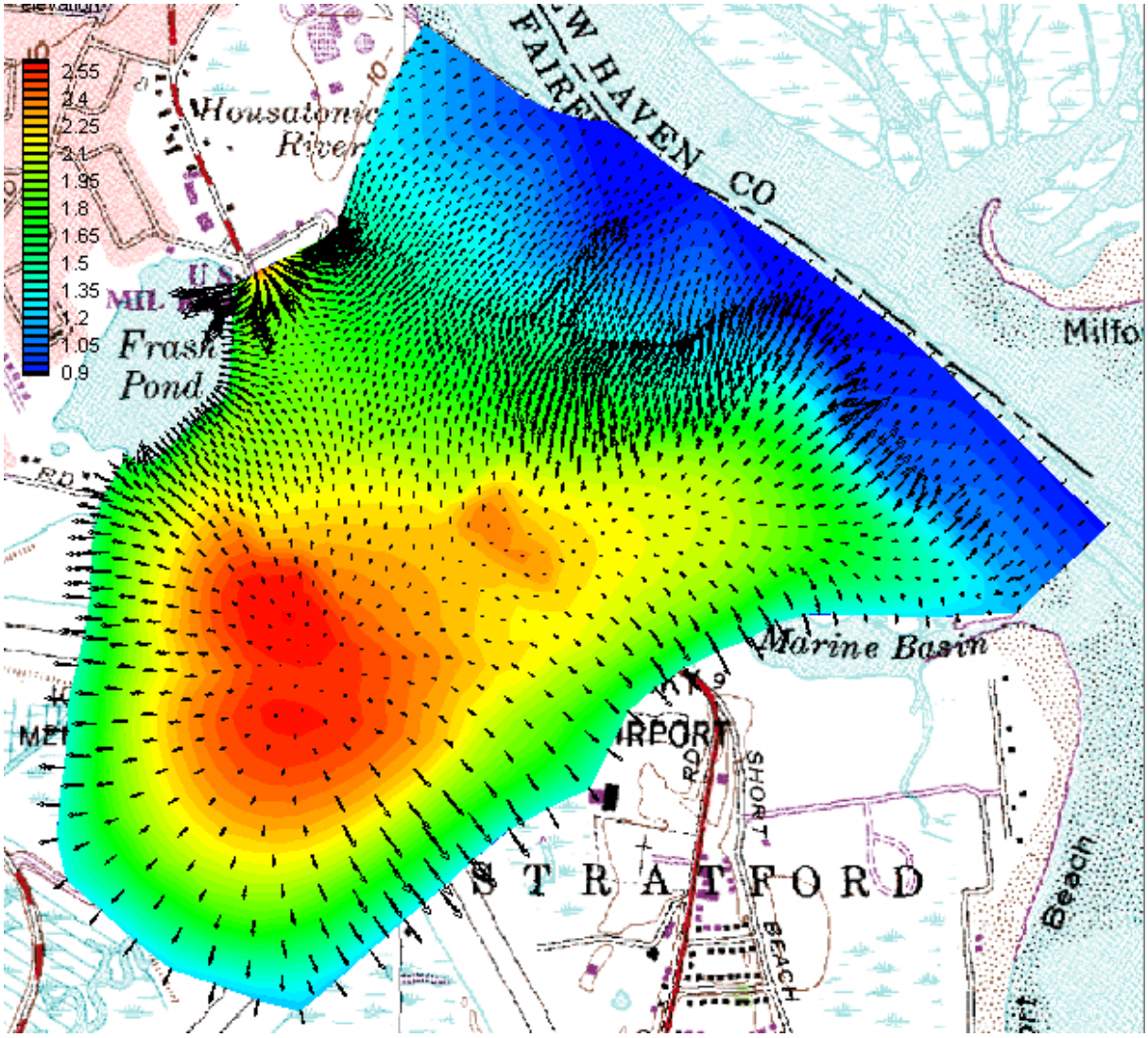

Figure 0.3. Total head color contours (in feet of head elevation) and steady-state flow vectors along the predominant flow direction toward the Housatonic River.

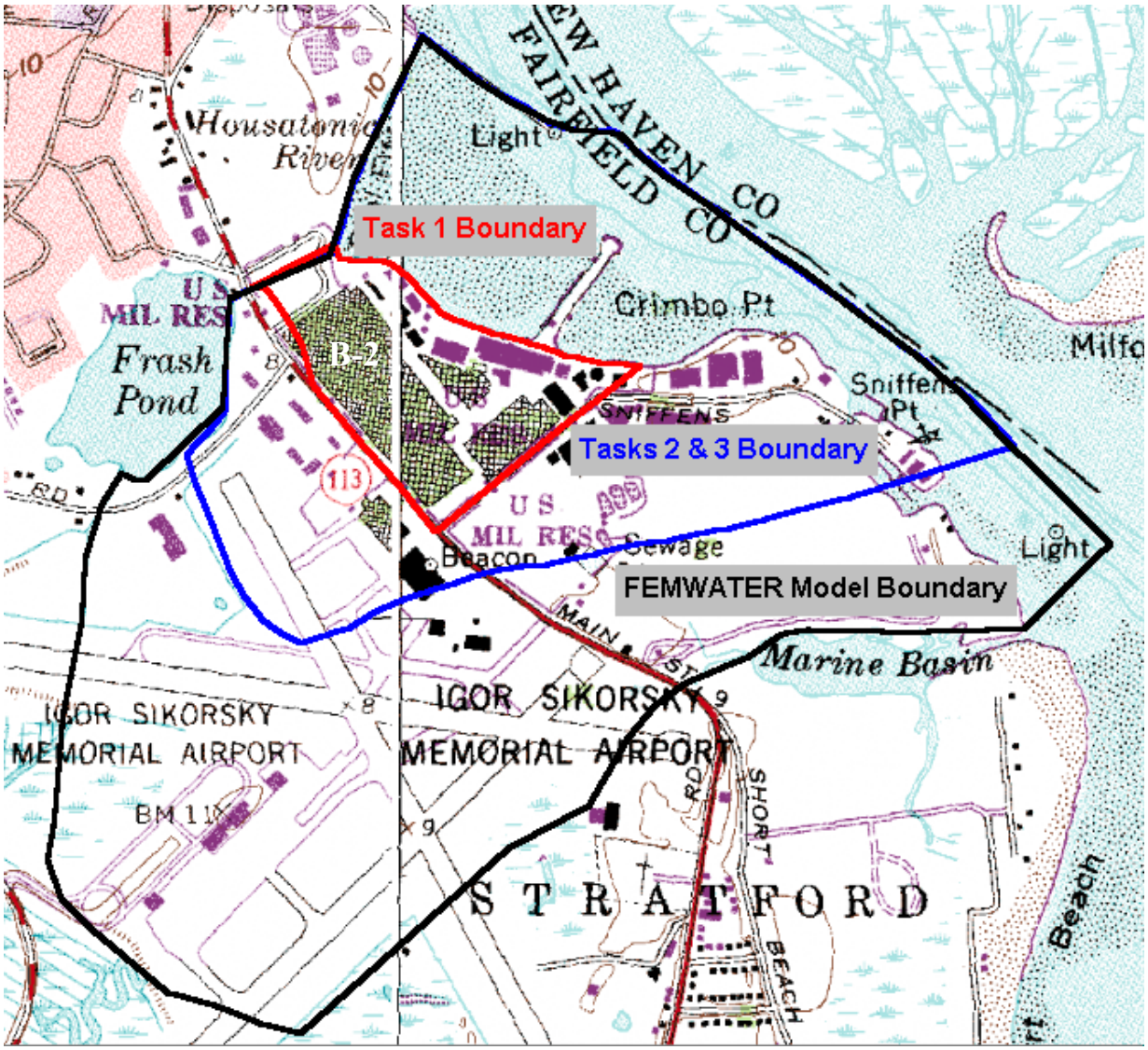

Figure 0.4. Locations of boundaries for the FEMWATER regional and two MODFLOW sub-models for Tasks 1, 2, and 3. Building B-2 is labeled.

Recharge Effects on Groundwater Flow

Conversion of the SAEP property to a public park or athletic fields has been proposed as one alternative. This likely would involve removal of all buildings and parking lots. The alteration in the recharge patterns conceivably could affect the rate and direction of contaminant transport. The FEMWATER model was used to evaluate the two different recharge scenarios.

Assessment of groundwater flow under present recharge conditions indicates a general flow direction toward the Housatonic River from a groundwater divide under the Sikorsky Airport (**Figure 0.5** and **0.3**). Recharge in the grassy areas is estimated to be 8 inches per year. This rate was estimated by calibrating the flow model to observed groundwater head distributions. While

this rate of recharge is at the lower end of the range of values tested in the calibration, it provided the best fit to the observed data. Given the grass and other vegetative cover in these areas of the model, interception, plant uptake and a layer of organic-rich soil at the surface all act to reduce the amount of rainfall that directly feeds the subsurface hydrologic system. Recharge to the extensive areas covered by SAEP buildings or parking lots is assumed to be essentially zero.

The scenario without SAEP structures was conducted by assigning a uniform recharge rate of about 8 inches per year. This condition resulted in a flow field (see **Figure 0.6**) similar to the flow scenario with the buildings present (**Figure 0.5**). Naturally, the greatest changes in head are directly beneath the locations of buildings and parking lots (**Figure 0.7**). Still, the largest increase in head was only +0.35 feet under building B-2. The differences in flow velocity induced by the hypothetical change in recharge distribution also are very small (**Figure 0.8**). The largest change is only +0.04 ft/d in a small zone of higher permeability in the glacial material.

Given that the hypothetical change in recharge has a negligible effect on the flow field, it was decided that these scenarios did not need to be evaluated in the assessments of natural attenuation. Attention was shifted to the assessment of alternative scenarios for the decay rates and the presence of DNAPL, which was expected to have a substantial effect on long-range predictions.

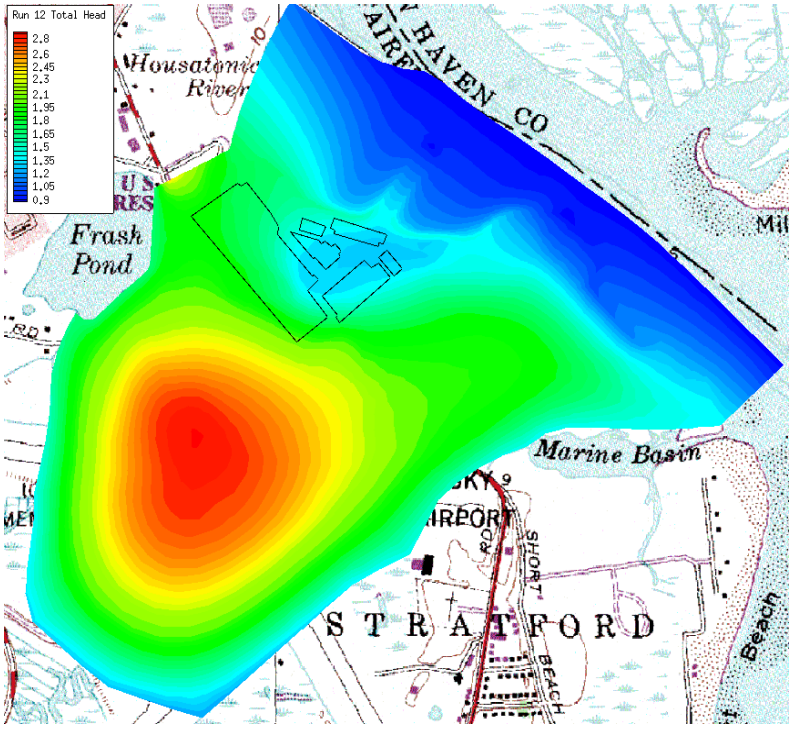

Figure 0.5. Total head contours at SAEP under current conditions as predicted with FEMWATER/GMS.

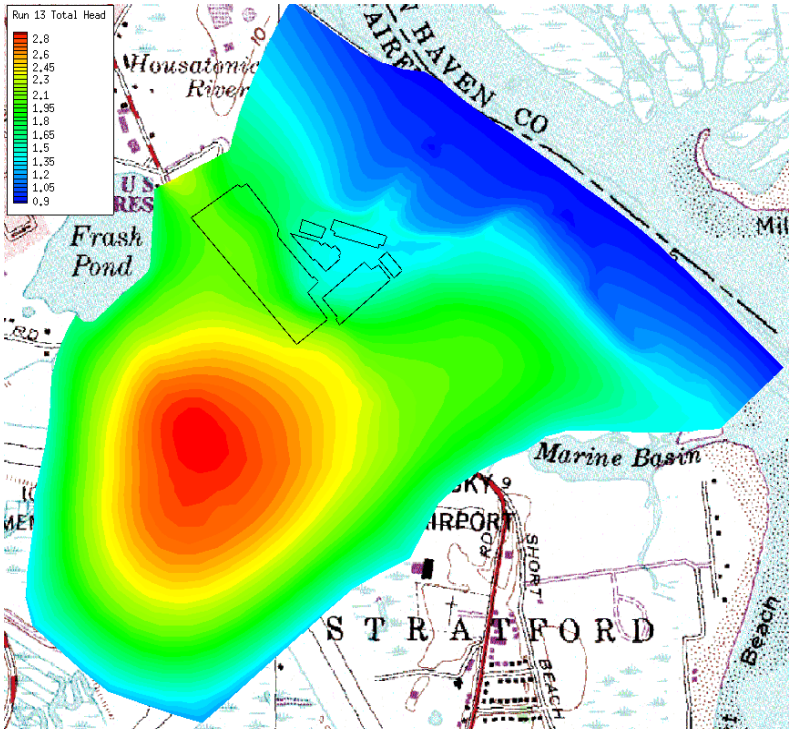

Figure 0.6. Total head contours at SAEP with site buildings and pavement removed (*i.e.* recharge equivalent to grassland recharge).

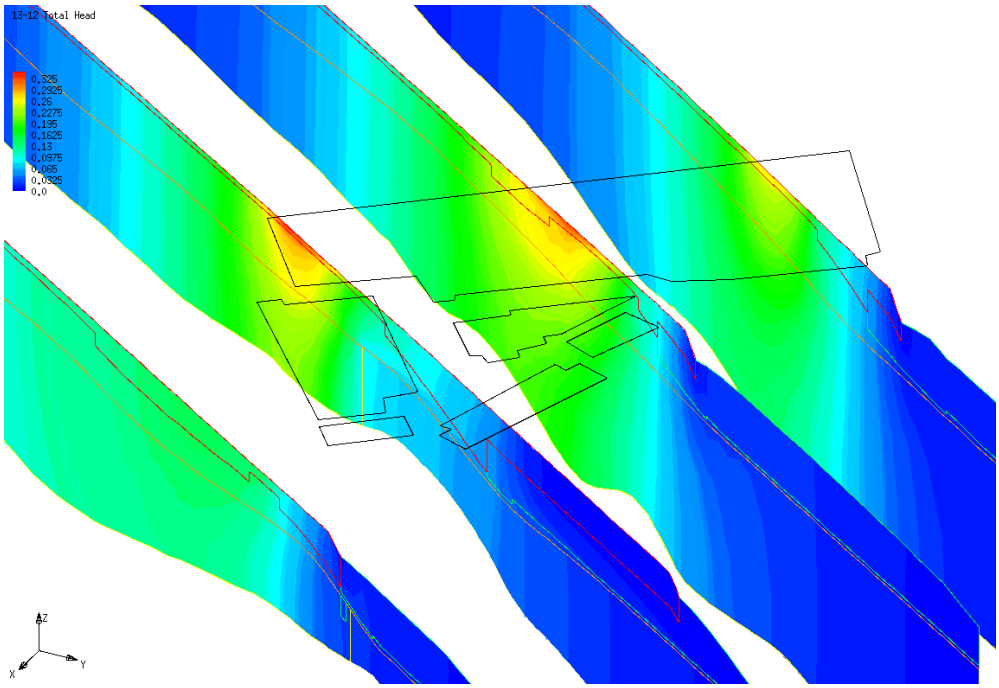

Figure 0.7. Cross sections under SAEP showing groundwater head differences between current and modified (*i.e.* no paved areas) recharge conditions. Black outlines indicate major SAEP buildings. The greatest head difference is +0.35 feet beneath Building B-2.

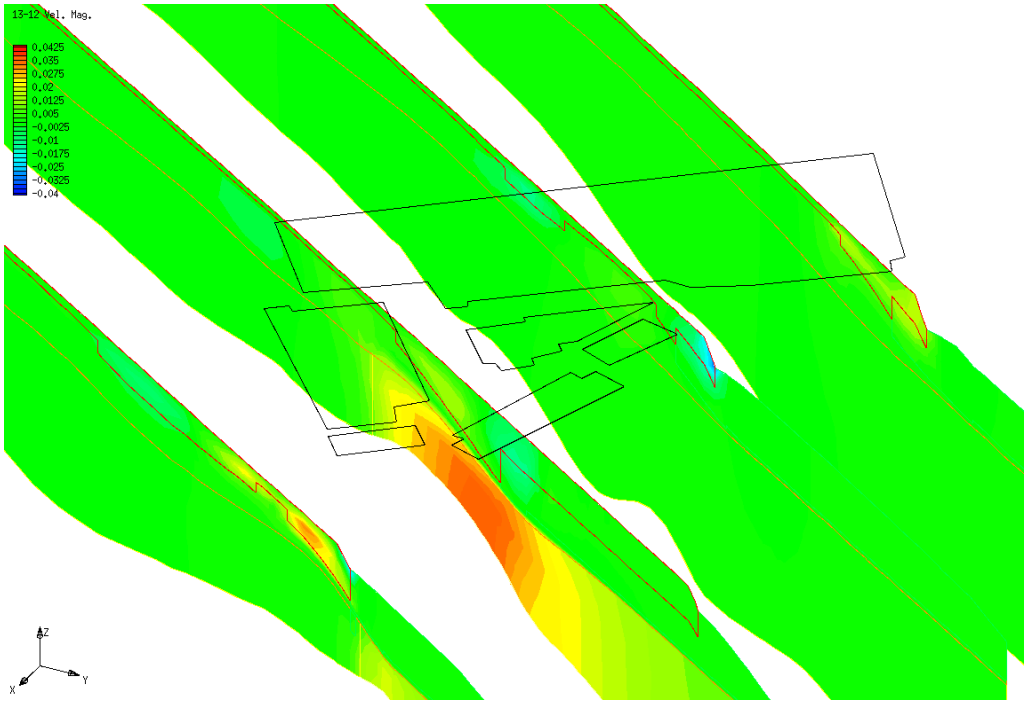

Figure 0.8. Cross sections under SAEP showing groundwater velocity magnitude differences between current and modified (*i.e.* no paved areas) recharge conditions. Black outlines indicate major buildings. The greatest velocity magnitude difference is +0.043 ft/day.

TASK-1. ASSESS EFFECTIVENESS OF SVE TREATMENT

1.1 PROBLEM SUMMARY

Extensive contamination of groundwater and soil air has been detected beneath several structures at the Stratford Army Engine Plant (SAEP). The contaminants include PCE, TCE, TCA, and their degradation products, including dichloroethenes (DCE), vinyl chloride (VC), and ethene. These volatile organic contaminants (VOCs) have impacted air quality within several buildings at SAEP, and may present a health risk.

Cleanup of the more severely contaminated portions of the shallow subsurface has been proposed to ameliorate the potential threat to indoor air quality. Three, multicomponent solvent "hot spots" have been identified that may impact air quality (see **Figures 1.1** and **1.2**). Thermally-enhanced vapor extraction – by steam injection or six-phase electrical heating – have been proposed as potential technologies to affect the cleanup.

The primary question to be addressed here is whether *any* cleanup action would be effective in the long-term reduction of indoor air impacts. It has been suggested that incomplete cleanup of the hot spots would constitute a temporary remedy that would be reversed by upward or lateral migration of residual contaminants. An additional issue concerns the depth to which any cleanup must be implemented to affect the long-term reduction of contamination at the water table. The focus of model predictions under this task is contaminant concentrations at the water table. The relationship between indoor air quality and contamination at the water table is being considered in an independent effort.

1.2 APPROACH

The reactive transport model RT3D has been applied to assess the long-term effectiveness of cleanup alternatives. The transport processes modeled include advection, dispersion, adsorption, and the sequential degradation of dissolved PCE, TCE, DCE, and VC. The detection of significant concentrations of transformation products (DCE, VC) supports the inclusion of degradation processes in these simulations. Additionally, transformation products are included because air quality standards are quite restrictive, particularly VC. TCA degradation is not modeled; it is assumed that TCA behavior would mimic that of PCE/TCE in terms of the current analysis.

The numerical grid proximal to the water table is refined to vertical dimensions (ΔZ) of approximately 5 feet in order to permit evaluation of multiple treatment depths as well as to minimize the effect of potential numerical dispersion. A uniform, relatively fine, ΔX and ΔY, grid spacing of 20 feet (*vs*. 40 feet in the Tasks 2 and 3 grids) is used to improve spatial resolution of contaminant distribution. Since the focus here is on the water table directly beneath SAEP buildings, the lateral extent of the numerical grid reduced (see Figure 0.4).

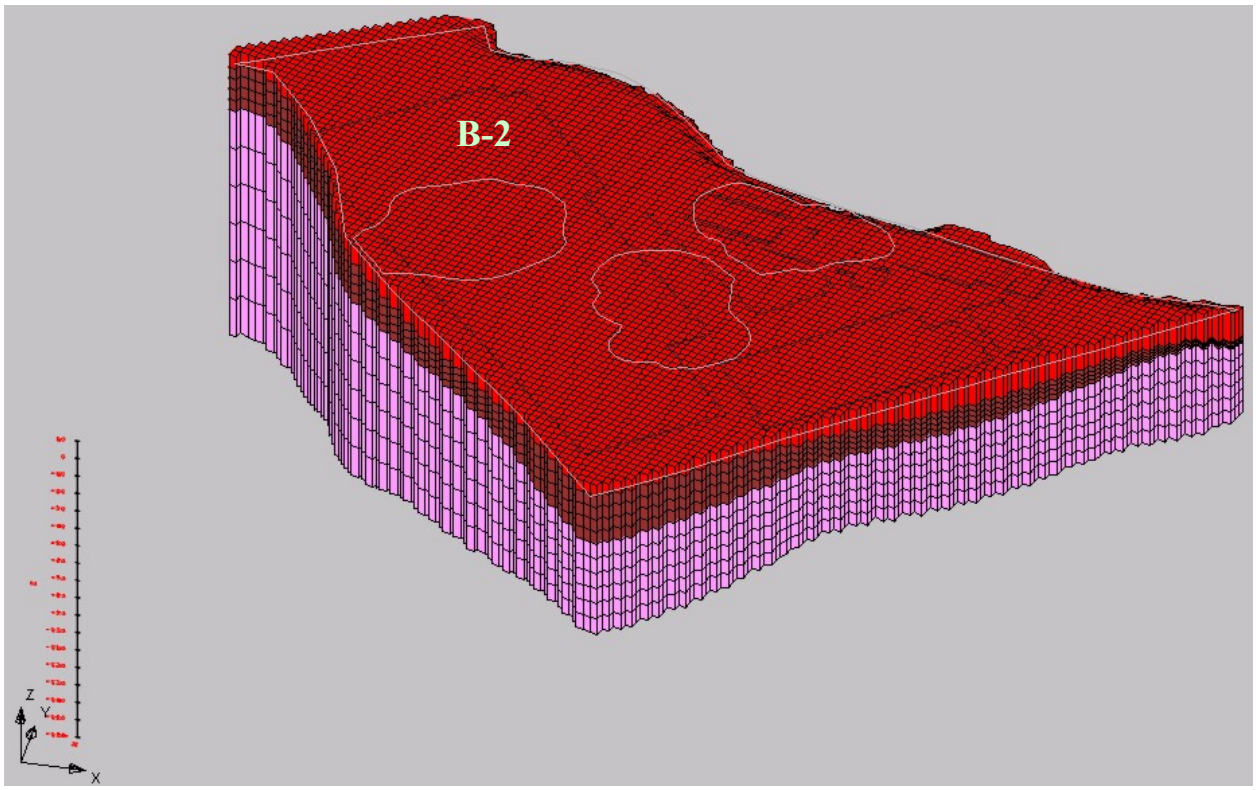

Figure 1.1. Numerical grid for the SVE assessments includes 11 numerical layers representing the three dominant hydrostratigraphic units. The ΔX and ΔY are uniformly 20 feet; ΔZ is variable, but approximately 5 feet in the upper layers. Z scale increments are 10 ft. The dark rectangular outlines on the surface indicate major SAEP buildings, *e.g.*, the large B-2 building. The irregular white outlines delineate the lateral extend of a hypothetical, plume core treatments.

Groundwater quality data from 1999, primarily from July sampling events, were used to define initial conditions for all three tasks. The data were extracted from an Access database provided by the New England District. The database query, data reduction, and reformatting for GMS use was conducted by ERDC. Some subjective screening of these data was required to extract a single representative value from multiple, disparate values in the database. Most of the subjective distillation arose from the nominal values reported as non-detect, which varied over several orders of magnitude. This issue appears to be rooted largely in the reporting of observations as the analytical detection limit, which will vary depending on the degree of any requisite sample dilution (common procedure when one or more analyte is present in excess of the calibration range). Generally, non-detects were reported as the smallest detection limit of 1 ppb. Confusion arose when data identified as non-detects were reported as 10 ppb, 100 ppb, or more. Where elevated non-detect values were proximal to established hot spots, the higher non-detect values were accepted. However, where uniform clusters of high non-detect values were reported in unlikely locations (not associated with one of the three target hot spots) a value of 1 ppb was assigned. The 3D dataset was mapped to the numerical grid using a

GMS interpolation scheme (inverse distance weighted method with the gradient plane option) that yielded hot spots of limited areal extent, reasonably consistent with previous conceptualizations (*e.g.,* Foster Wheeler / Harding-Lawson, FW/HL).

The VOC stripping process was not modeled explicitly (though the GMS includes models with this capability). Cleanup was implemented by manually editing the concentrations within the treatment zone to nominal levels. The lateral extent of the treatment zone was defined by cells in which the initial concentration of TCE or PCE exceeded 20,000 ppb within the treated layers. The areal extent of the treatment zones was larger than those actually proposed (FW/HL), probably reflecting differences in contouring. The initial concentration *of each contaminant in each treated cell* was reduced to 11 ppb. However, if the initial concentration of any constituent was already low (~100 ppb), the value was reduced to 1.1 ppb. These arbitrary values afforded the modeler a "fingerprint" of the cells that had been edited. These concentrations represent an optimistic level of cleanup efficiency, in some cases in excess of 99.9% removal. Actual cleanup efficiencies achieved by steam stripping or six-phase heating may be lower. There is no data from this site to justify *any* particular efficiency. The issue can be revisited if deemed important, but is not critical to the immediate question of contaminant rebound.

The hypothetical cleanup process was applied to assess treatment to three different depths, with the extent of the treatment area being expanded with depth to incorporate lateral shifts in the threshold (PCE/TCE above 20 ppm). The three depths were defined as the cleanup of 2, 4, and 6-7 numerical grid layers. Grid thickness varies spatially, but under most of the site, these treatment levels translate to elevations of approximately –10, -20, and –30-40 feet (surface elevation is approximately 7 feet). The deeper treatment represents cleanup of all three shallow hot spots, but not the deeper lobe associated with hot spot #3.

To resolve the potential contribution of lateral transport *versus* upward rebound of contaminants, the intermediate and deep treatments were run assuming *complete* removal of all solvents. Concentrations in the entire treated layers were set to the lowest detection limit (1 ppb).

Adsorption of the VOCs is described with a linear isotherm model. Estimation of the distribution coefficients (K_d) is discussed more thoroughly under Task-2 (Natural Attenuation). Distribution coefficients (K_d's) for PCE, TCE, DCE, and VC are summarized in Table 2.2.

The sequential dechlorination reaction pathway PCE-TCE-DCE-VC(-Ethene) was adopted for these simulations, though ethene is not modeled explicitly. This pathway is simulated with one of the standard reaction package in RT3D/GMS. Additional reaction pathways are possible (*e.g*., multiple DCE isomers), but the simple, sequential, dechlorination pathway with 1,1-DCE (dominant isomer) is supported by the bulk of the observation data. The reaction rates utilized here may be characterized as typical rates for the natural attenuation of chlorinated solvents. The rates are of the same order of magnitude as those described in Task-2, for which an attempt was made to adjust rates to more closely approximate the trends suggested by limited, post-1999 data. The presence

of DNAPL was not considered in these calculations, but could certainly have an impact on longer-range predictions.

1.3 RESULTS

The modeling results presented here provide an overview of the assessment of the long-range effectiveness of treatment to three depths and two lateral extents: (1) *shallow core treatment* to an elevation of approximately –10 feet, (2) *intermediate core treatment* to an elevation of approximately –20 feet, (3) *deep core treatment* to approximately –30 to –40 feet elevation to affect removal of the shallower plume cores, (4) *intermediate complete treatment* to approximately –10 feet elevation, and (5) *deep complete treatment* to approximately –40 feet (top 7 grid layers).

Figures 1.2 to 1.13 represent contaminant distributions conditioned on 1999 observation data. These pre-treatment conditions provide a common starting point for each of the five treatment scenarios.

Figures 1.14 to 1.29 represent initial and 10-year conditions for each component after shallow treatment of the hot spot cores to approximately -10 feet elevation (grid layers 1 and 2). Contaminant rebound is rapid and extensive.

Figures 1.30 to 1.49 summarize results from the intermediate-depth treatment of the hot spot cores to approximately -20 feet elevation (grid layers 1-4). Initial conditions at the water table would be very similar to those represented in Figures 1.14 to 1.29.

Figures 1.50 to 1.77 summarize results from the deep treatment of the hot spot cores tow approximately –30 to -40 feet elevation (6 or 7 grid layers). Treatment to these depths would largely encompass the shallower contaminant zone, but not the deeper plume associated with only hot spot #3.

Figures 1.78 to 1.97 summarize the effects of complete plume treatment (decapitation) to the intermediate depth of approximately –20 feet elevation (4 grid layers). Contaminant rebound is still observed.

Figures 1.98 to 1.115 summarize the effects of complete and deep, plume treatment (decapitation) to the –40 feet elevation (7 grid layers). PCE and TCE do not rebound significantly within 30 years. However, much reduced levels of DCE and VC are predicted to reach the surface over a limited area within approximately 10 years.

Figures 1.116 to 1.119 present concentration profiles for PCE at 10 years after each of the intermediate and deep treatments.

1.4 CONCLUSIONS

The relative success of each treatment level must be determined by the estimate of its effect on indoor air quality, which will be estimated independently. However, is appears that the shallow treatment would be insufficient due to significant levels of contaminant rebound after only 10 years. The intermediate treatment appears marginally successful. The deep treatment is the most effective.

Temporal trends in the post-treatment contaminant profiles suggest that most of the contamination re-entering the treatment zone originates from lateral migration of any residual plume halo (GMS film loops show this phenomenon better than a series of static plots; these avi files can be provided separately). Influx from sources outside SAEP was not considered beyond their contribution to initial conditions. The upward flux of contaminant reaches the water table within 10 years for the shallow treatment, and within ~18 years after the intermediate treatment. Extension of the treatment zones laterally to include the entire grid layer indicate that upward transport contributes significantly to contaminant rebound at the water table. However, upward transport of contaminant from below –30 feet elevation appears to be insufficient to reach the water table before degradation is well advanced. These observations highlight the need for careful plume delineation to assure that any treatment "decapitates" the plume rather than creating only a divot. Treatment to a depth of –30 ft elevation appears to be sufficient to eliminate significant recontamination at the water table from depth. Further commentary is offered in the figure captions below.

Notes for all Task-1 Figures

All figures are contour plots of solvent concentration on a particular numerical grid plane – either an areal view of the SAEP facility (usually at the water table, top grid layer) or a vertical profile through the plume along the predominant flow direction (coincident with a numerical grid plane). Profile (cross section) images are generally identified by the associated transect (A-A' or B-B') delineated on the areal view. The grid layer number increase with depth; the profile grid plane indicator (*e.g.*, I=75) increases to the east.

Concentrations. All solvent concentrations are reported in units of parts-per-billion (ppb; μg/L) and are contoured using a uniform, logarithmic scale.

Spatial scales. The X-Y or Y-Z axes in each diagram provide reference length scales. In the map views the X-Y axes are 1000-feet in length, marked in 100-foot increments. The profile views include Y-Z axes with the same 1000-foot Y axis, but a Z axis of only 100 feet with 10-foot increments. Note that the vertical exaggeration is 2.0 in all profiles views, *i.e.*, the Z dimension is expanded by a factor of 2 in order to reveal details of plume and grid structure. The uniform dX and dY grid spacings of 20 feet provide another scale for all horizontal distances; grid thickness varies.

Outlines. The rectangular, black (or gray) outlines represent the major SAEP buildings as a uniform reference in all map views. The very large building B-2 is labeled in several figures. The irregular, circular, gray (or black) outlines delineate the approximate lateral extent of the hypothetical treatment zones. Actually, the lines are a trace of the TCE 10,000 ppb isopleth, which encompasses all treated cell values exceeding 20,000 ppb TCE or PCE.

Water Table. All profiles include, within the uppermost grid layer, a nearly horizontal, thin, blue line that represents the MODFLOW delineation of the steady-state water table. Note that the cells along the Housatonic boundary are flooded, *i.e.*, the water table is above the ground surface. Note that references to "at the water table" and "grid layer 1" are synonymous.

Pre-Treatment Conditions

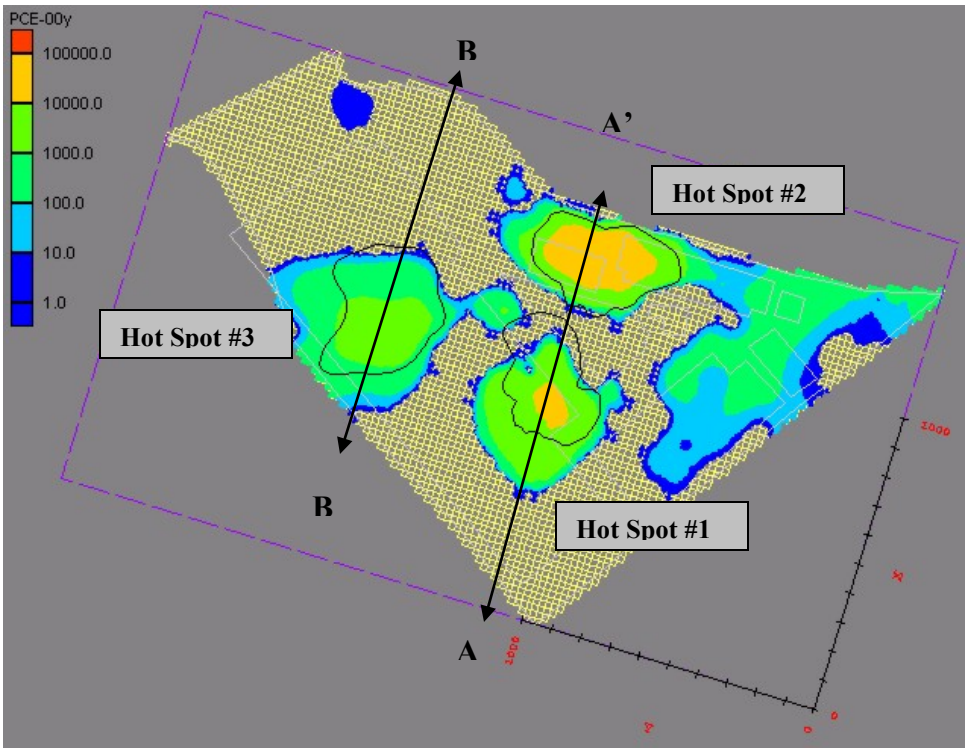

Figure 1.2. PCE concentrations (ppb) at the water table, conditioned on 1999 data, represent the pre-treatment distribution.

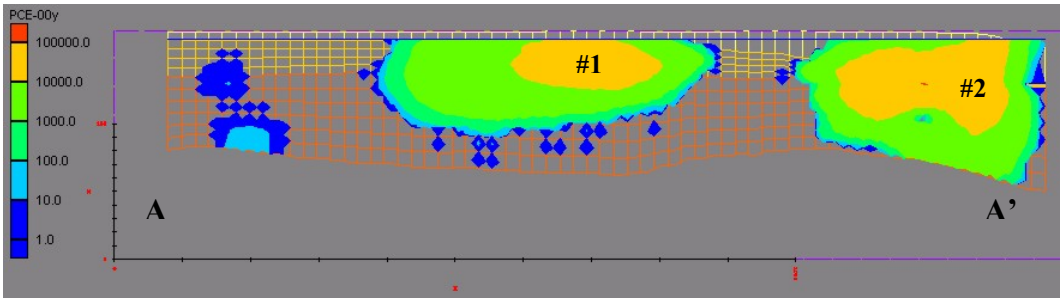

Figure 1.3. PCE concentration (ppb) profile along A-A' (Fig. 1.2) through hot spots #1 (left) and #2 [grid plane I=75].

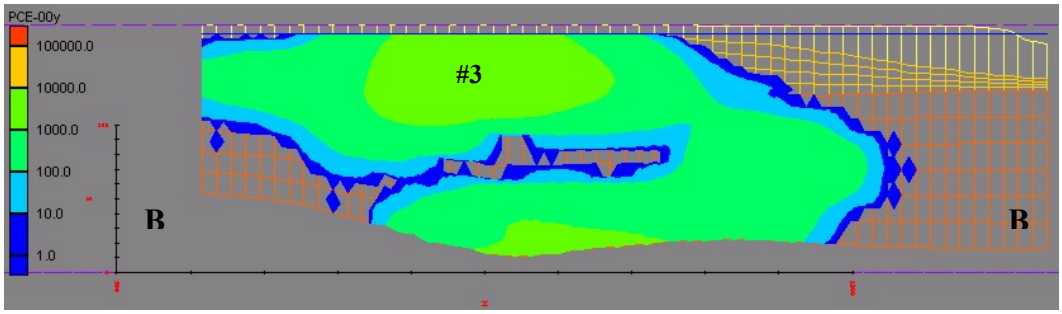

Figure 1.4. PCE concentration profile along B-B' (Fig. 1.2) through hot spot #3 [I=47]

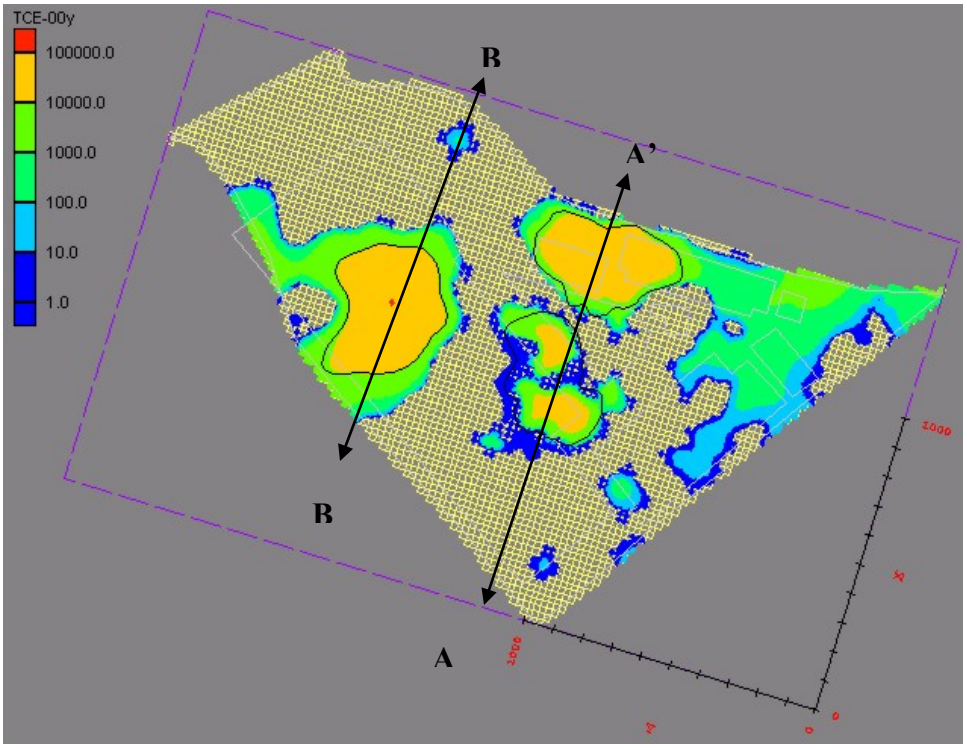

Figure 1.5. TCE concentrations at the water table, conditioned on 1999 data, taken as the pre-treatment distribution.

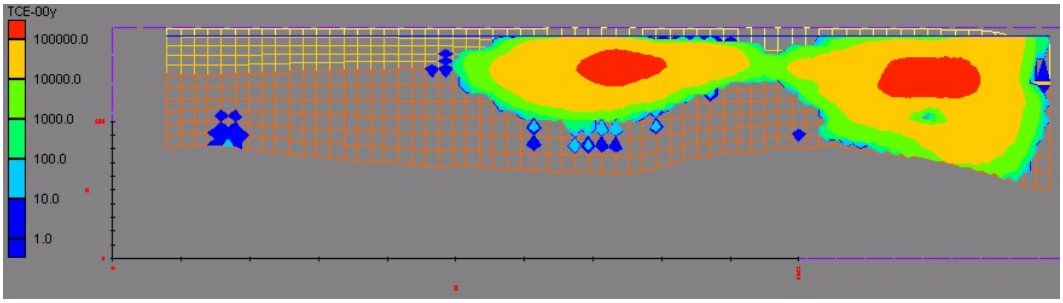

Figure 1.6. TCE concentration profile at A-A' (Fig. 1.5)

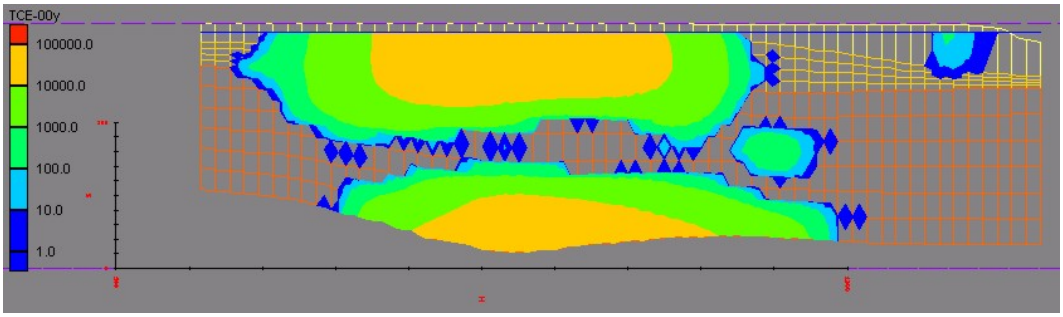

Figure 1.7. TCE concentration profile at B-B' (Fig. 1.5).

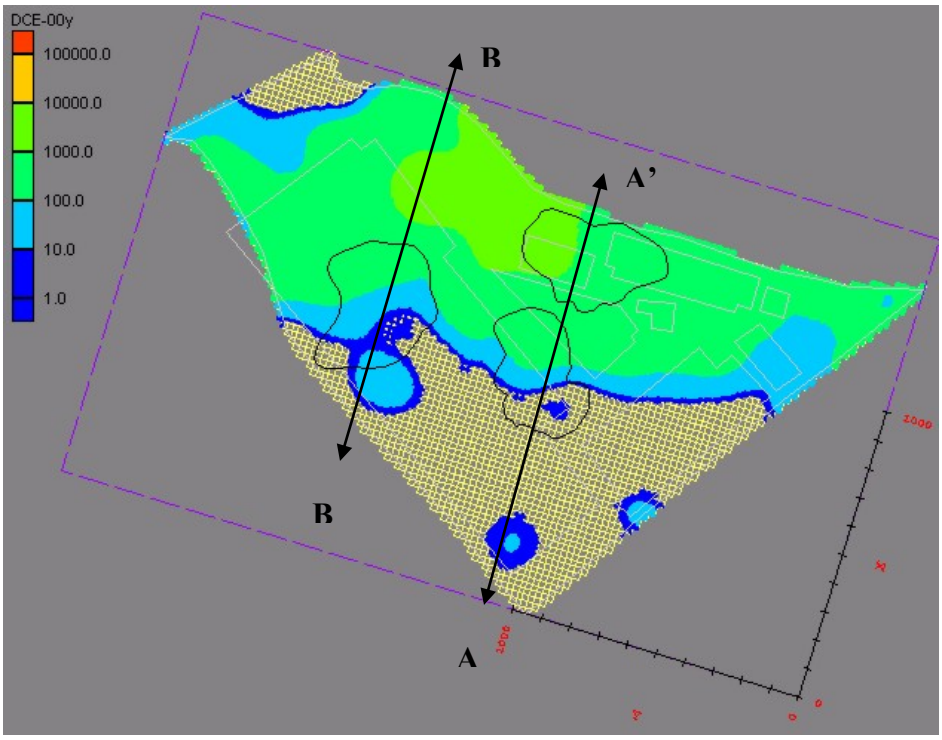

Figure 1.8. DCE concentrations at the water table, conditioned on 1999 data, taken as the pre-treatment distribution

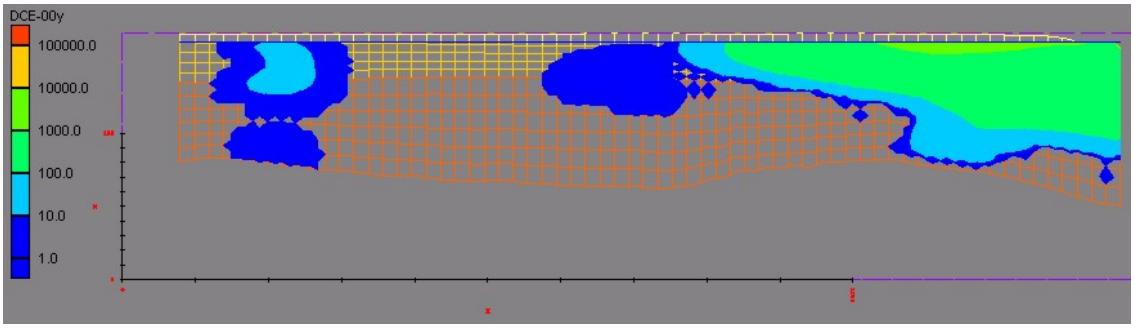

Figure 1.9. DCE profile along A-A' [I=75]

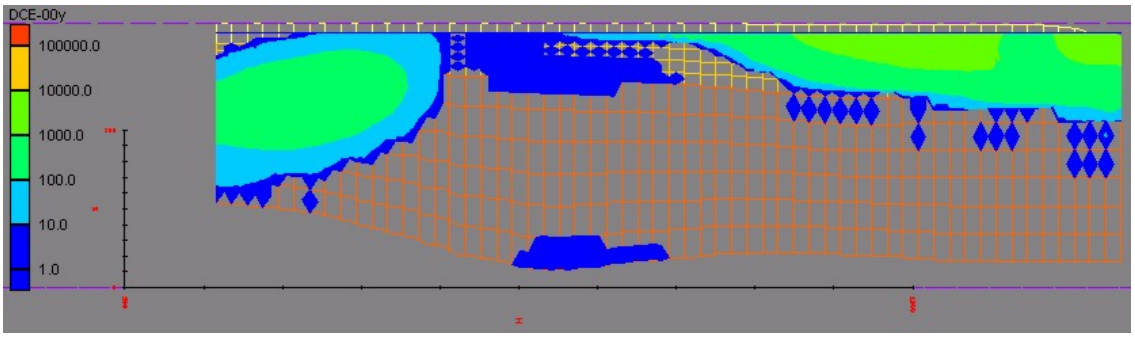

Figure 1.10. DCE profile along B-B' [I=47]

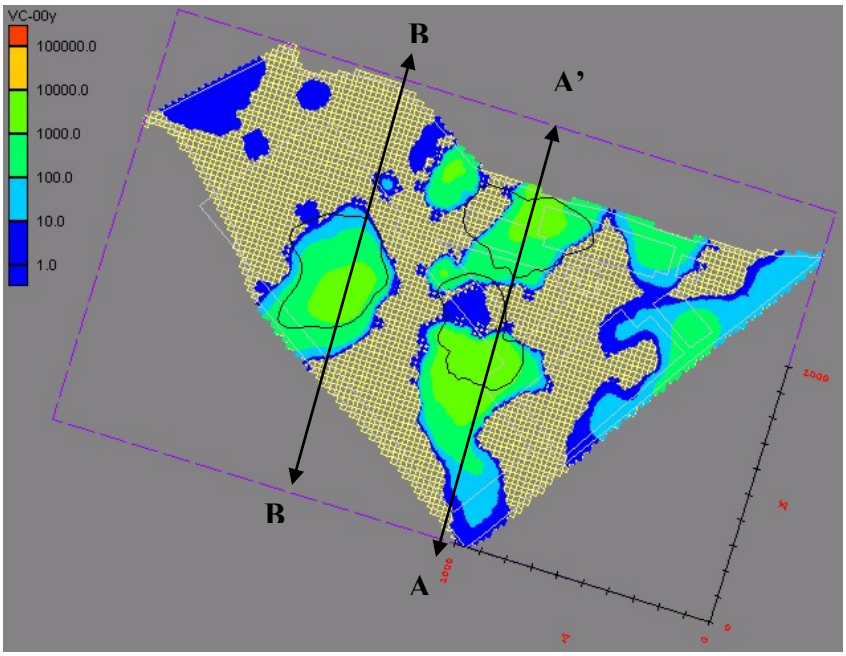

Figure 1.11. VC concentrations at the water table, conditioned on 1999 data, taken as the pre-treatment distribution.

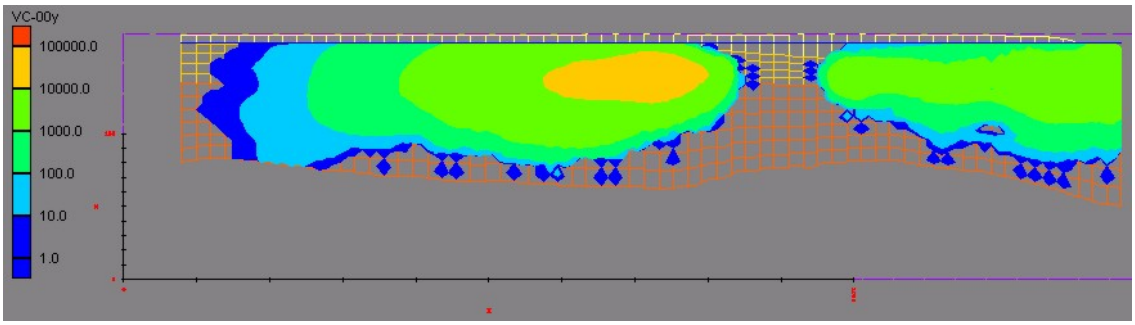

Figure 1.12. VC profile on A-A' transect in Figure 1.11. [I=75]

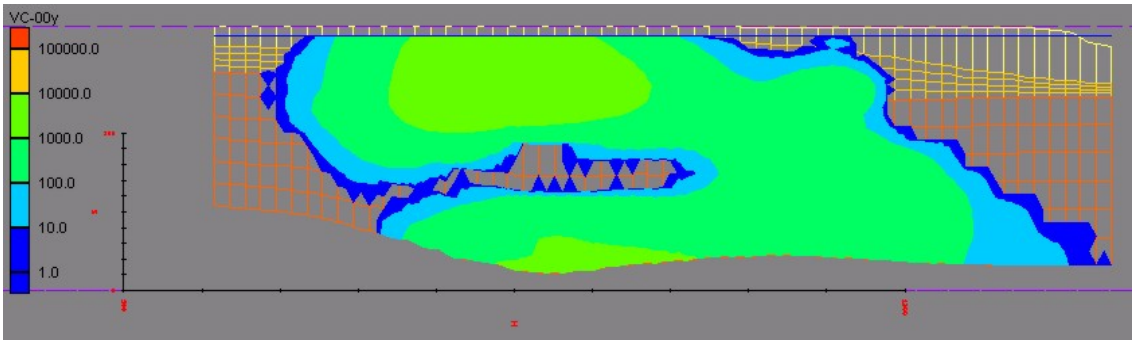

Figure 1.13. VC profile on B-B' transect in Figure 1.11.

Shallow Treatment of Plume Core (2 grid layers)

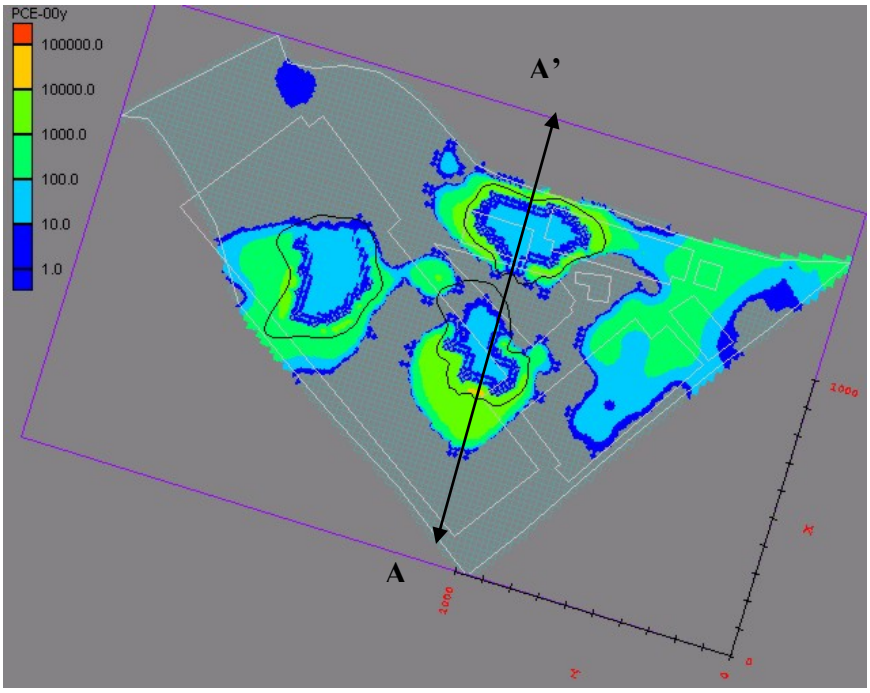

Figure 1.14. PCE concentrations (ppb) at the water table immediately after shallow treatment of the plume cores.

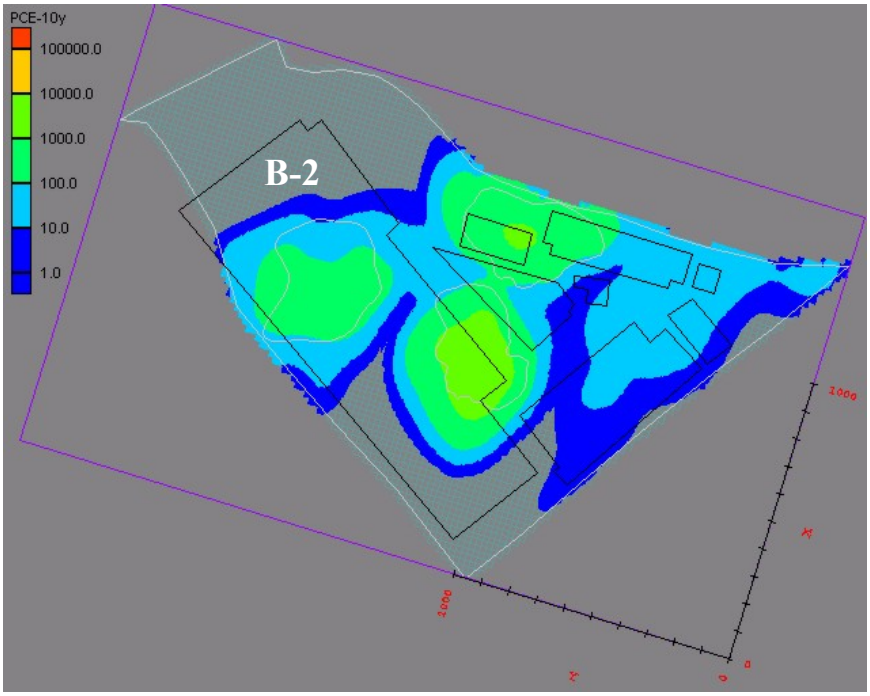

Figure 1.15. PCE (ppb) distribution at the water table, only 10 years after shallow treatment of plume cores. Though an improvement over untreated conditions (Figure 1.2), contaminant rebound is evident.

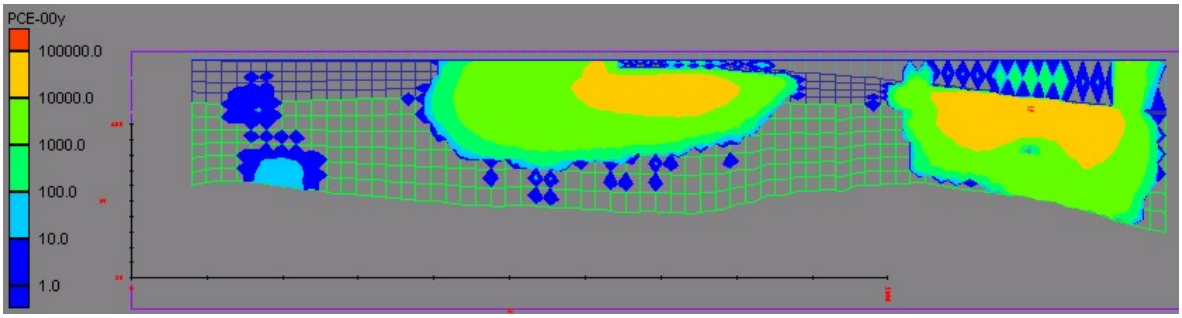

Figure 1.16. PCE concentrations (ppb) along section A-A' in Figure 1.14 after shallow treatment of the plume cores. [I=75]

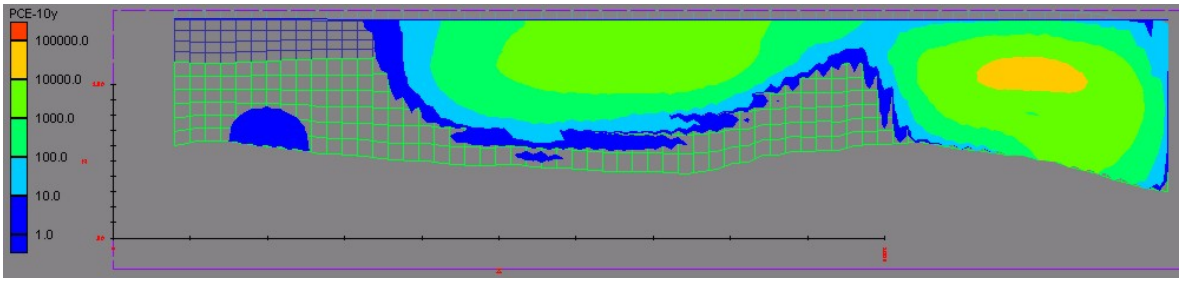

Figure 1.17. PCE concentrations (ppb) along section A-A' (Figure 1.14), 10 years after shallow treatment of the plume cores. [I=75]

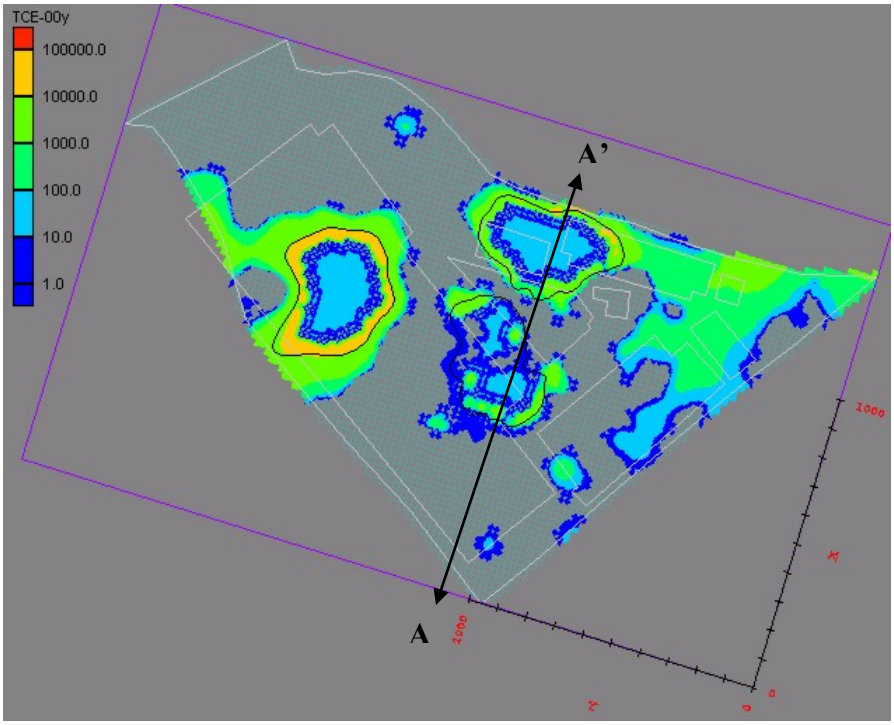

Figure 1.18. TCE concentrations (ppb) at the water table immediately after shallow treatment of the plume cores

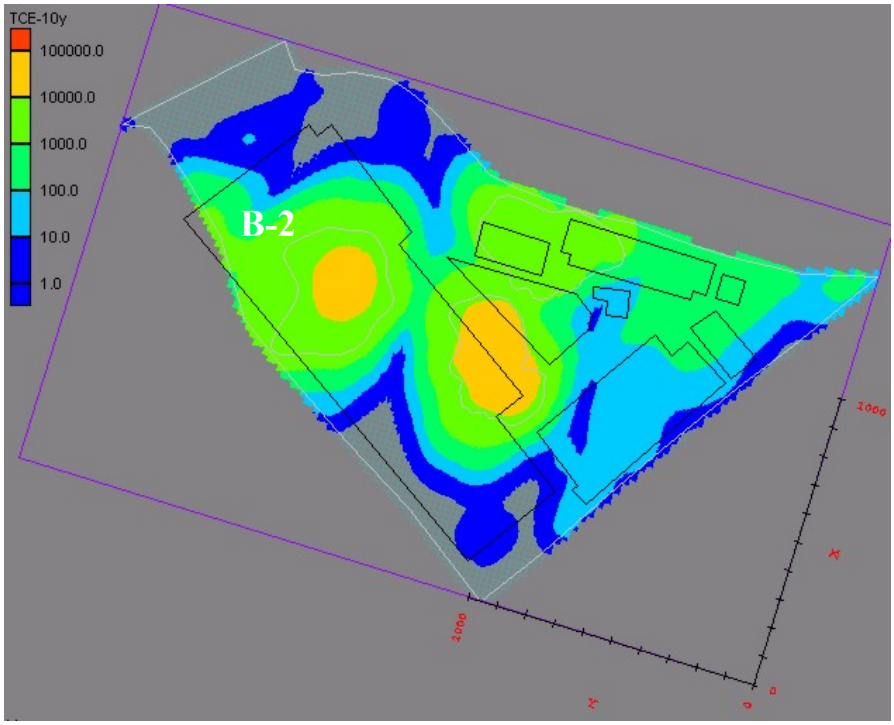

Figure 1.19. TCE (ppb) distribution at the water table, only 10 years after shallow treatment of plume cores. Contaminant rebound is evident.

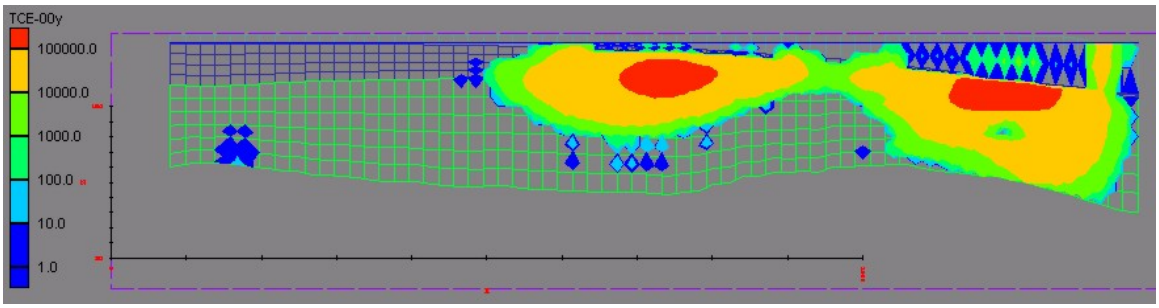

Figure 1.20. TCE concentrations along section A-A' in Figure 1.18, immediately after shallow treatment of plume cores. [I=75]

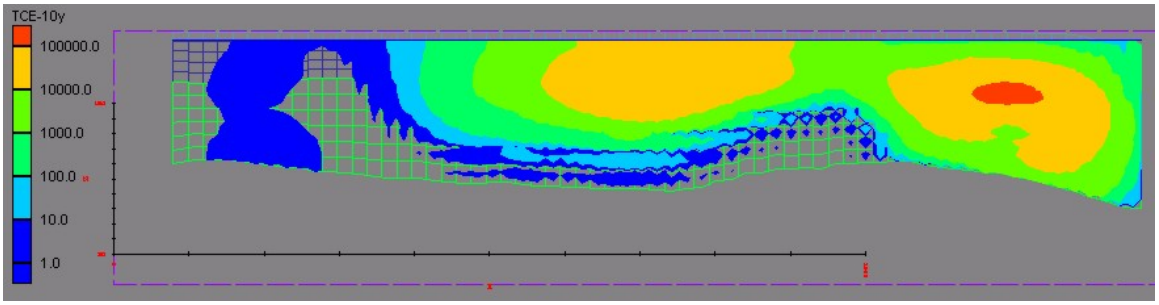

Figure 1.21. TCE concentrations along section A-A’ (Figure 1.18) 10 years after shallow treatment of plume cores. [I=75]

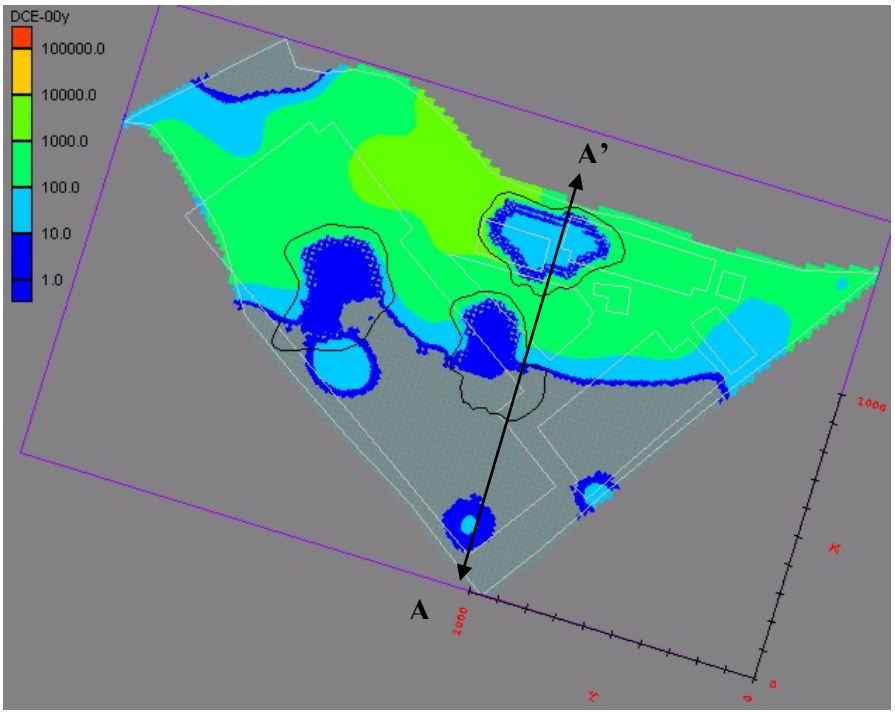

Figure 1.22. DCE (ppb) distribution at the water table immediately after shallow treatment of the plume cores.

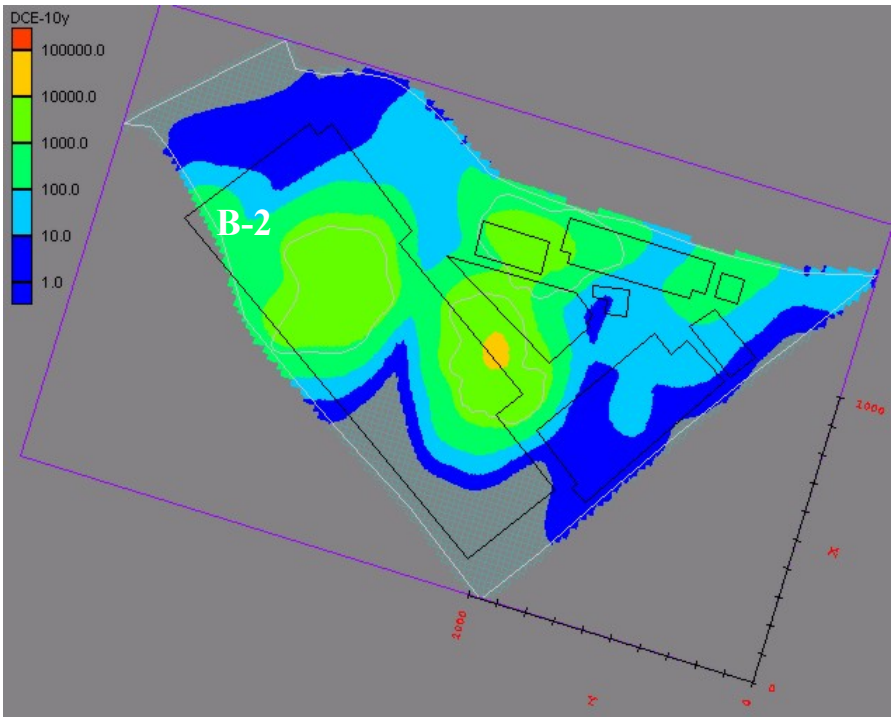

Figure 1.23. DCE (ppb) distribution at the water table, only 10 years after shallow treatment of plume cores. Contaminant rebound derived from continued solvent degradation is evident.

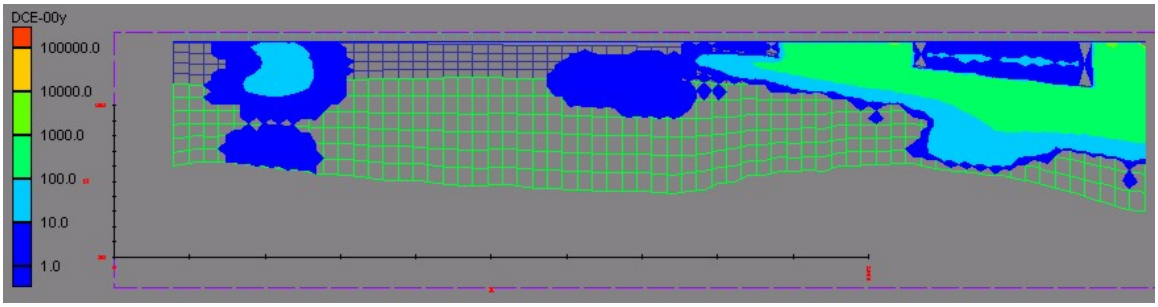

Figure 1.24. DCE distribution along section A-A' in Figure 1.22, immediately after shallow treatment of the plume cores. [I=75]

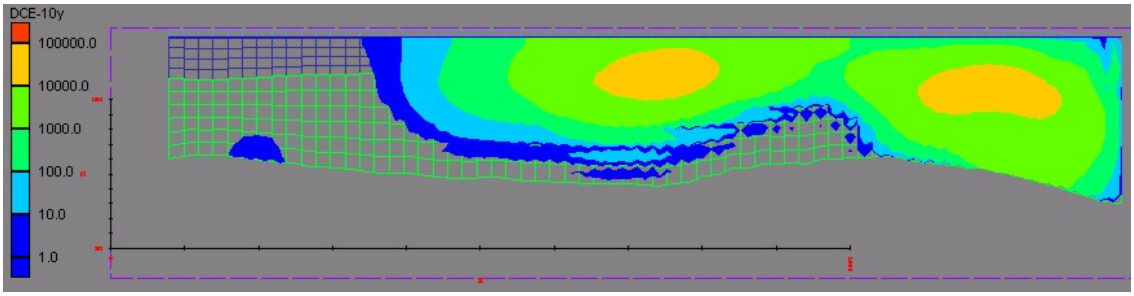

Figure 1.25. DCE distribution along section A-A' (Figure 1.22), 10 years after shallow treatment of the plume cores. Contaminant rebound is evident, apparently derived from continued solvent degradation and upward migration. [I=75]

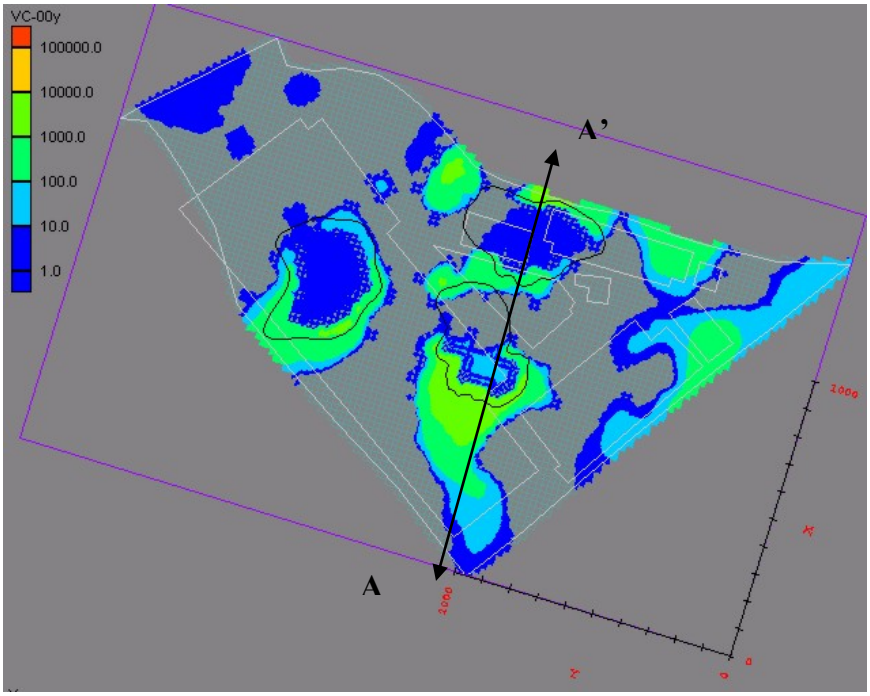

Figure 1.26. VC concentrations at the water table immediately after shallow treatment of plume cores.

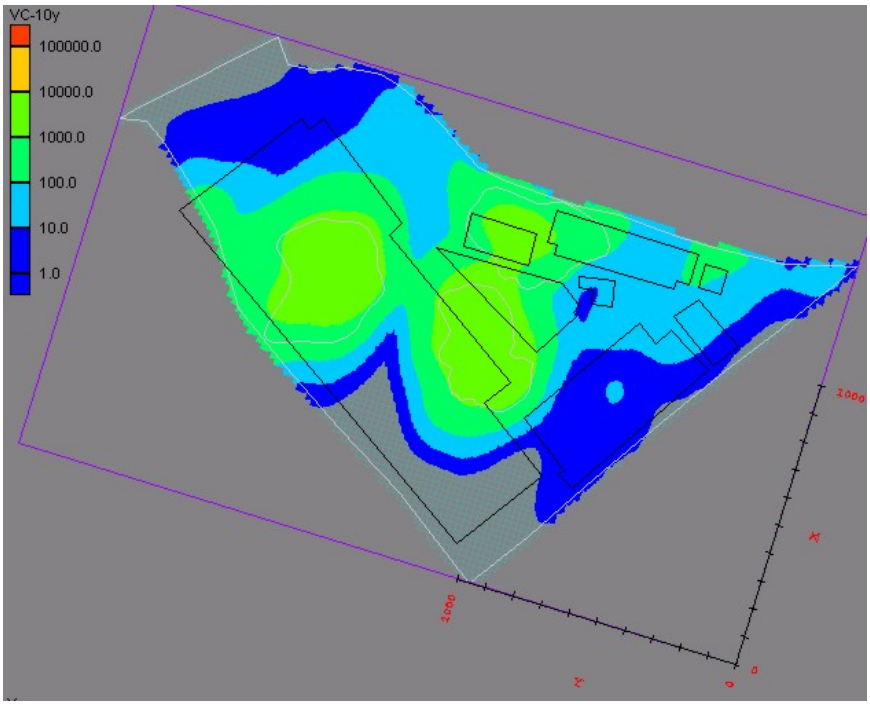

Figure 1.27. VC (ppb) distribution at the water table, only 10 years after shallow treatment of plume cores. Contaminant rebound is evident.

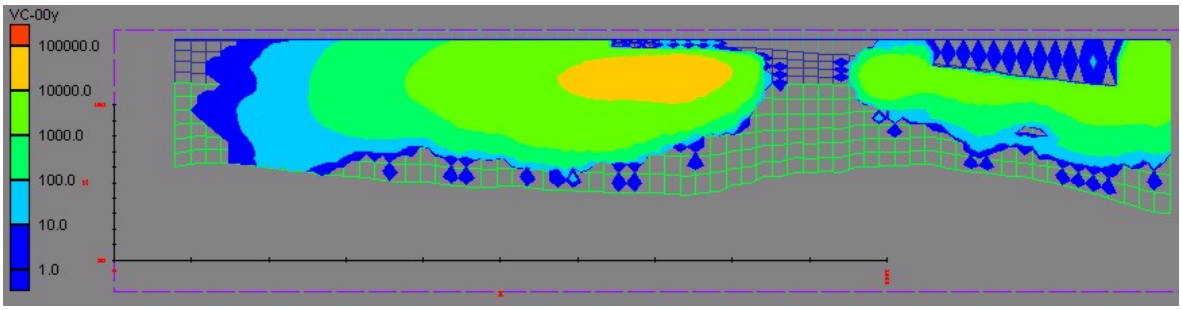

Figure 1.28. VC concentrations along section A-A' (Figure 1.26) after shallow treatment of plume cores [I=75]

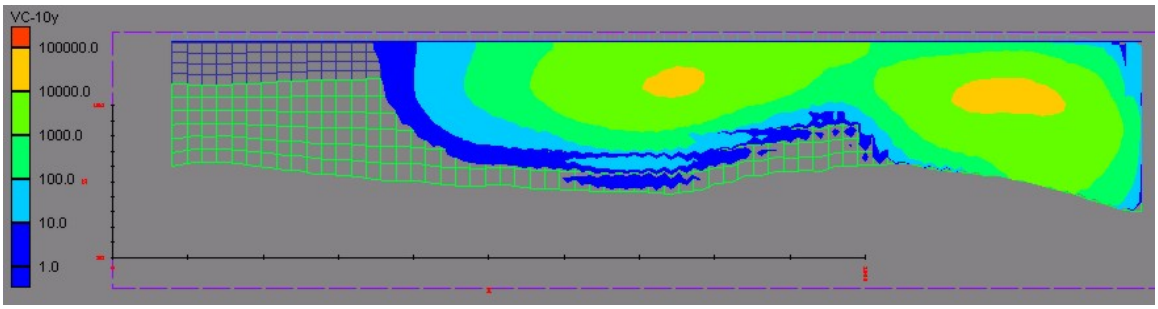

Figure 1.29. VC concentrations (ppb) along section A-A' (Figure 1.26), 10 years after shallow treatment of the plume cores. [I=75]

Intermediate Treatment of Plume Core (4 grid layers)

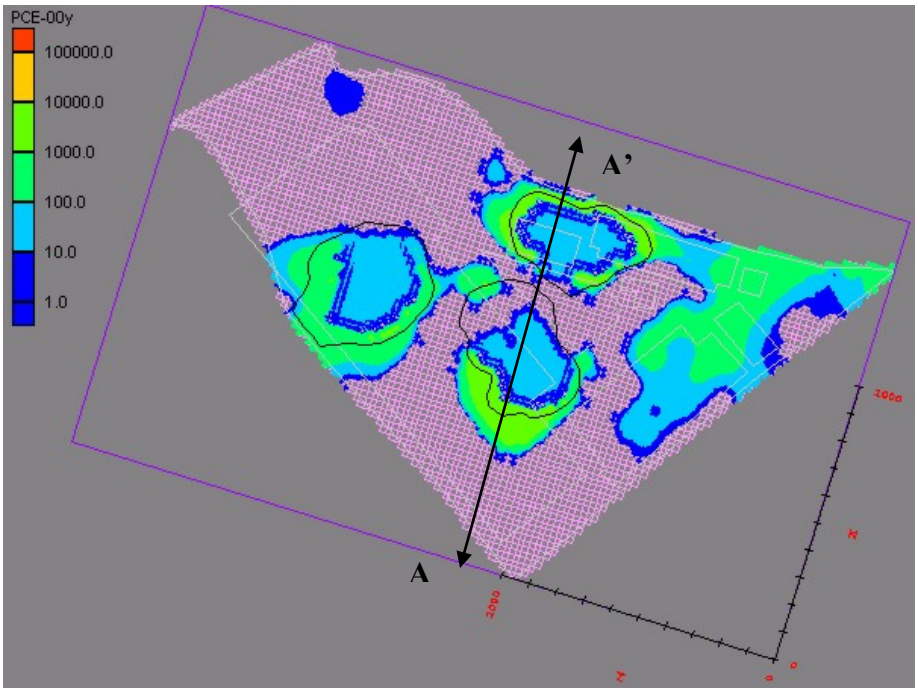

Figure 1.30. PCE concentrations (ppb) at the water table immediately after treatment of plume cores to the intermediate depth (4 grid layers).

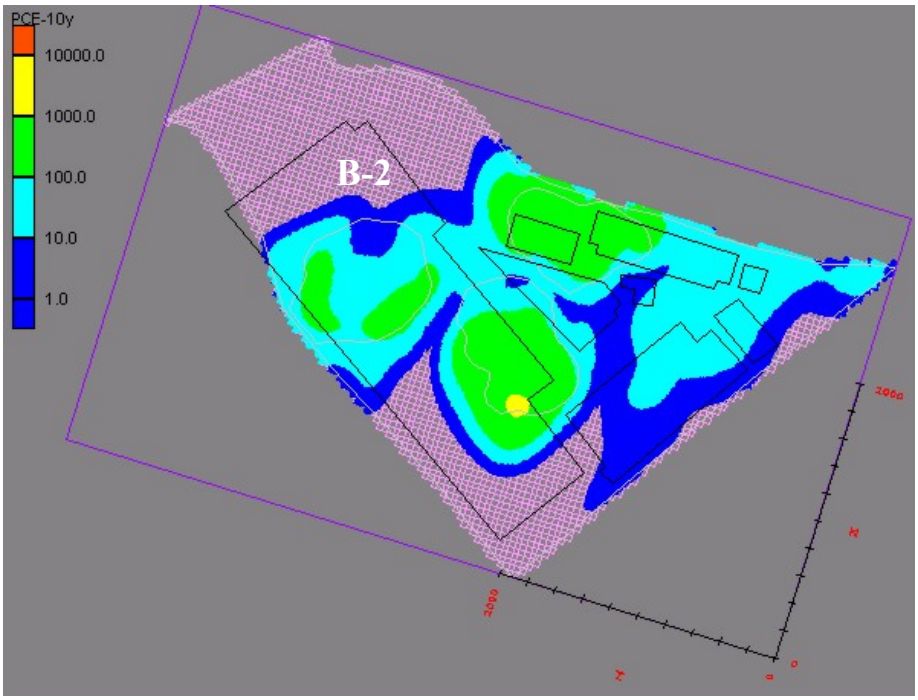

Figure 1.31. PCE (ppb) at the water table, 10 years after intermediate, core treatment; contaminant rebound is evident.

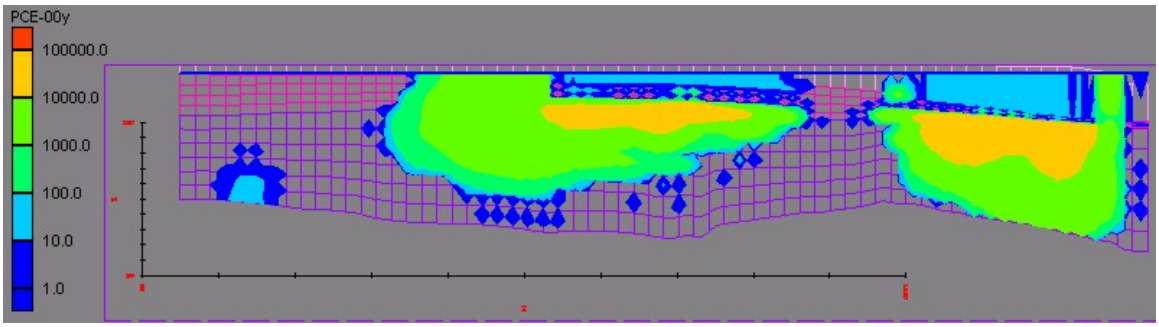

Figure 1.32.. PCE concentrations (ppb) along section A-A' (Figure 1.30) after the hypothetical intermediate-depth treatment of plume cores. [I=73]

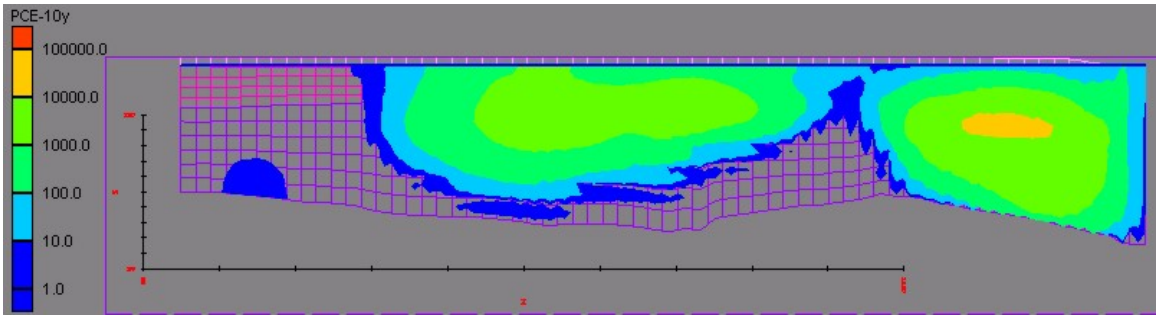

Figure 1.33. PCE concentrations (ppb) along section A-A' (Figure 1.30) 10 years after the intermediate-depth treatment of plume cores. [I=73]

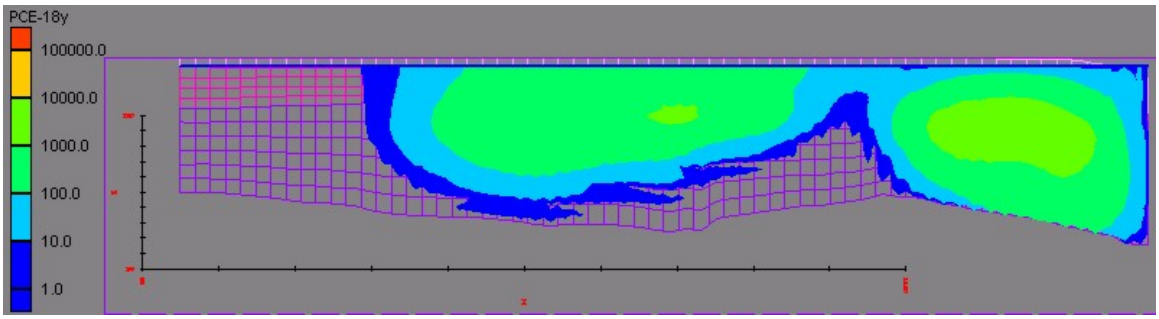

Figure 1.34. PCE concentrations (ppb) along section A-A' (Figure 1.30) 18 years after the intermediate-depth treatment of plume cores. [I=73]

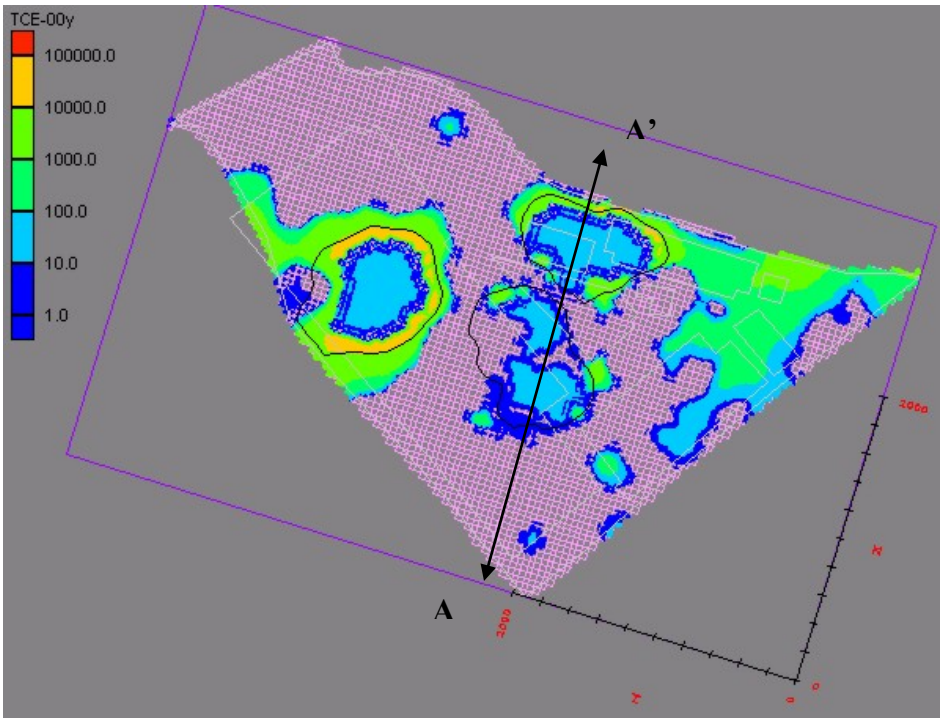

Figure 1.35. TCE concentrations (ppb) at the water table after intermediate-depth treatment of plume cores.

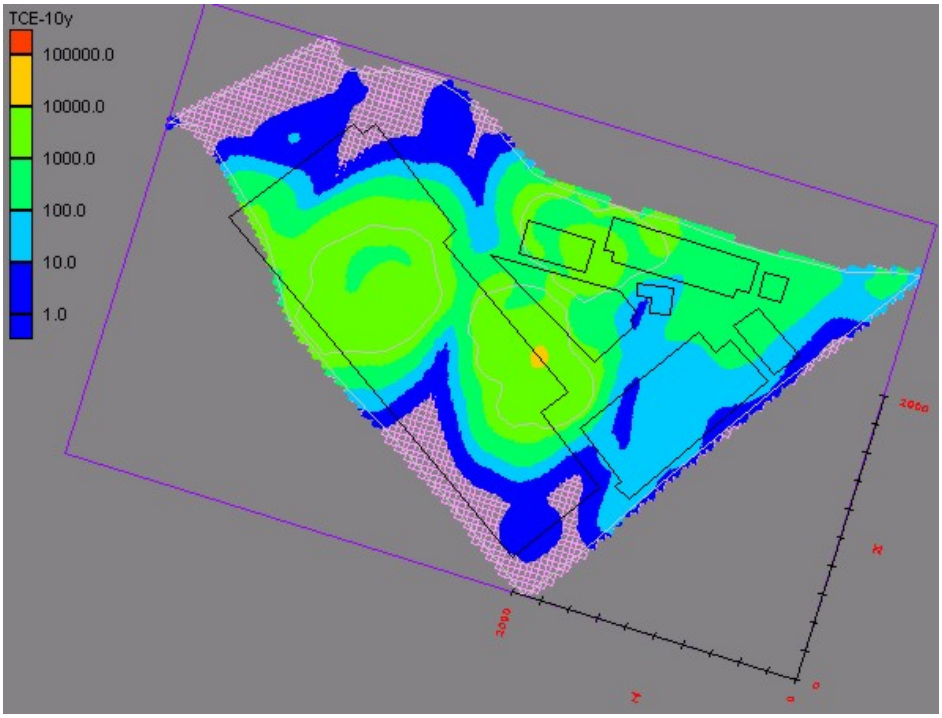

Figure 1.36. TCE concentrations (ppb) at the water table 10 years after intermediate-depth treatment of plume cores; contaminant rebound is evident.

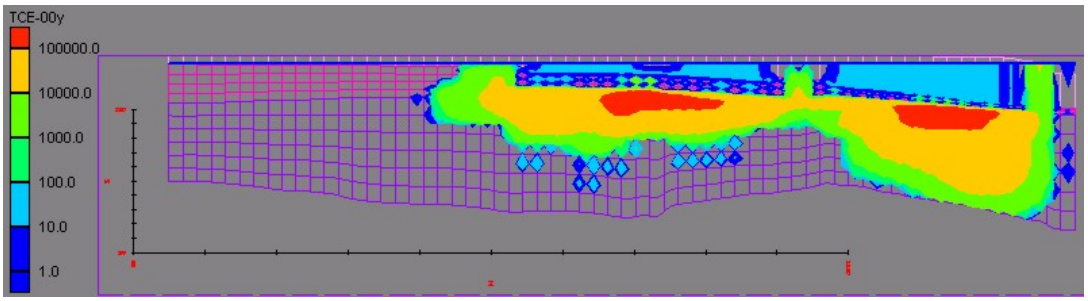

Figure 1.37. TCE concentrations (ppb) along section A-A' (Figure 1.35) after intermediate-depth treatment of the plume cores. [I=73]

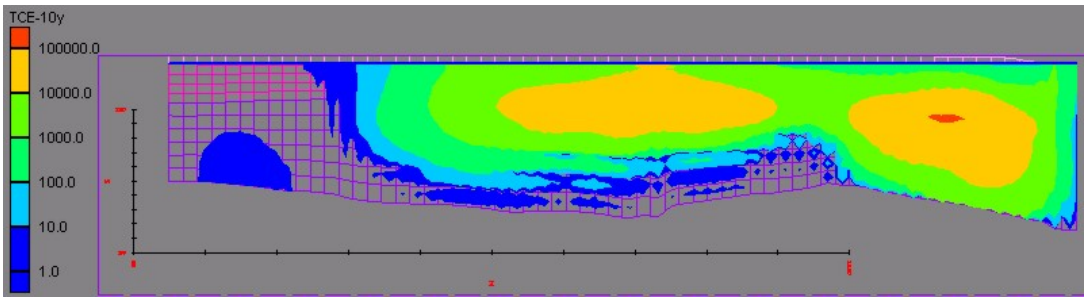

Figure 1.38. TCE concentrations (ppb) 10 years after intermediate-depth treatment of the plume core**.** [I=73]

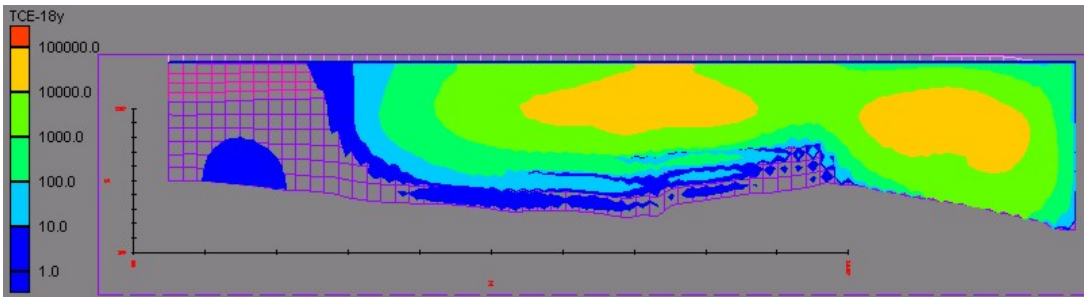

Figure 1.39. TCE concentrations (ppb) 18 years after the intermediate-depth treatment of the plume cores. [I=73]

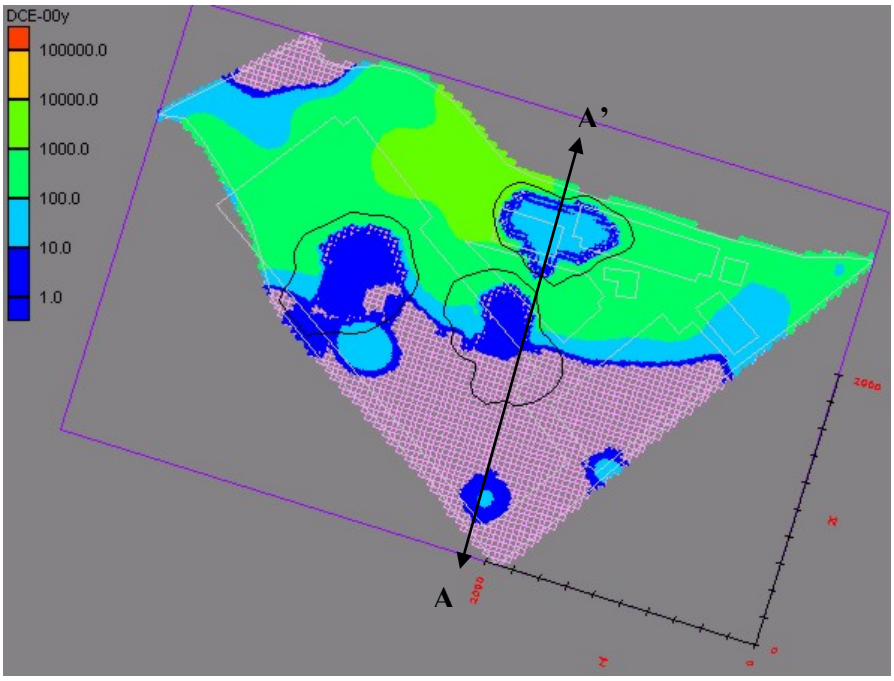

Figure 1/40. DCE concentrations (ppb) at the water table after intermediate-depth treatment of plume cores.

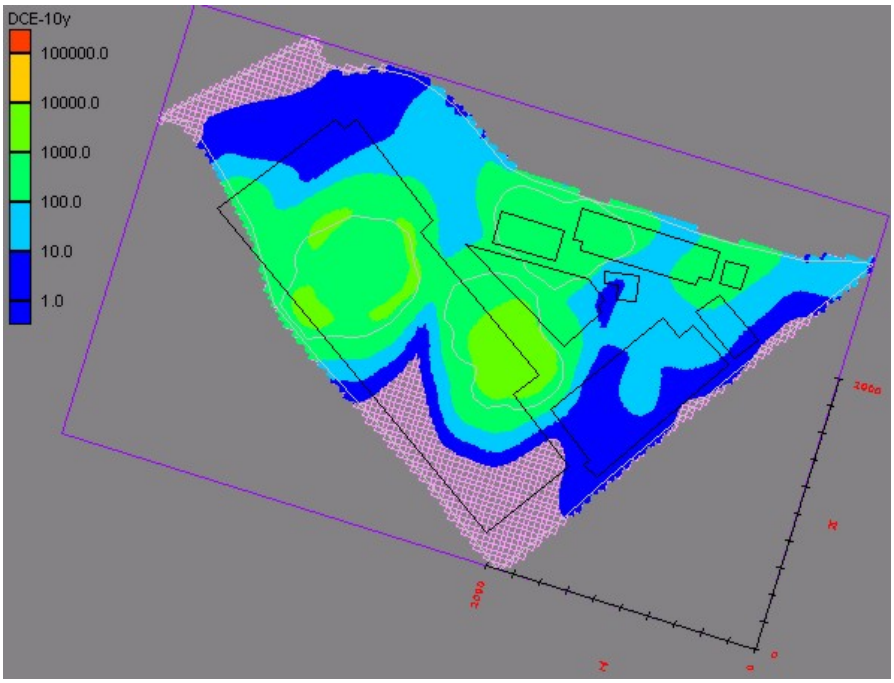

Figure 1.41. DCE concentrations (ppb) at the water table, 10 years after intermediate-depth treatment of plume cores; contaminant rebound is evident.

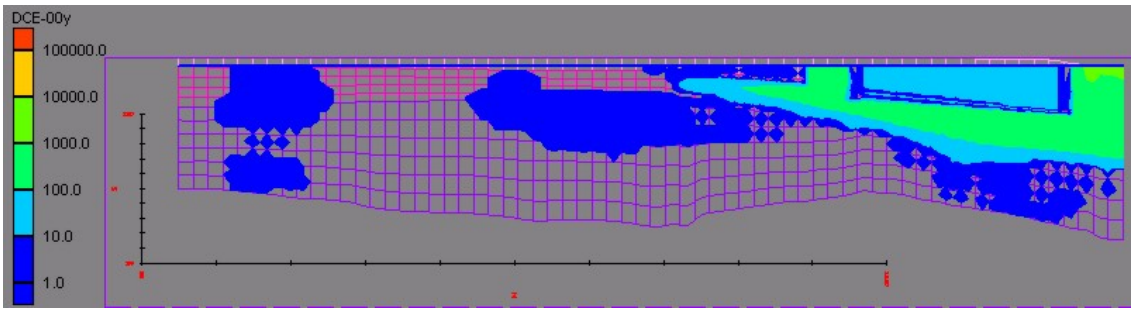

Figure 1.42. DCE concentrations (ppb) along section A-A' (Figure 1.40) after intermediate-depth treatment of the plume cores. [I=73]

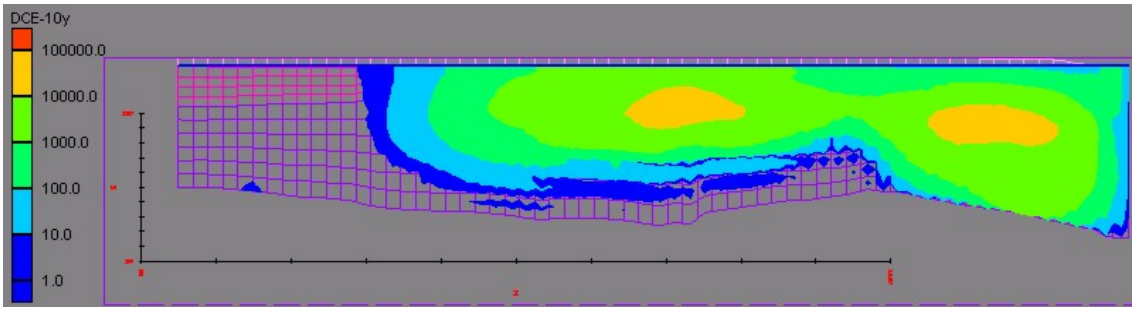

Figure 1.43. DCE concentrations (ppb) along section A-A' (Figure 1.40) 10 years after the intermediate-depth treatment of the plume cores. [I=73]

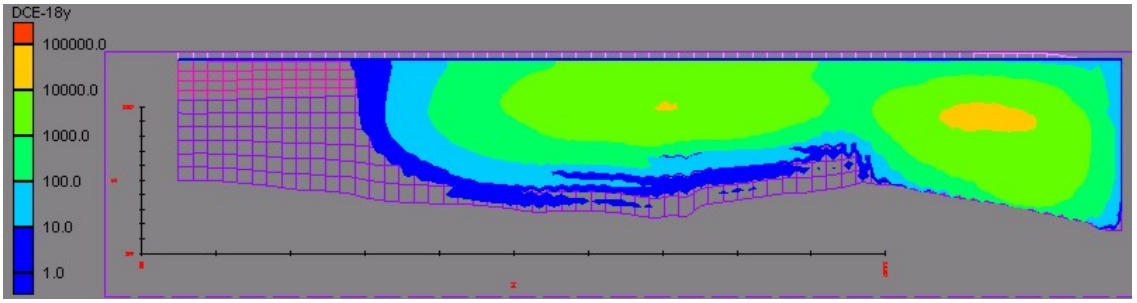

Figure 1.44 DCE concentrations (ppb) along section A-A' (Figure 1.40) 18 years after the intermediate-depth treatment of the plume cores. [I=73]

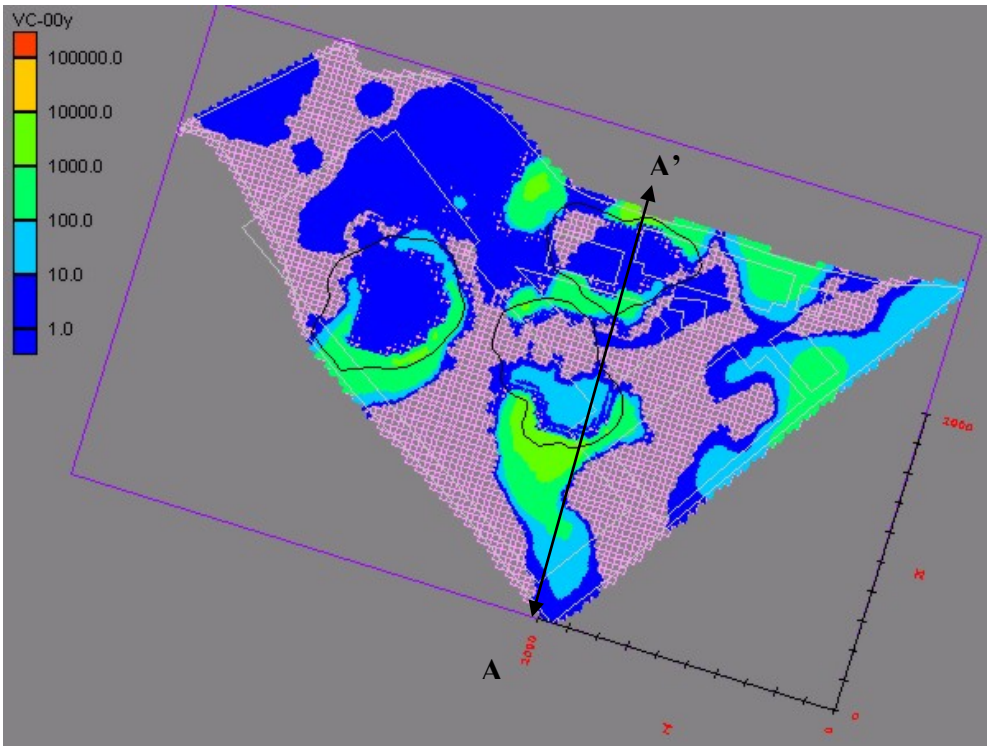

Figure 1.45. VC concentrations (ppb) at the water table after intermediate-depth treatment of plume cores.

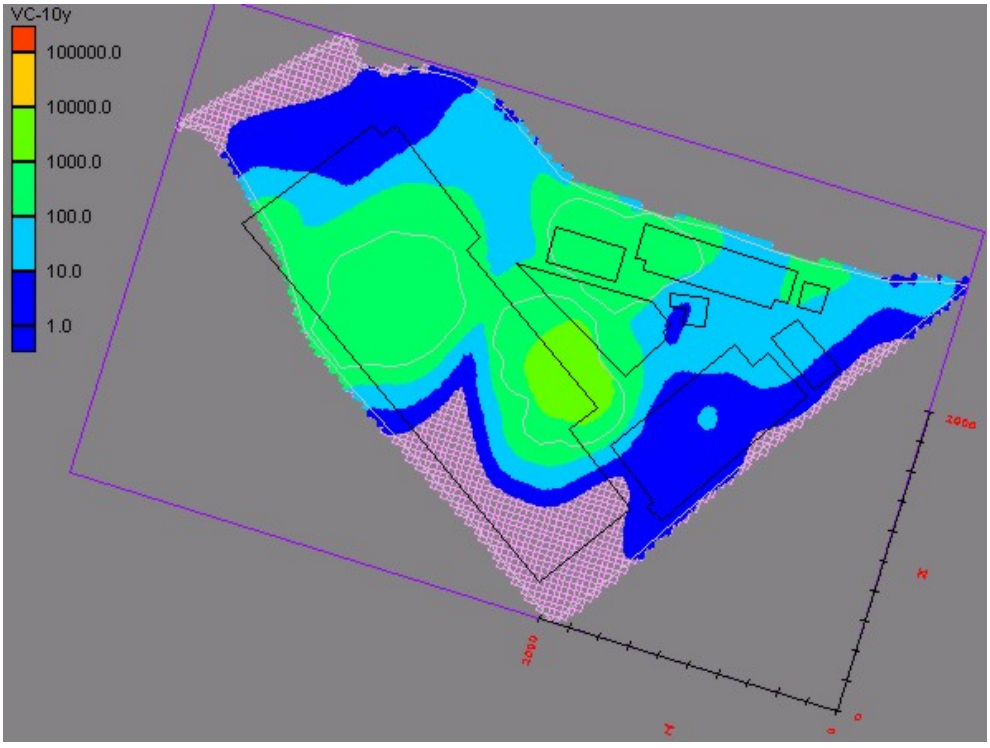

Figure 1.46. VC concentrations at the water table 10 years after intermediate-depth treatment of plume cores; contaminant rebound is evident.

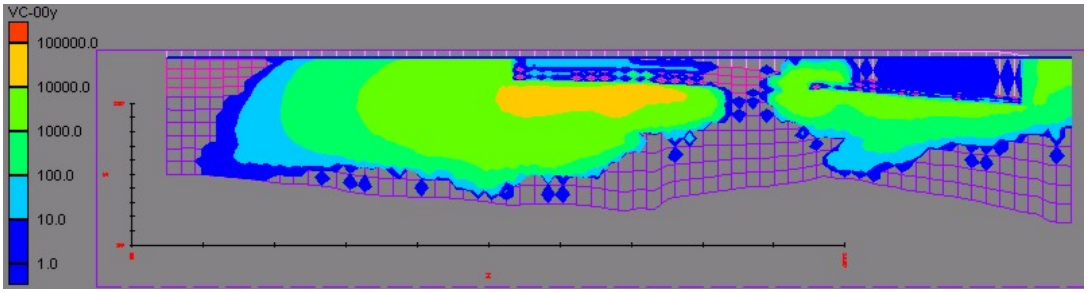

Figure 1.47. VC concentrations (ppb) along section A-A' (Figure 1.40) after intermediate-depth treatment of the plume cores. [I=73]

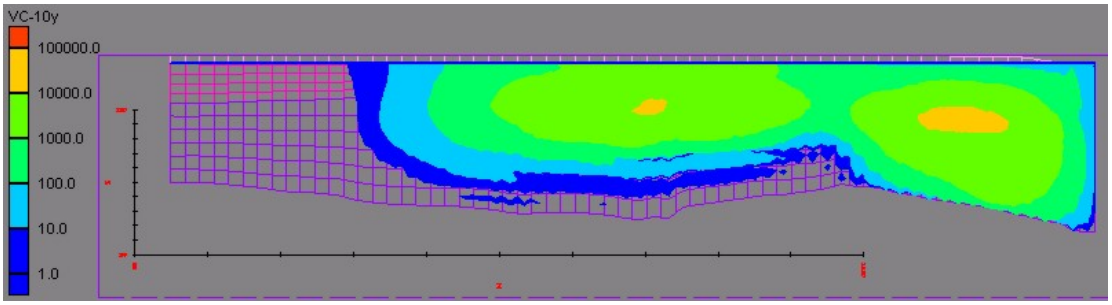

Figure 1.48. VC concentrations (ppb) along section A-A' (Figure 1.40) 10 years after intermediate-depth treatment of the plume cores. [I=73]

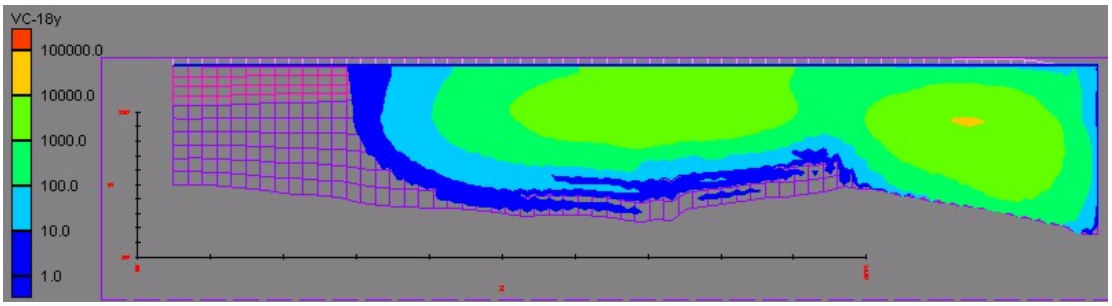

Figure 1.49. VC concentrations (ppb) along section A-A' (Figure 1.40) 18 years after intermediate-depth treatment of the plume cores. [I=73]

Deep Treatment of Plume Core (6-7 grid layers)

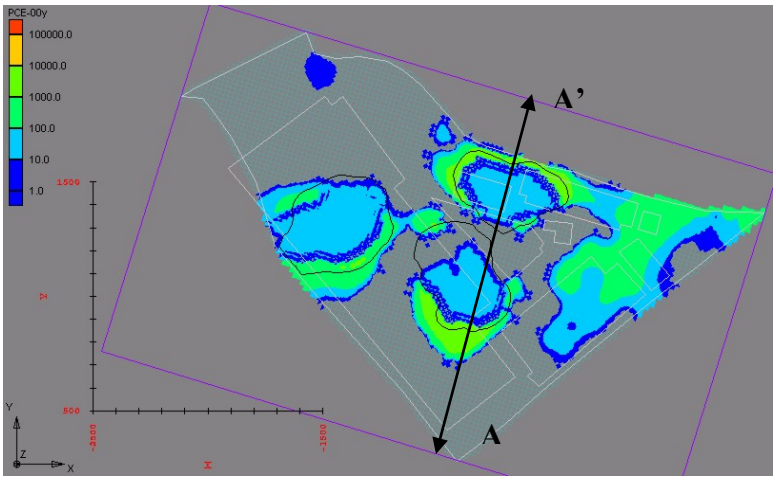

Figure 1.50. PCE (ppb) at water table after deep treatment of plume cores.

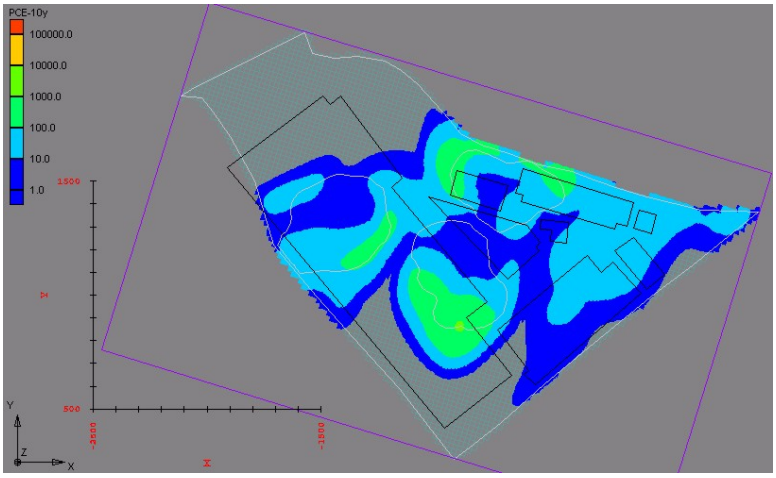

Figure 1.51. PCE (ppb) at water table, 10 years after deep treatment of plume cores.

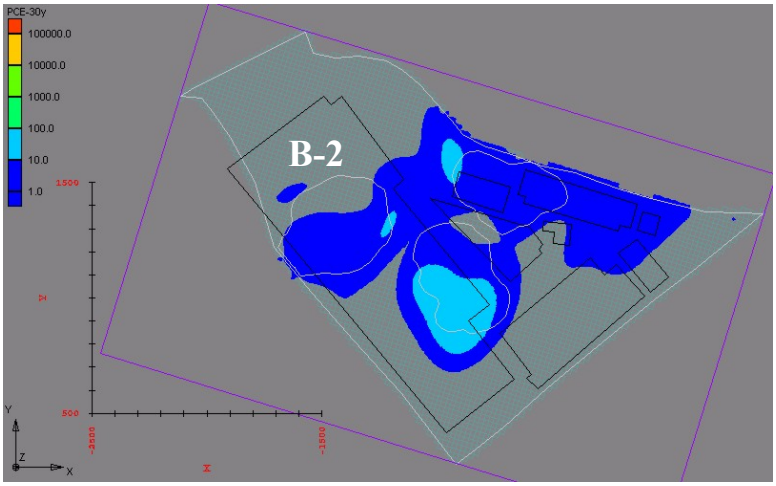

Figure 1.52. PCE (ppb) at water table, 30 years after deep treatment of plume cores.

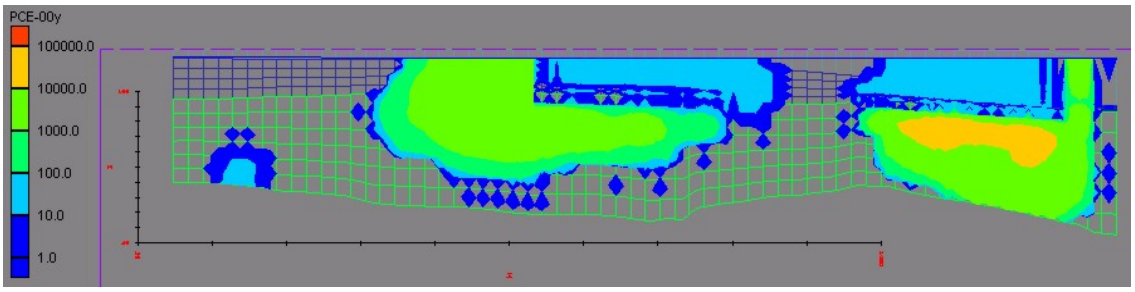

Figure 1.53. PCE profile along A-A' (Fig. 1.50) after deep core treatment [I=73]

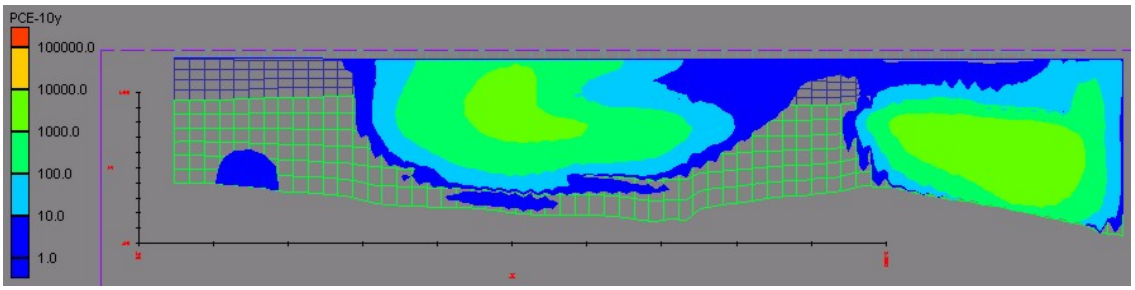

Figure 1.54. PCE profile along A-A' (Fig. 1.50) 10 years after deep core treatment [I=73]

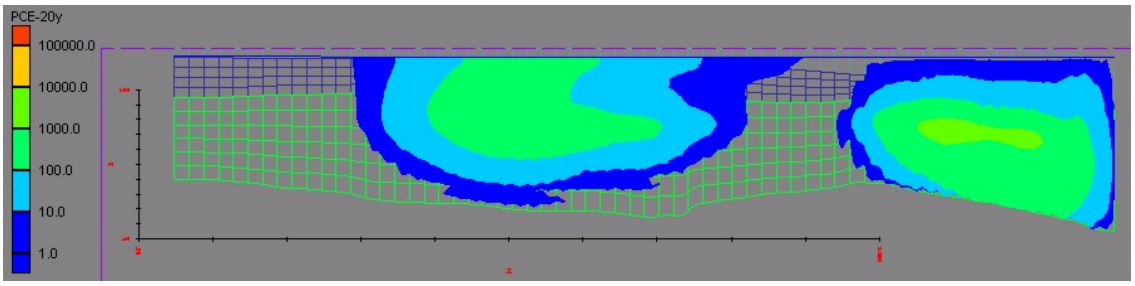

Figure 1.55. PCE profile A-A' (Fig. 1.50) 20 years after deep core treatment [I=73]

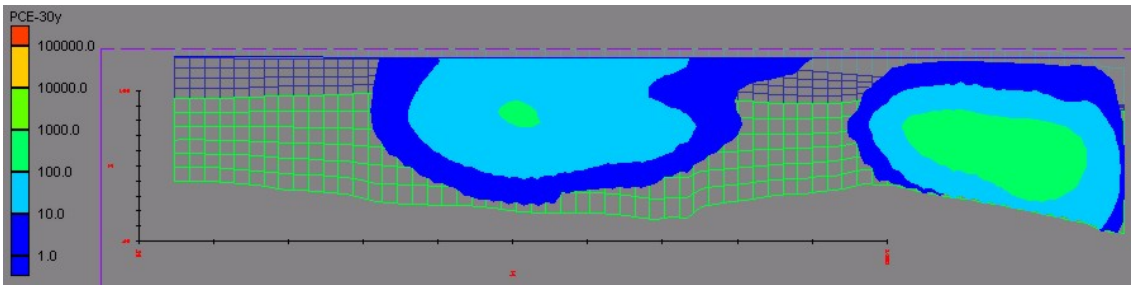

Figure 1.56. PCE profile A-A' (Fig. 1.50) 30 years after deep core treatment [I=73]

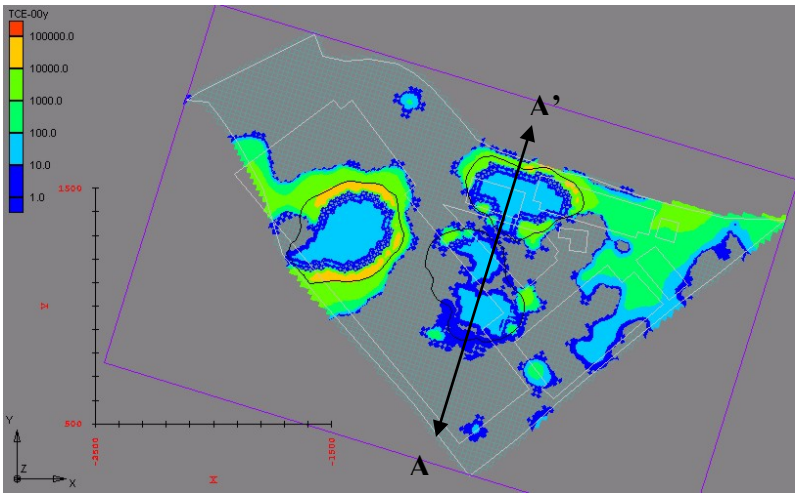

Figure 1.57. TCE (ppb) at water table after deep treatment of plume cores.

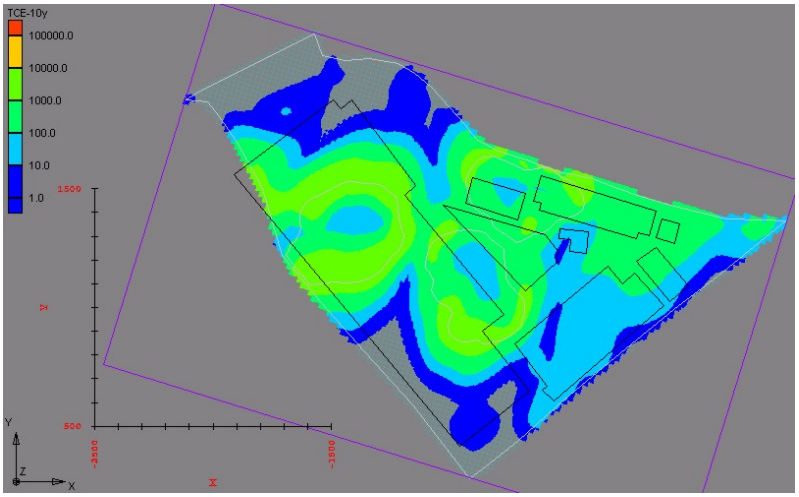

Figure 1.58. TCE (ppb) at water table, 10 years after deep treatment of plume cores

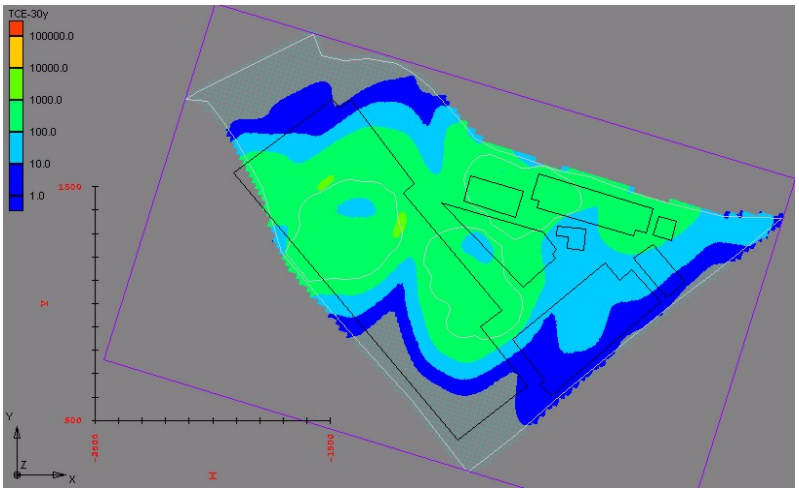

Figure 1.59. TCE (ppb) at water table, 30 years after deep treatment of plume cores

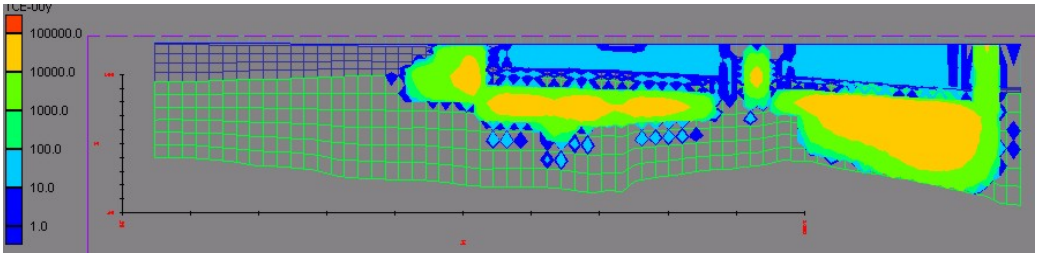

Figure 1.60. TCE profile along A-A' (Fig. 1.57) after deep core treatment [I=73]

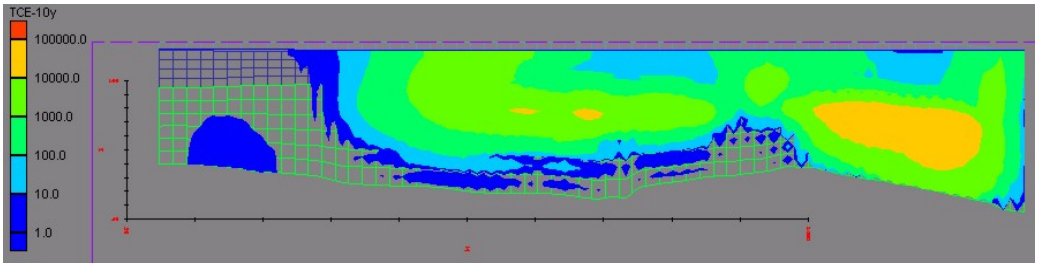

Figure 1.61. TCE profile at A-A' (Fig. 1.57) 10 years after deep core treatment [I=73]

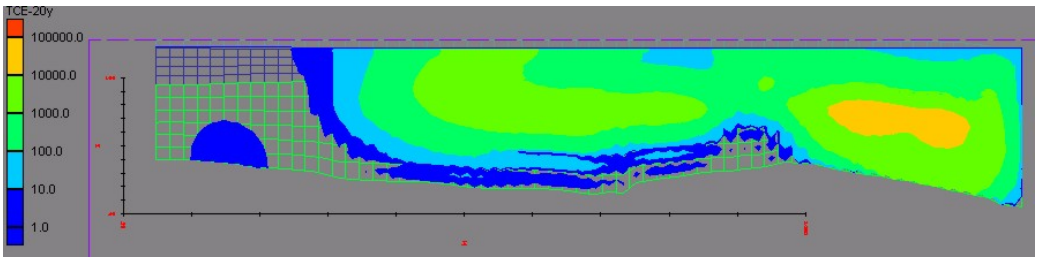

Figure 1.62. TCE profile at A-A' (Fig. 1.57) 20 years after deep core treatment [I=73]

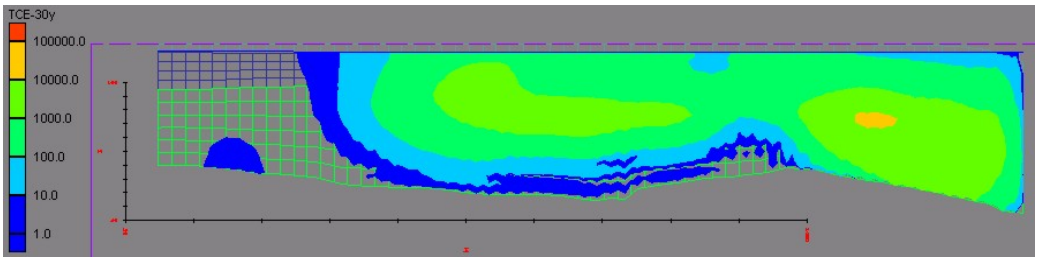

Figure 1.63. TCE profile at A-A' (Fig. 1.57) 30 years after deep core treatment [I=73]

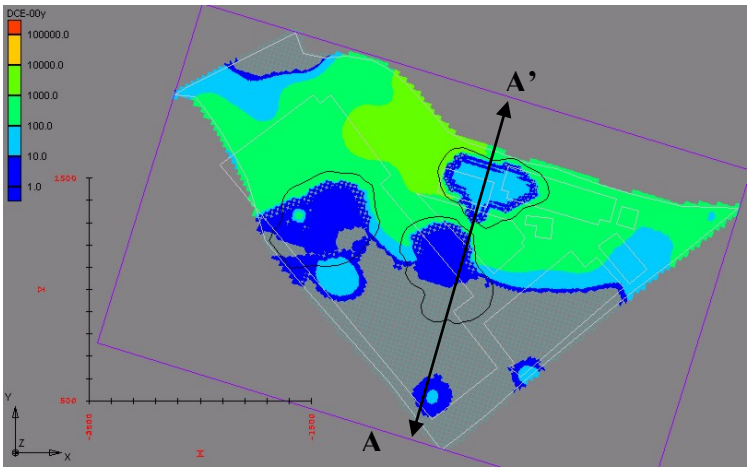

Figure 1,64. DCE (ppb) at water table after deep treatment of plume cores.

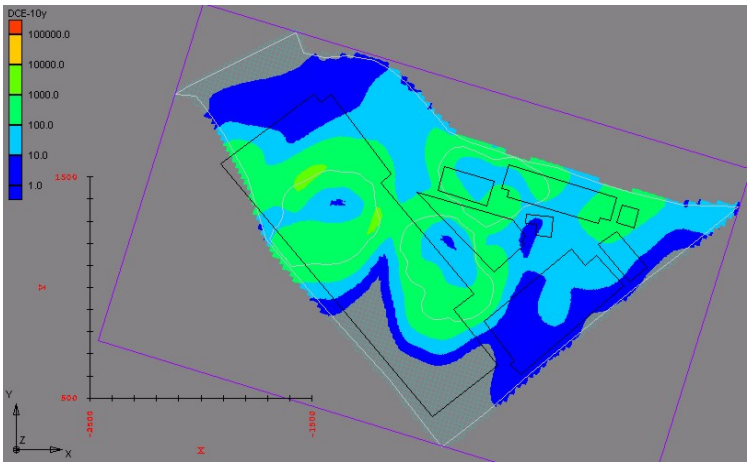

Figure 1.65. DCE (ppb) at water table 10 years after deep treatment of plume cores

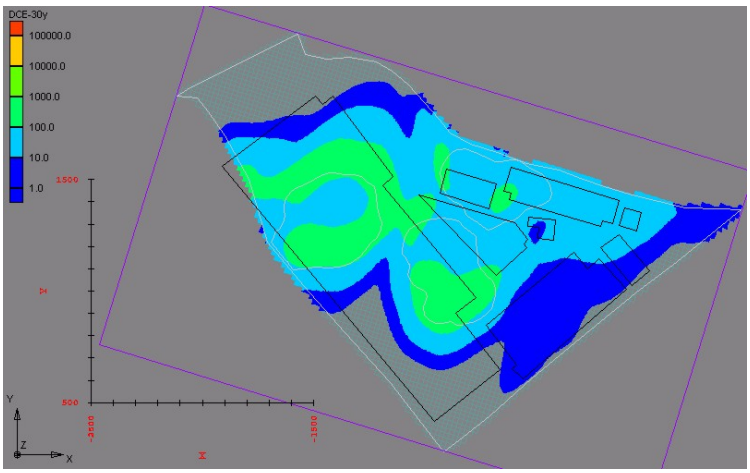

Figure 1.66. DCE (ppb) at water table 30 years after deep treatment of plume cores

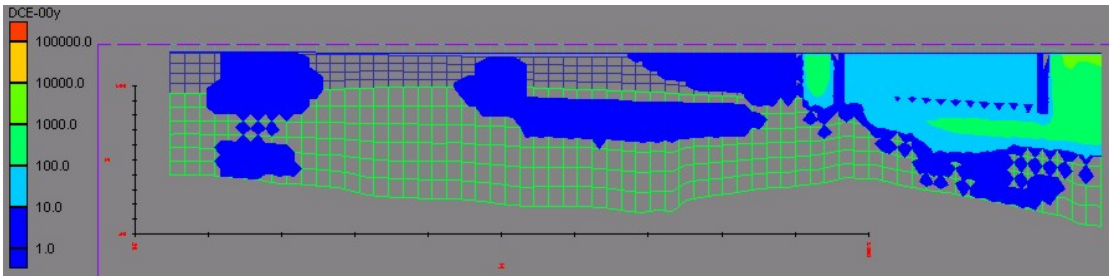

Figure 1.67. DCE profile along A-A' (Fig. 1.64) after deep core treatment [I=73]

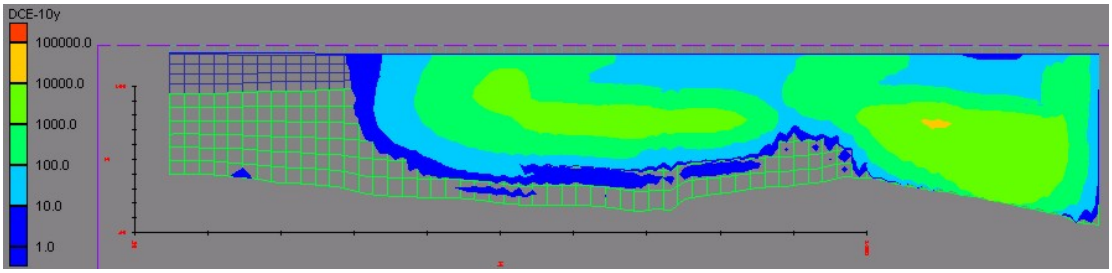

Figure 1.68. DCE profile at A-A' (Fig. 1.64) 10 years after deep core treatment. [I=73]

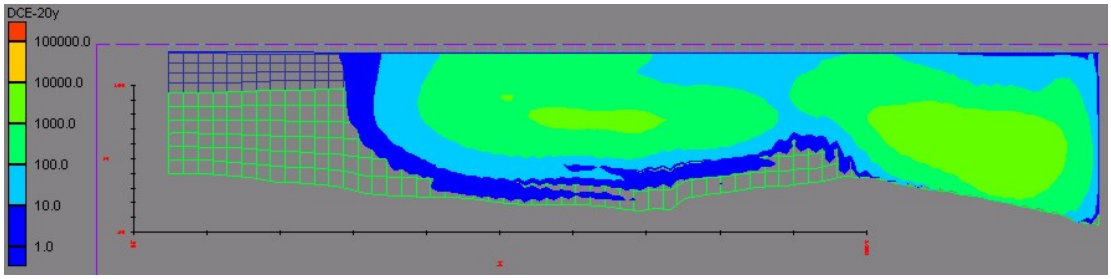

Figure 1.69. DCE profile at A-A' (Fig. 1.64) 20 years after deep core treatment. [I=73]

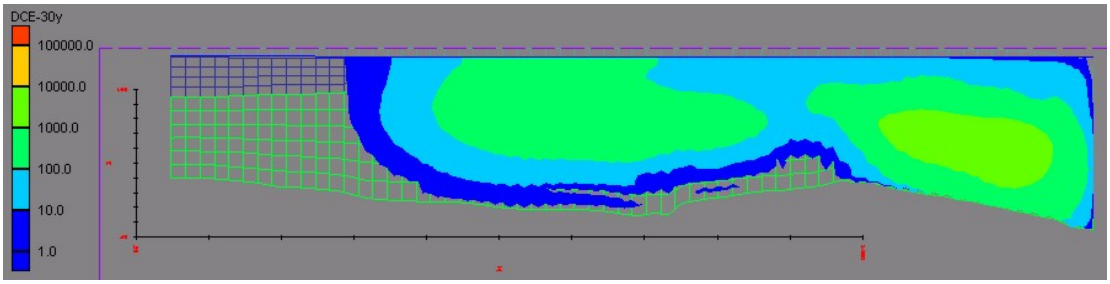

Figure 1.70. DCE profile at A-A' (Fig. 1.64) 30 years after deep core treatment. [I=73]

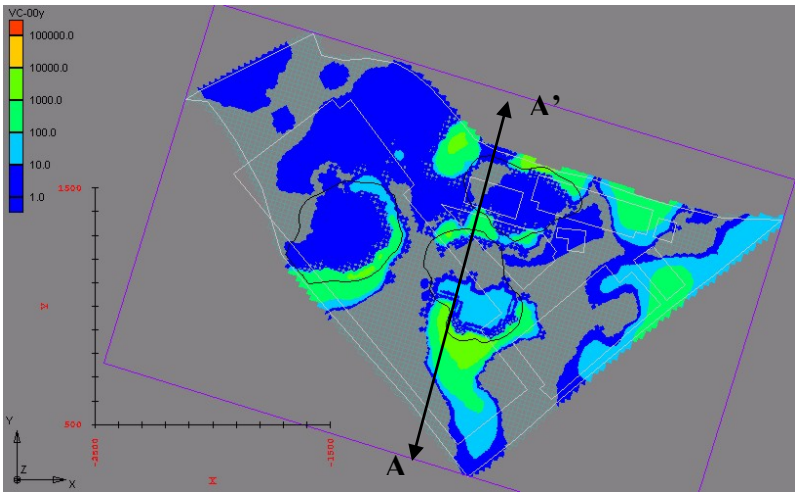

Figure 1.71. VC (ppb) at water table after deep treatment of plume cores.

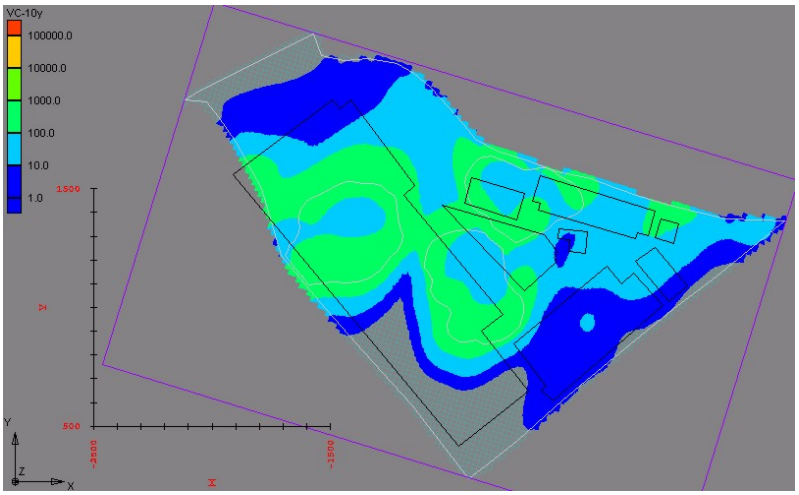

Figure 1.72. VC (ppb) at water table 10 years after deep treatment of plume cores.

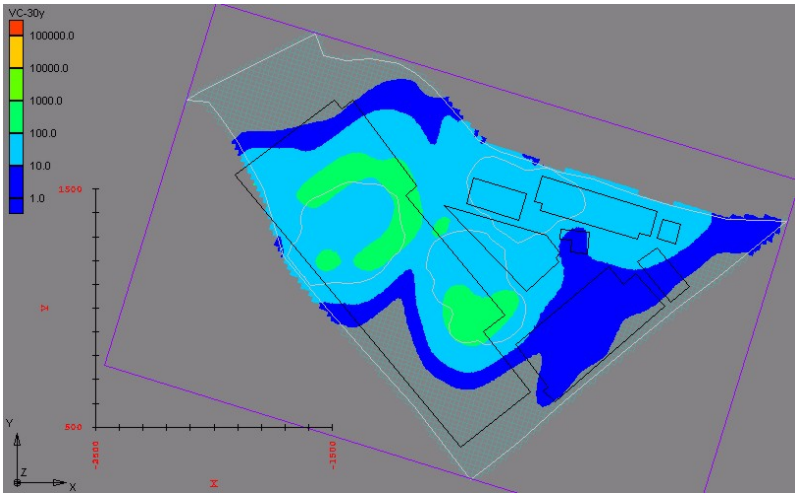

Figure 1.73. VC (ppb) at water table 30 years after deep treatment of plume cores.

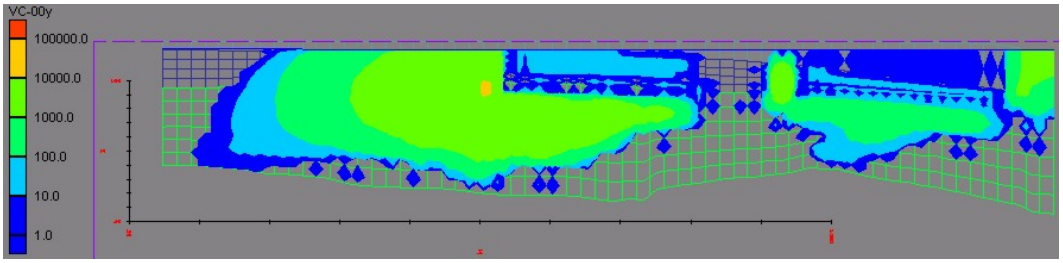

Figure 1.74. VC profile along A-A' (Fig. 1.71) after deep core treatment [I=73]

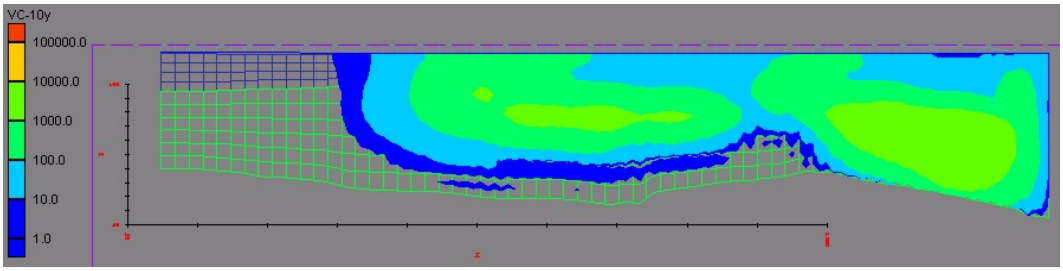

Figure 1.75. VC profile at A-A' (Fig. 1.71) 10 years after deep core treatment [I=73]

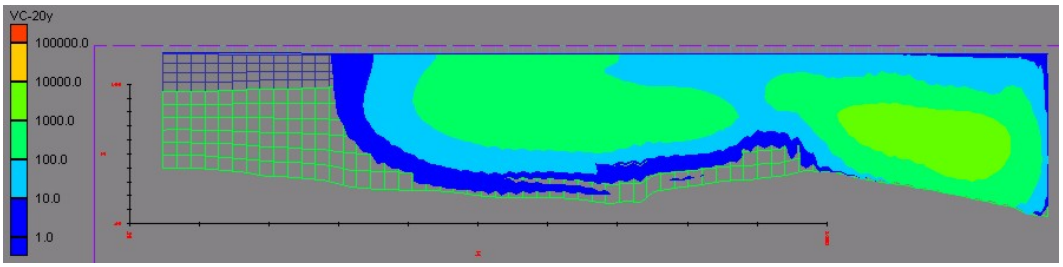

Figure 1.76. VC profile at A-A' (Fig. 1.71) 20 years after deep core treatment [I=73]

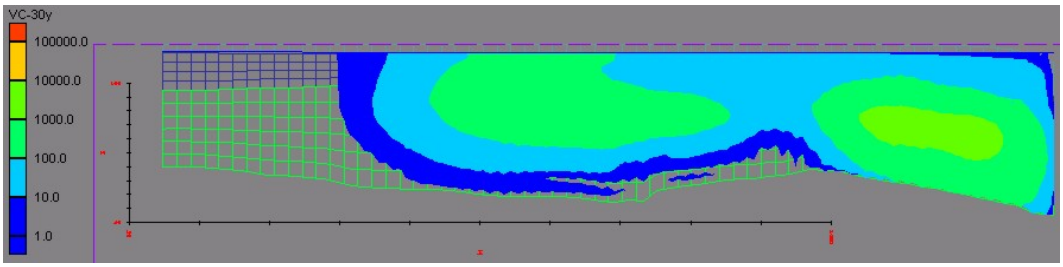

Figure 1.77. VC profile at A-A' (Fig. 1.71) 30 years after deep core treatment [I=73]

Intermediate Treatment of Entire Plume (4 grid layers)

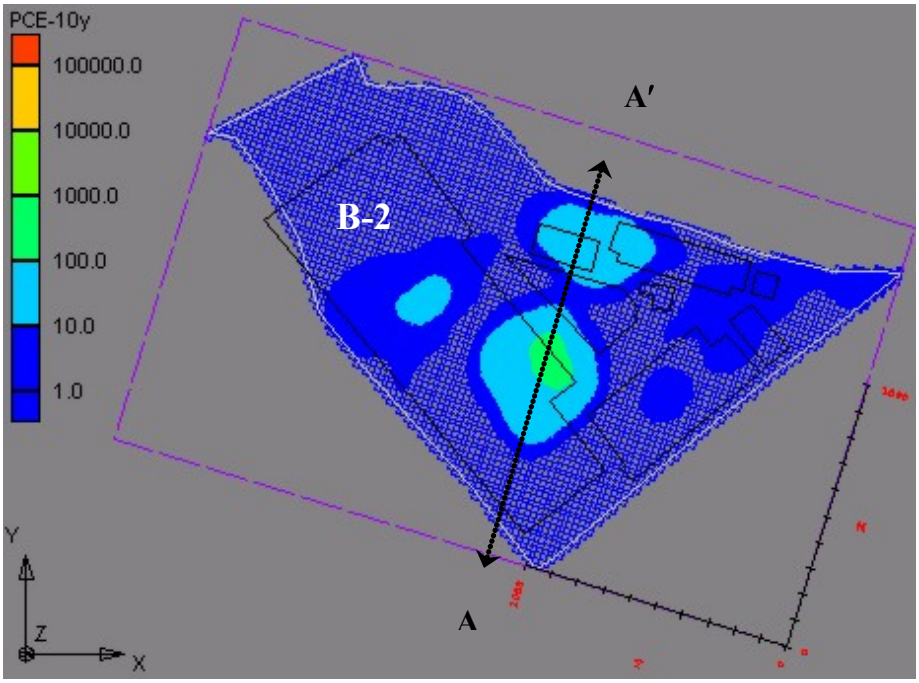

Figure 1.78. PCE concentrations (ppb) immediately below the hypothetical, complete treatment zone (~30 ft bgs; upper 4 grid layers).

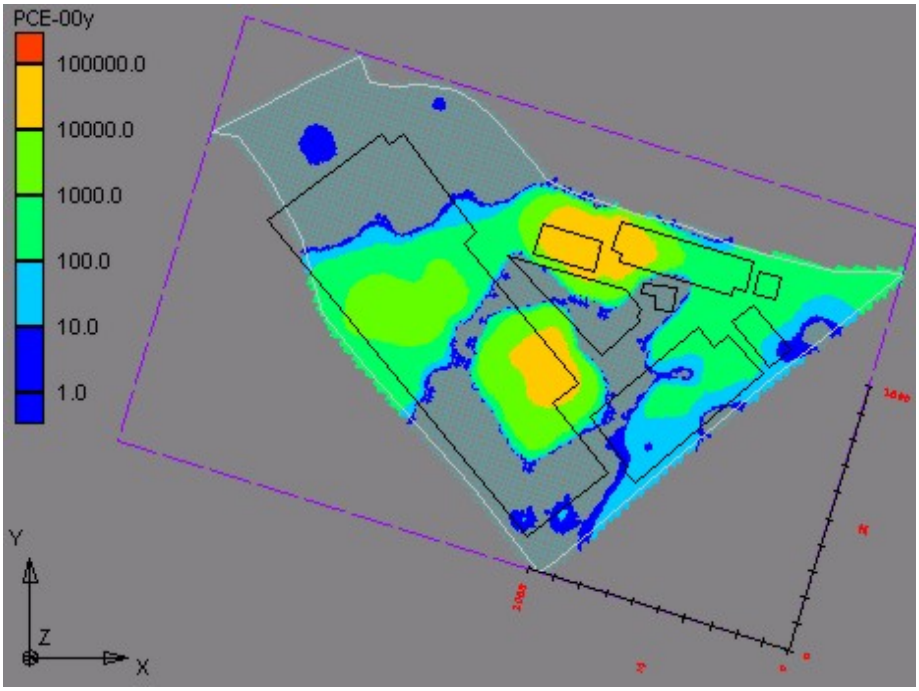

Figure 1.79. PCE concentrations (ppb) at water table (grid layer 1) only 10 years after the complete treatment to the intermediate depth. [Note: as previous.]

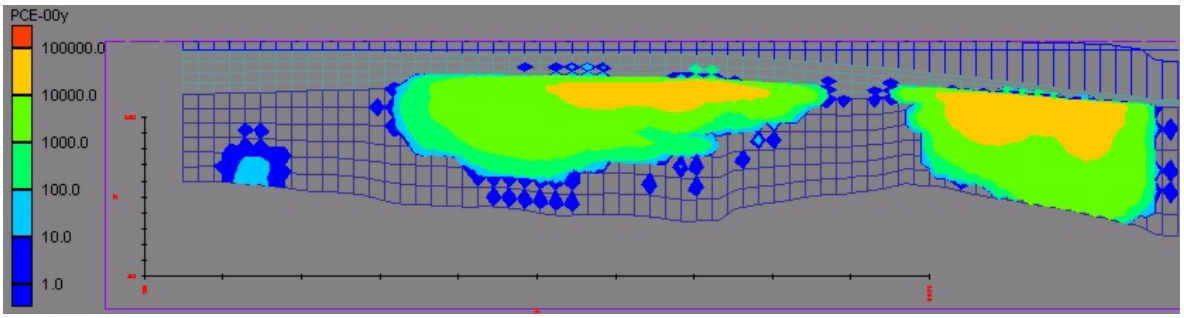

Figure 1.80. PCE concentrations (ppb) profile along section A-A' (Figure 1.78) after the hypothetical, complete treatment to intermediate depth (upper ~30 feet; 4 grid layers). [I=73]

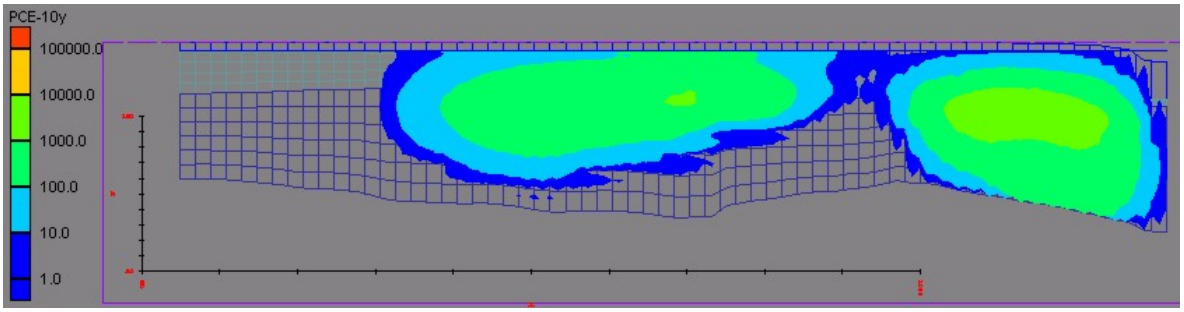

Figure 1.81. PCE concentration (ppb) profile at A-A' 10 years after intermediate depth treatment. [I=73]

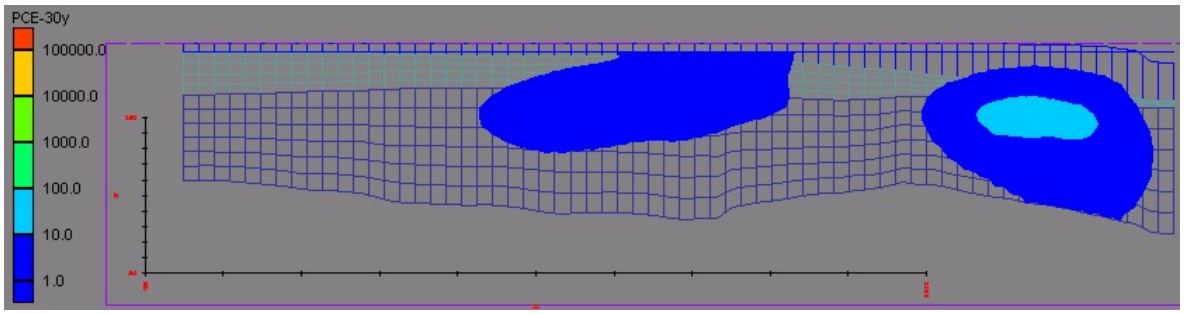

Figure 1.82. PCE concentration (ppb) profile at section A-A' 30 years after intermediate depth treatment. [I=73]

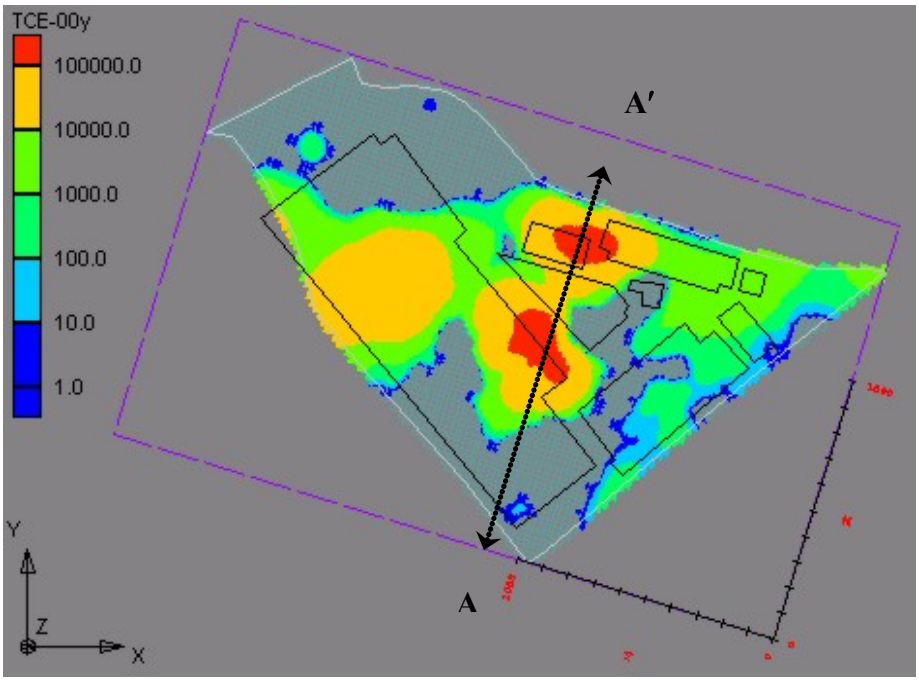

Figure 1.83. TCE concentrations (ppb) immediately below the hypothetical, complete, intermediate-depth, treatment zone (to approximately 30 ft bgs; upper 4 grid layers).

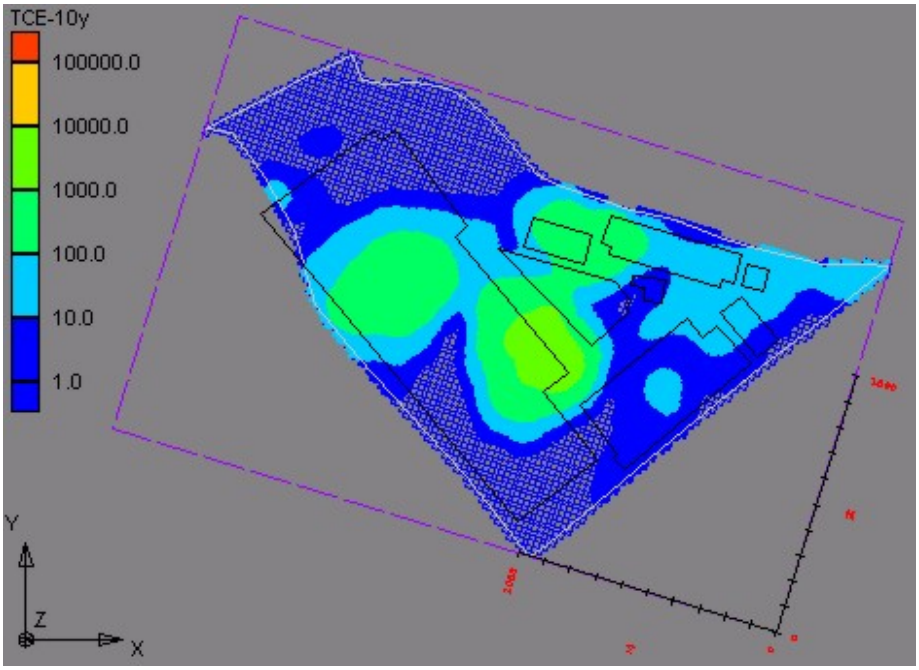

Figure 1.84. TCE concentrations (ppb) at water table (grid layer 1) only 10 years after the intermediate depth treatment.

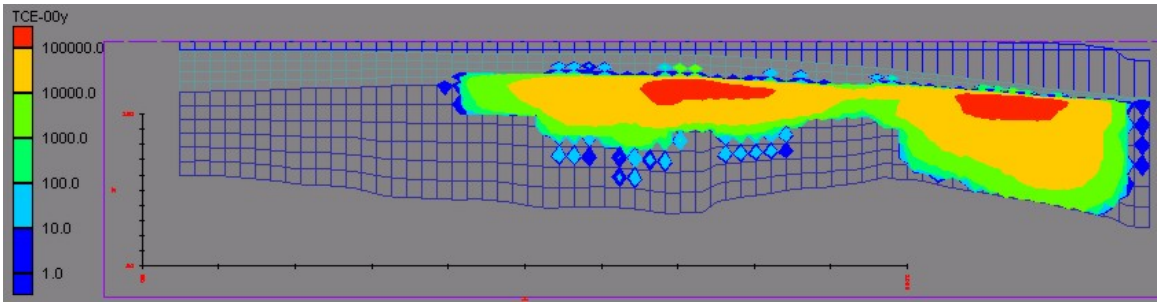

Figure 1.85. TCE concentration (ppb) profile along section A-A' (Figure 1.83) after the hypothetical, complete treatment to the intermediate depth (~30 feet; upper 4 grid layers). [I=73]

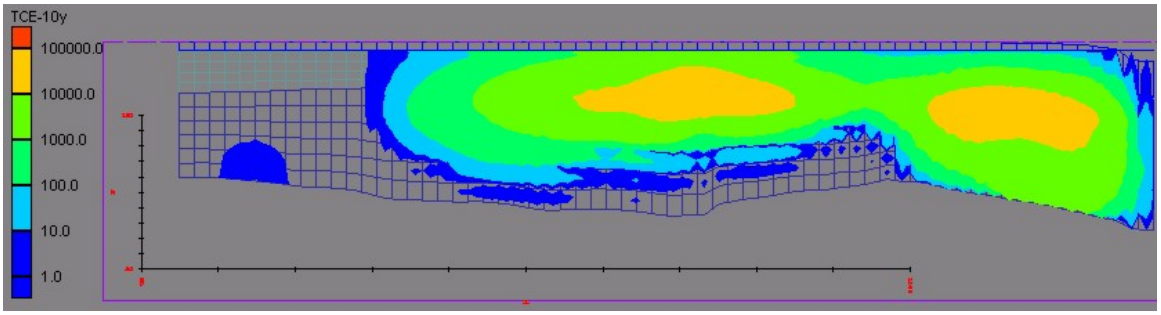

Figure 1.86. TCE concentration (ppb) profile at section A-A' 10 years after complete, intermediate-depth treatment. [I=73]

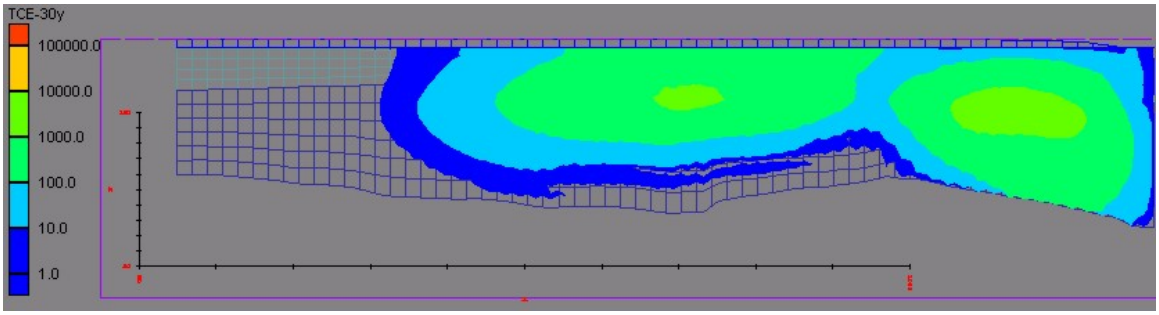

Figure 1.87. TCE concentration (ppb) profile at section A-A' 30 years after complete intermediate-depth treatment. [I=73]

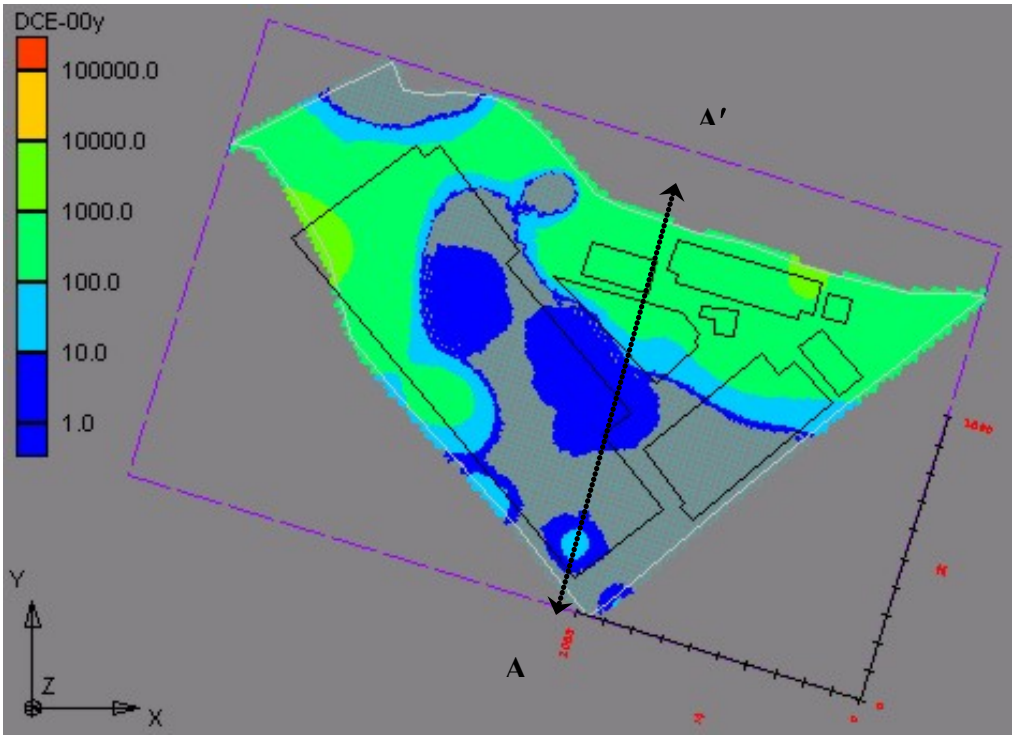

Figure 1.88. DCE concentrations (ppb) immediately below the hypothetical, complete treatment zone to intermediate depth (approx. 30 ft bgs; upper 4 grid layers).

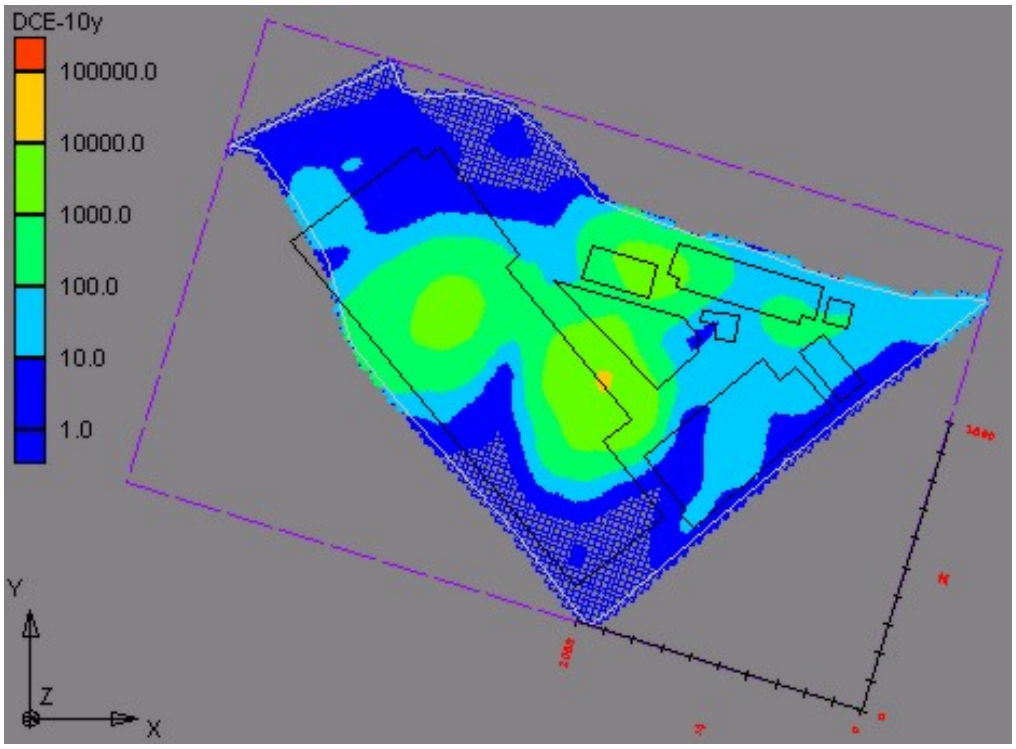

Figure 1.89. DCE concentrations (ppb) at water table 10 years after the hypothetical, complete treatment to the intermediate depth.

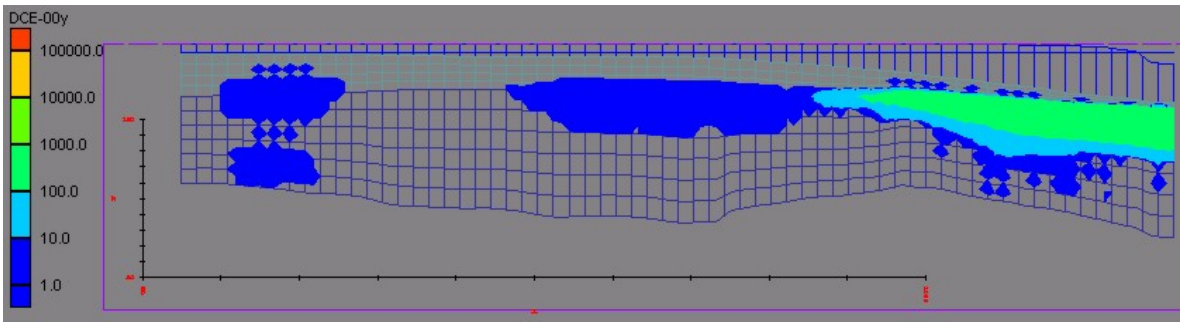

Figure 1.90. DCE concentration (ppb) profile along section A-A' (Figure 1.88) after complete treatment to intermediate depth (~30 feet bgs; upper 4 grid layers). [I=73]

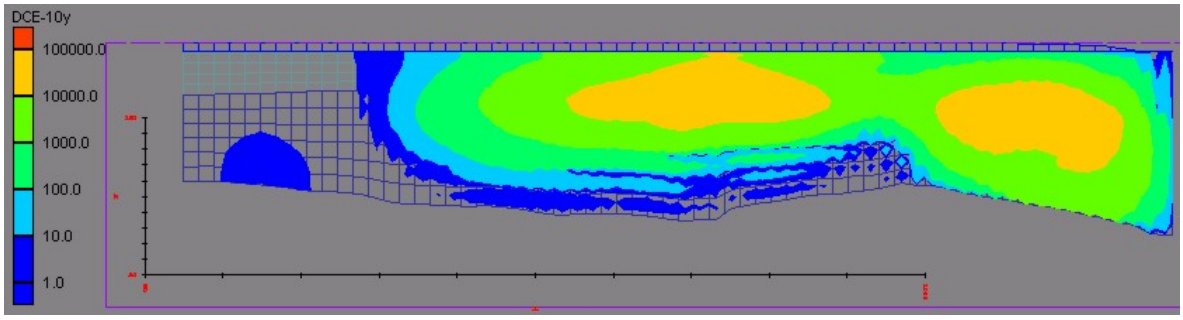

Figure 1.91. DCE concentration (ppb) profile at section A-A' 10 years after the complete, intermediate-depth treatment. [I=73]

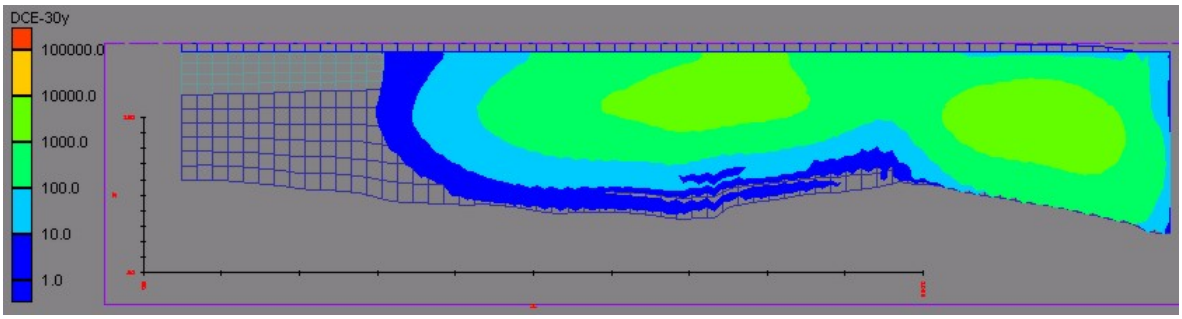

Figure 1.92. DCE concentration (ppb) profile at section A-A' 30 years after the complete treatment to the intermediate depths. [I=73]

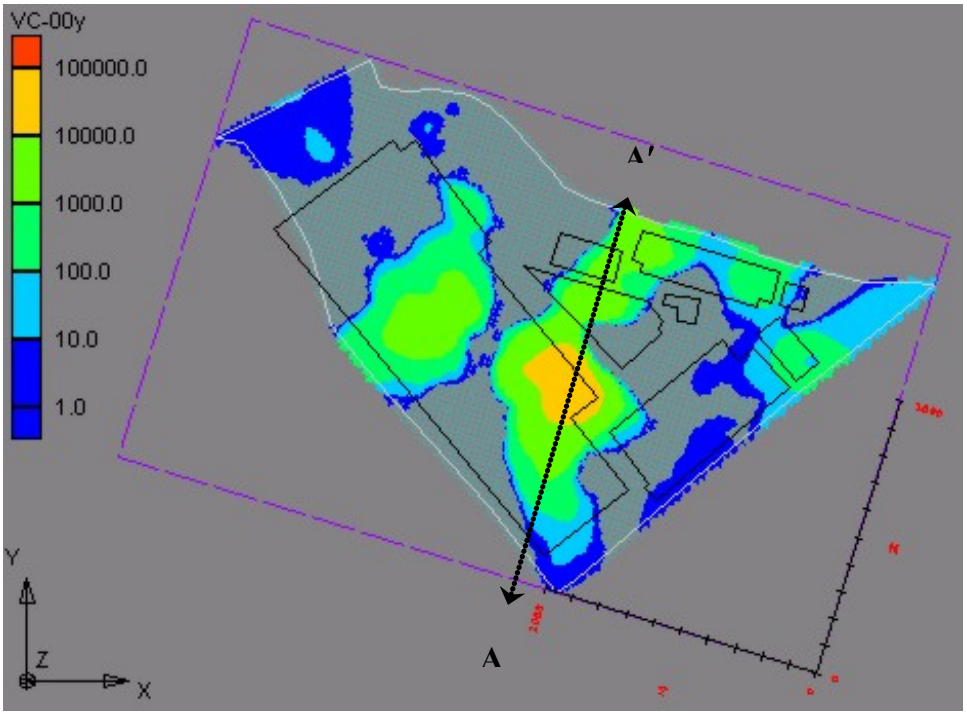

Figure 1.93. VC concentrations (ppb) immediately below the hypothetical, complete, treatment zone to the intermediate-depth (~30 ft bgs; upper 4 grid layers).

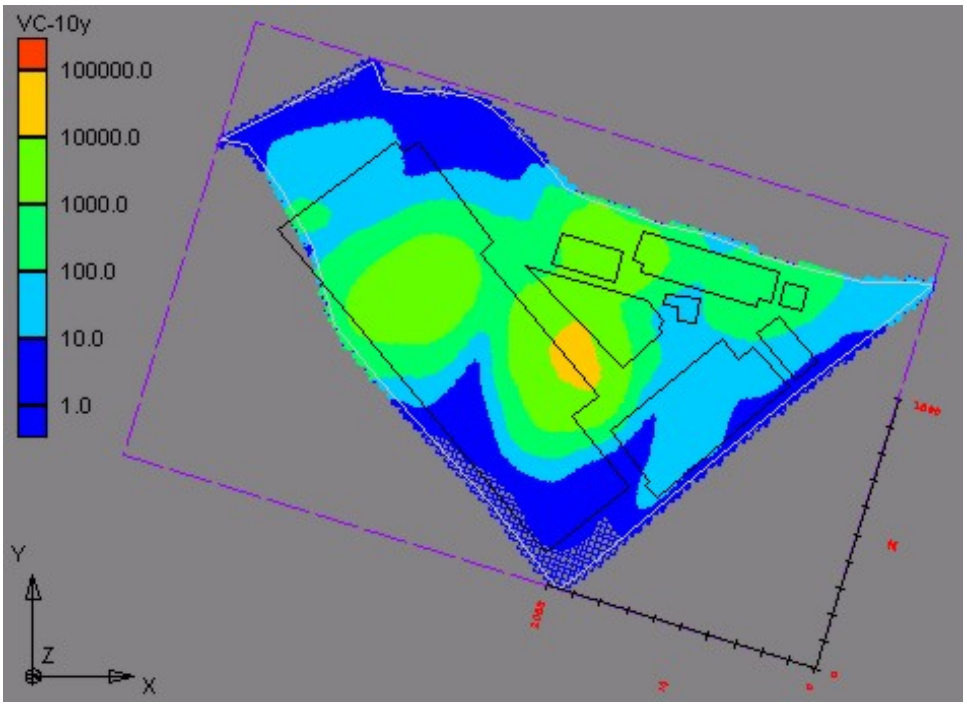

Figure 1.94. VC concentrations (ppb) at water table 10 years after the complete, intermediate depth treatment.

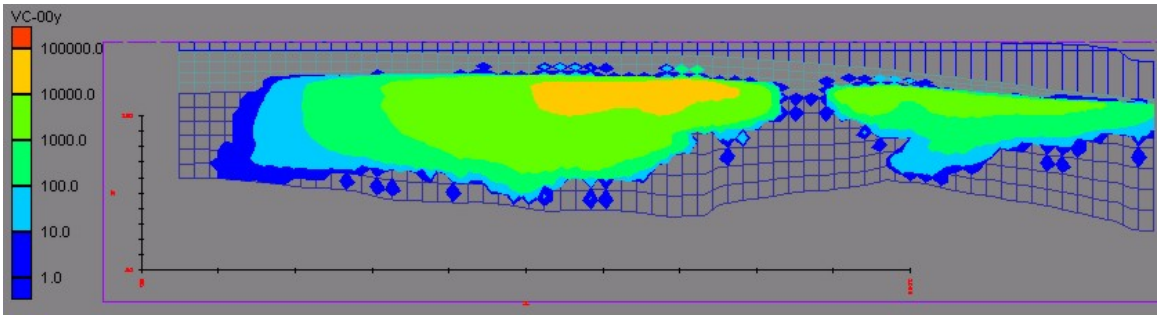

Figure 1.95. VC concentration (ppb) profile along section A-A' (Figure 1.93) after complete treatment to the intermediate depths (upper 4 grid layers). [I=66].

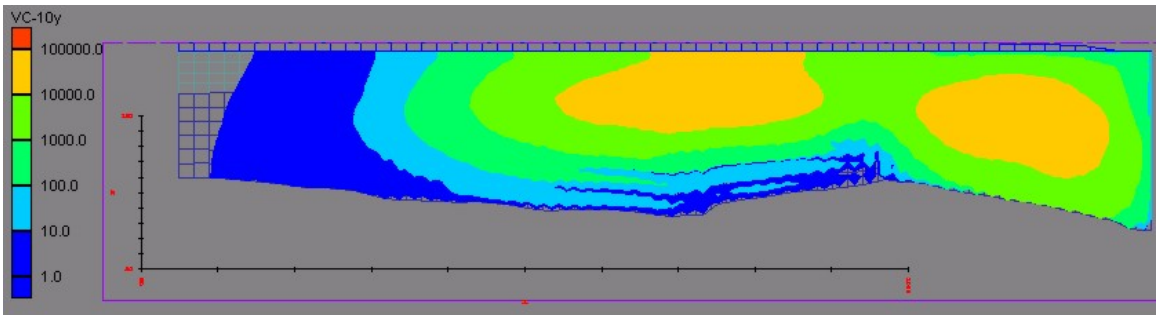

Figure 1.96. VC concentration (ppb) profile at section A-A' 10 years after complete, intermediate-depth treatment. [I=66]

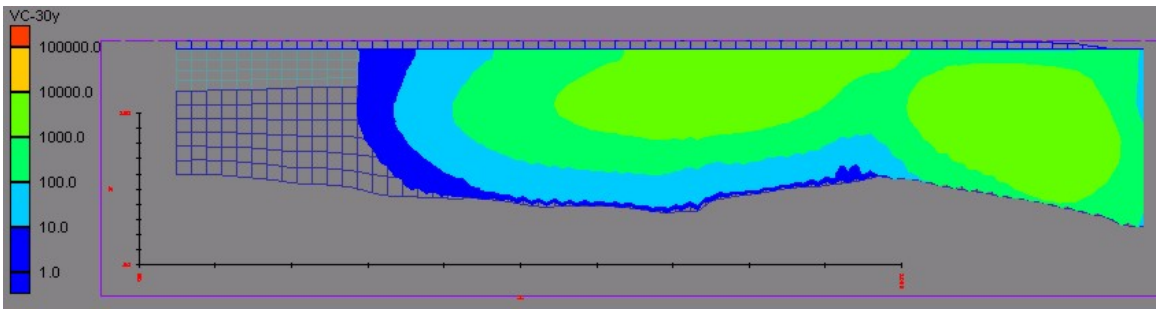

Figure 1.97. VC concentration (ppb) profile at section A-A' 30 years after complete, intermediate-depth treatment. [I=66]

Deep Treatment of Entire Plume (7 grid layers)

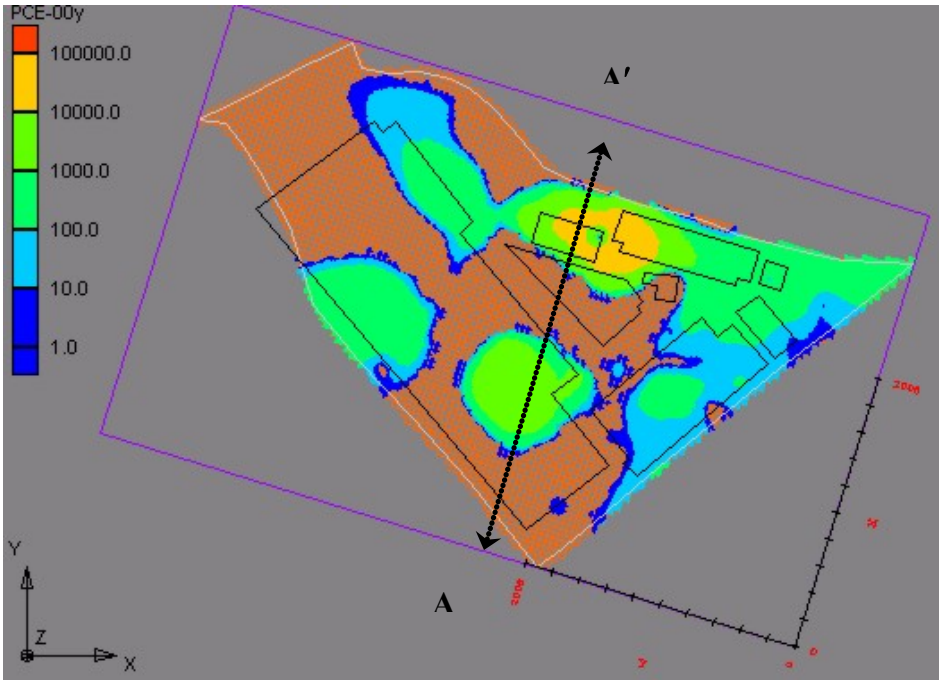

Figure 1.98. PCE concentrations (ppb) immediately below the hypothetical, complete, deep treatment to approximately 50 ft bgs. PCE is initially absent in the upper 7 grid layers.

Figure 1.99. PCE concentrations (ppb) at the top of glacial sediments (grid layer 6), 30 years after the complete, deep treatment. PCE is absent above this level.

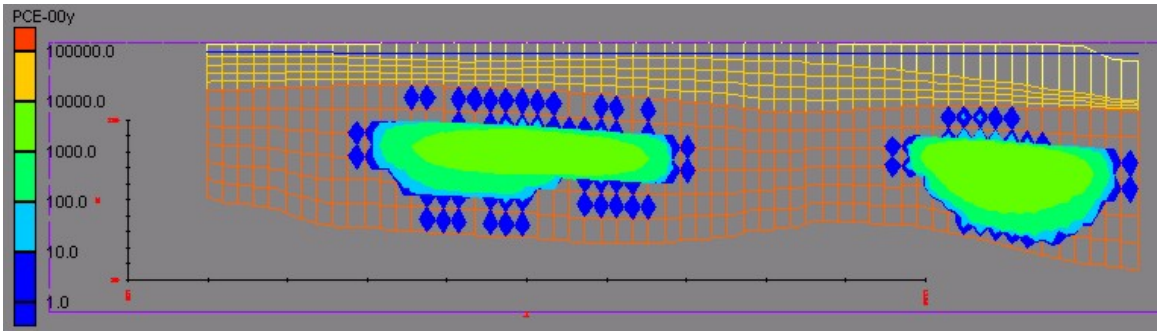

Figure 1.100. PCE concentration (ppb) profile along section A-A' (Figure 1.98) after the hypothetical, complete, deep treatment (upper 7 grid layers). [I=66]

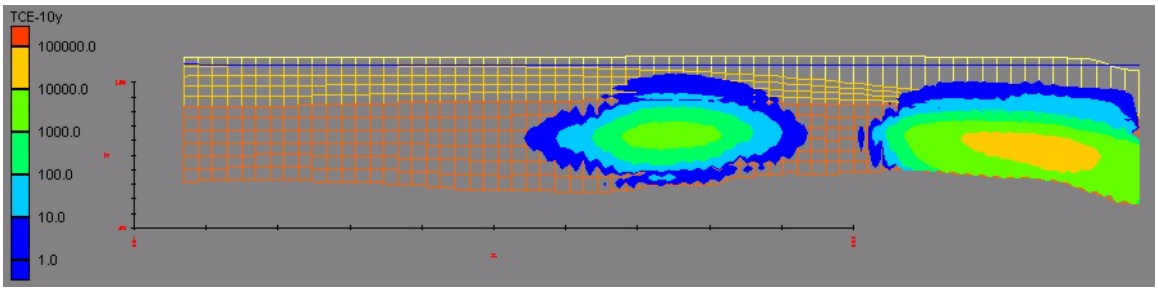

Figure 1.101. PCE concentration (ppb) profile at a section ~230 feet east of A-A' [I=79]; depicts the highest PCE concentrations observed 10 years after treatment.

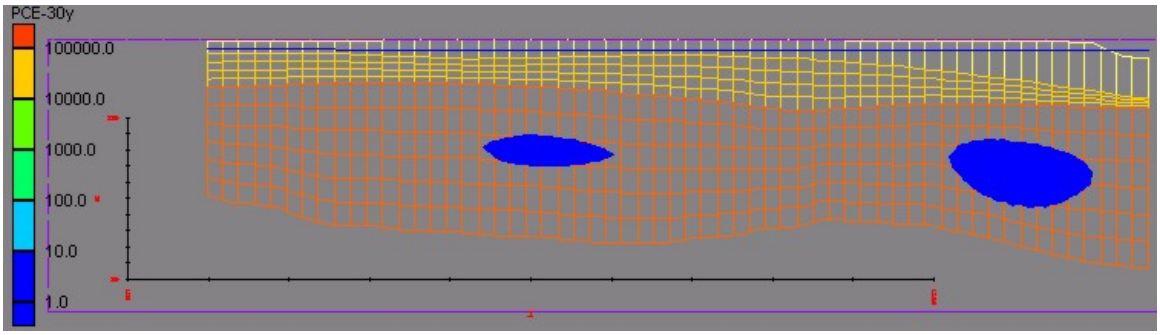

Figure 1.102. PCE concentration (ppb) profile at section A-A' 30 years after the complete, deep treatment. [I=66]

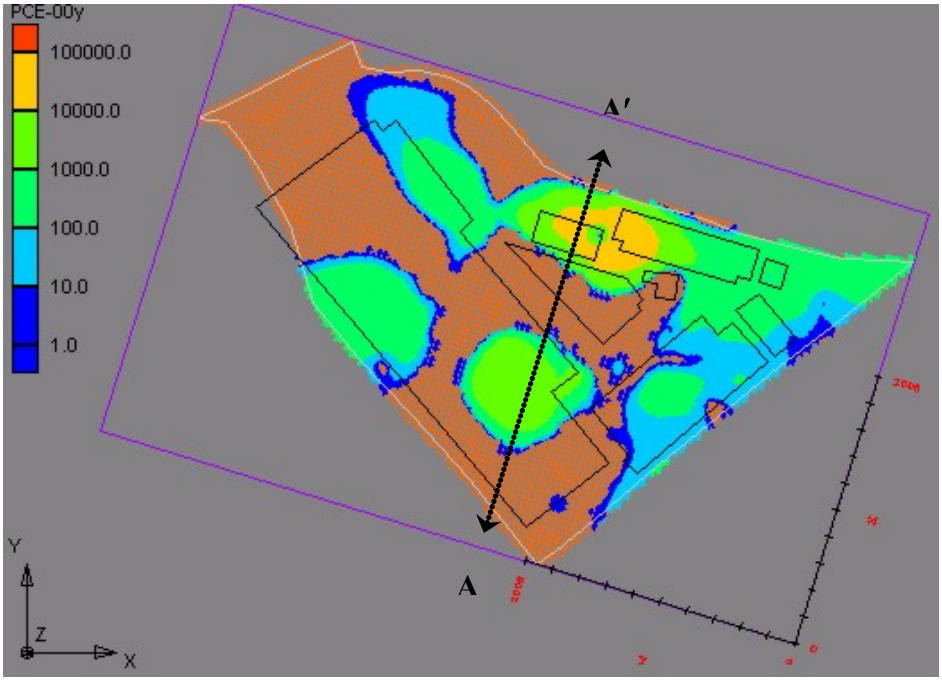

Figure 1.103. TCE concentrations (ppb) immediately below the hypothetical, complete, deep treatment zone to~50 ft bgs. TCE is initially absent in the upper 7 grid layers.

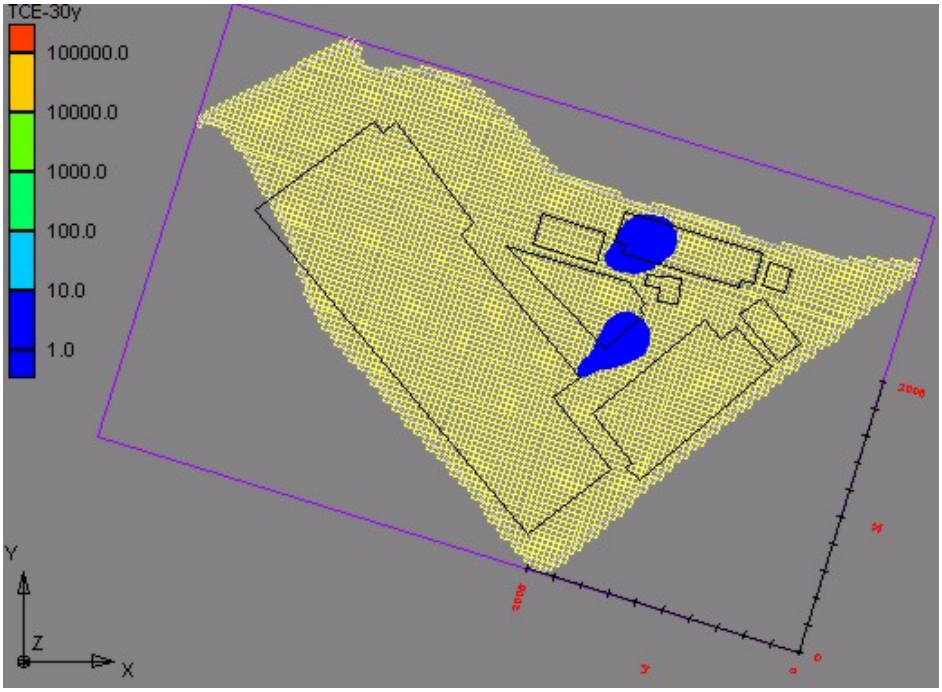

Figure 1,104. TCE concentrations (ppb) at the top of glacial sediments (grid layer 6), 30 years after the complete, deep treatment. TCE is absent above this level.

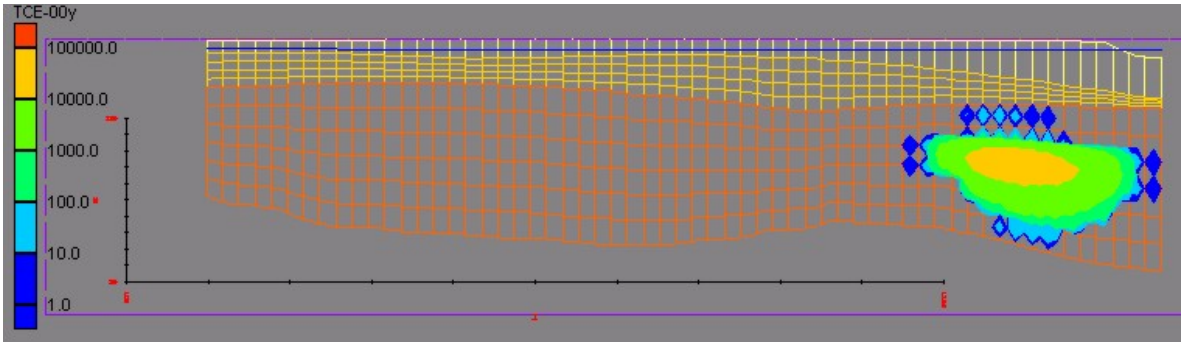

Figure 1.105. TCE concentration (ppb) profile along section A-A' (Figure 1.103) after the hypothetical, complete, deep treatment through the upper 7 grid layers. [I=66.]

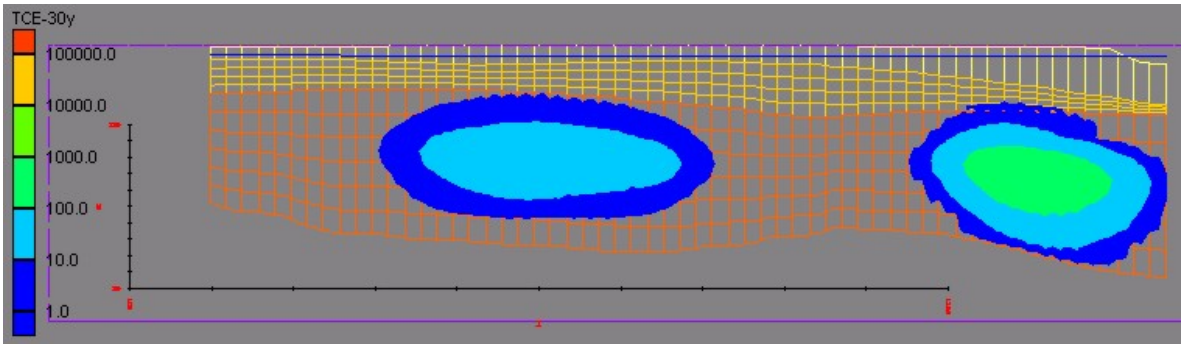

Figure 1.106. TCE concentration (ppb) profile at section A-A' [I=66] 30 years after the complete, deep treatment.

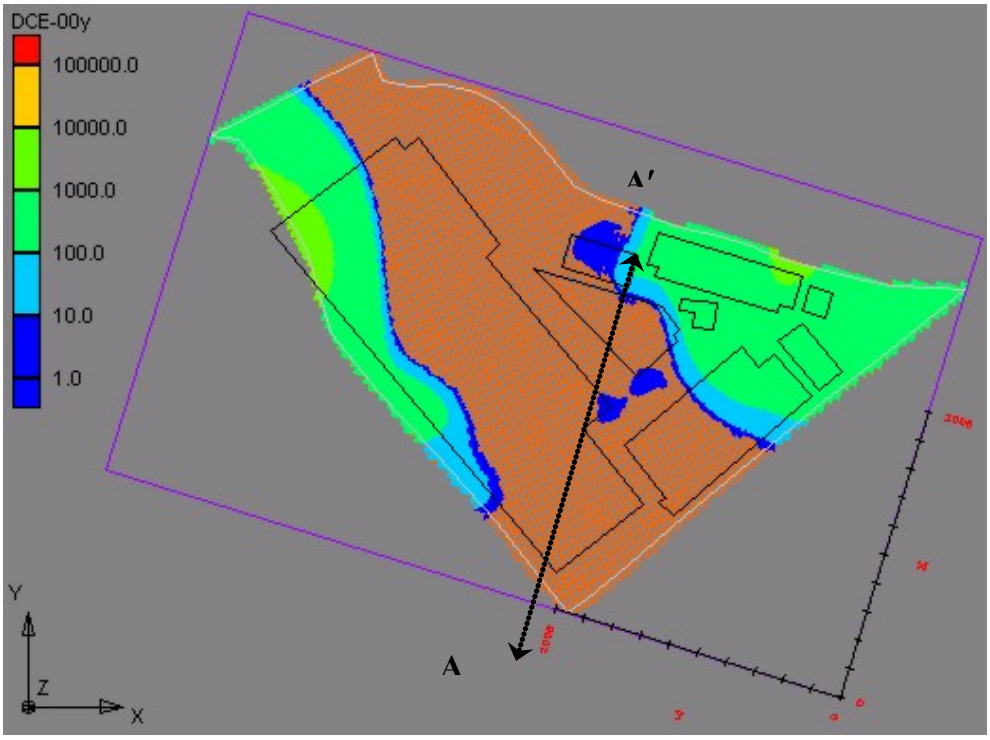

Figure 1.107. DCE at grid layer 8 after complete and deep treatment. DCE concentrations are redefined as less than 1 ppb in overlying grid levels.

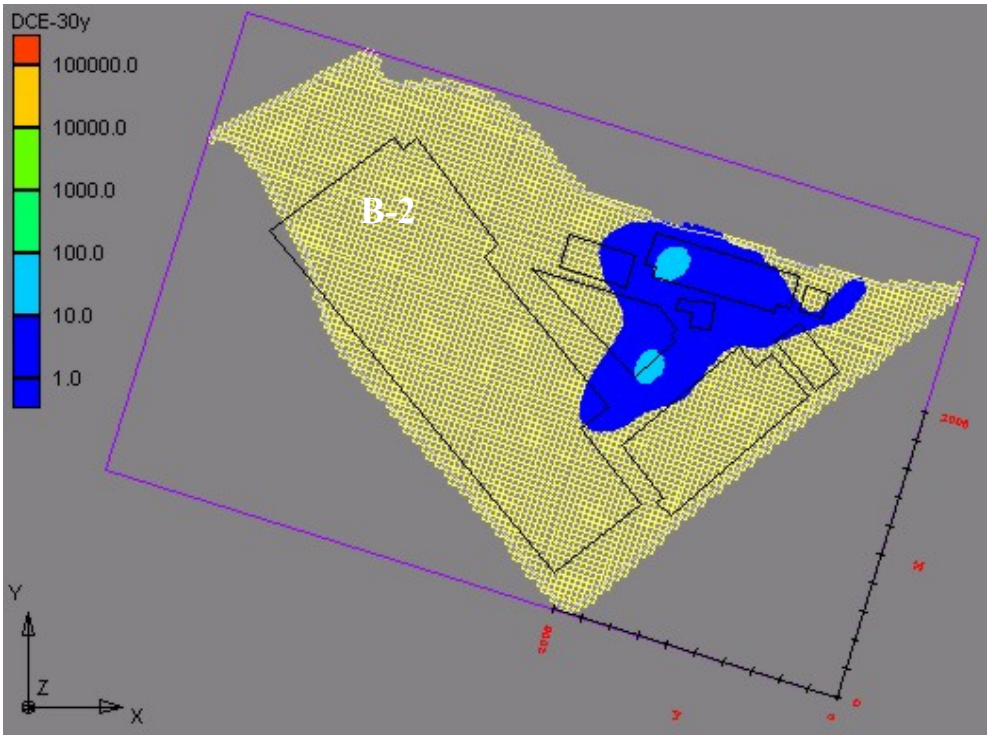

Figure 1.108. DCE concentrations (ppb) predicted at the water table 30 years after the complete, deep treatment. The same view is virtually identical at 10 years, though with a slightly greater lateral extent of the sub-10 ppb area.

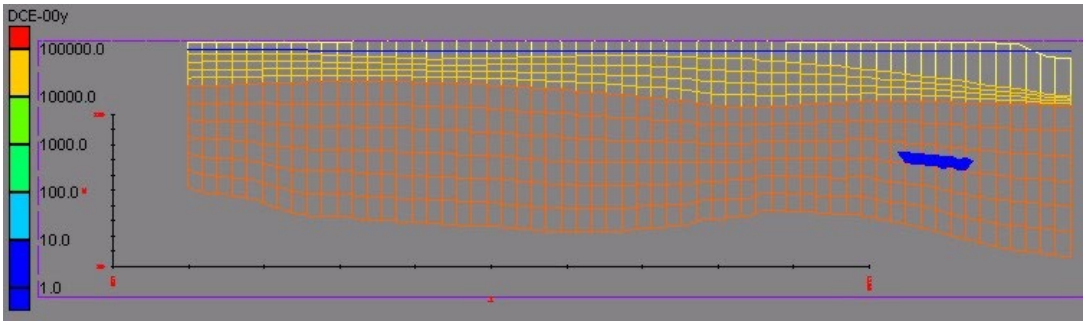

Figure 1.109. DCE concentration profile along section A-A' (Figure 1.107) after the complete, deep treatment of the upper 7 grid layers. [I=66]

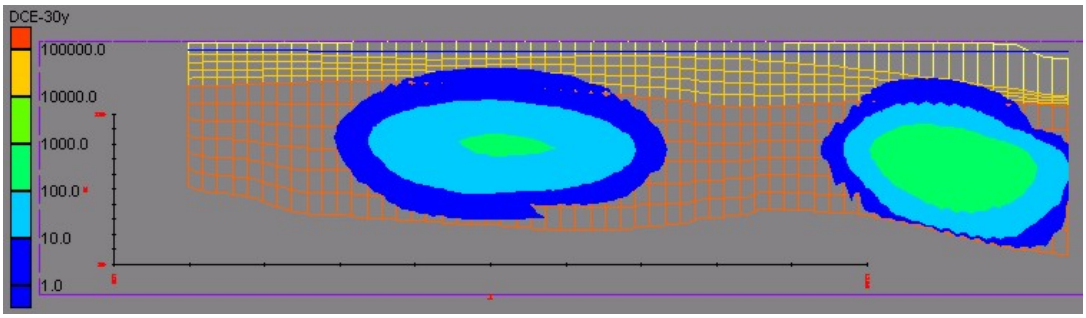

Figure 1.110. DCE concentration profile at section A-A' 30 years after the complete, deep treatment. DCE increases significantly due to production by TCE transformation, but then declines. . [I=66]

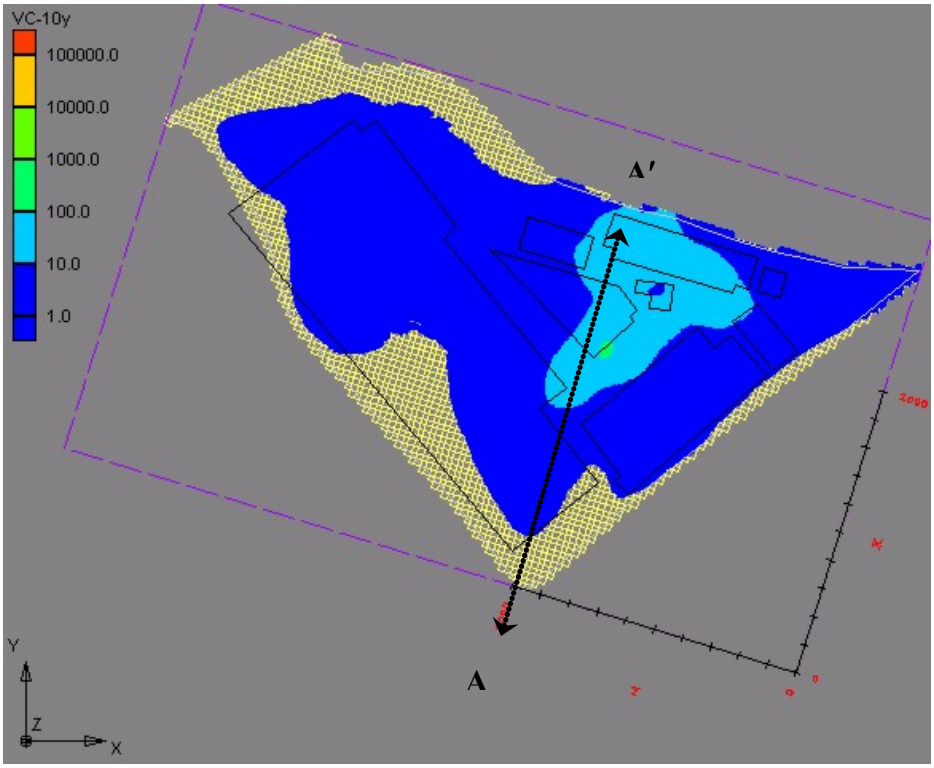

Figure 1.111. VC concentrations (ppb) at the water table, 10 years after the hypothetical, complete treatment of the upper 7 grid layers. Low levels of VC are predicted to rebound at the water table within 10 years (though little under B-2).

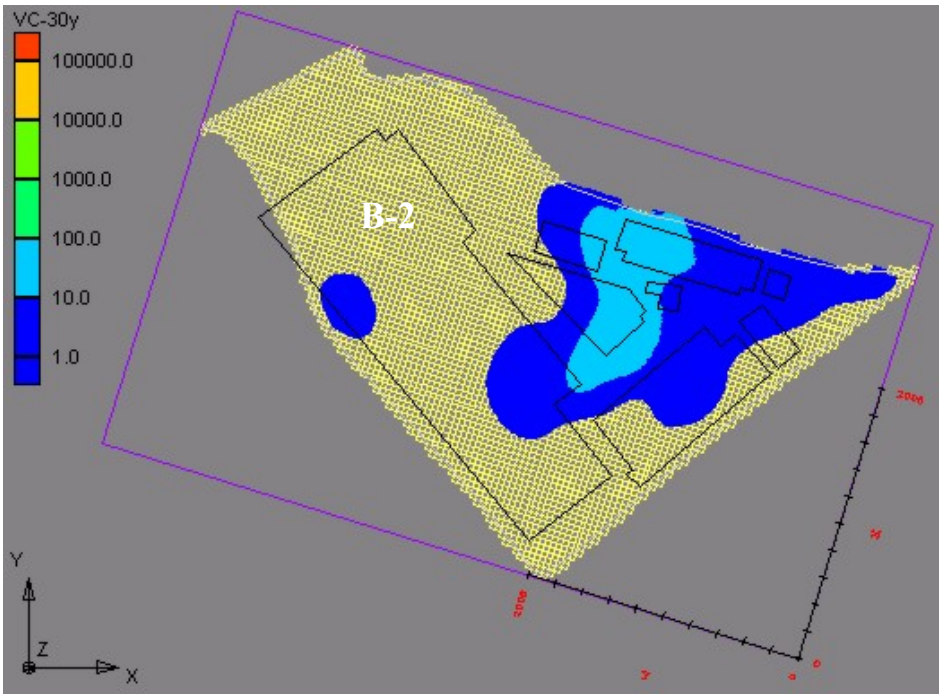

Figure 1.112. VC concentrations (ppb) at the water table, 30 years after the complete, deep treatment.

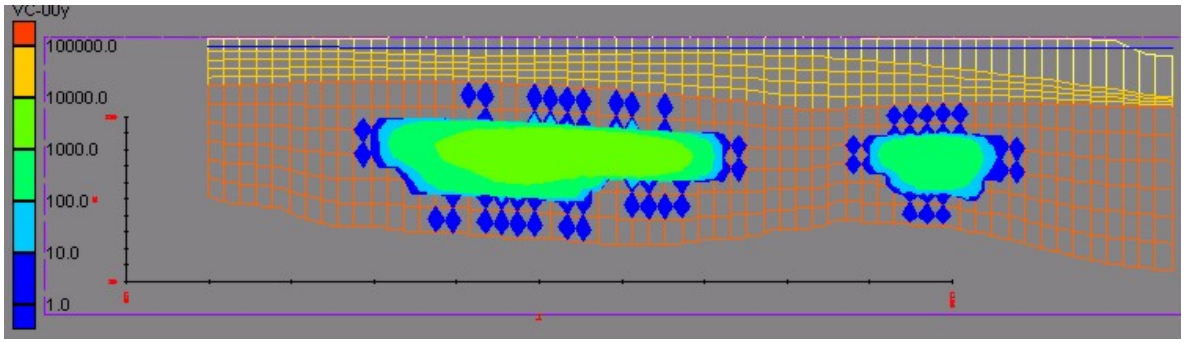

Figure 1.113. VC concentration (ppb) profile along section A-A' (Figure 1.111) immediately after complete treatment of the upper 7 grid layers. [I=66]

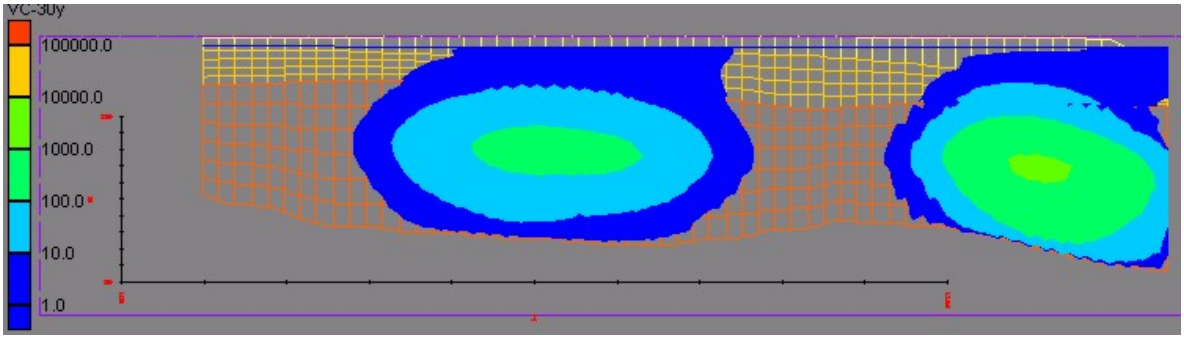

Figure 1.114. VC concentration (ppb) profile at section A-A' [I=66] 30 years after complete treatment of the upper 7 grid layers..

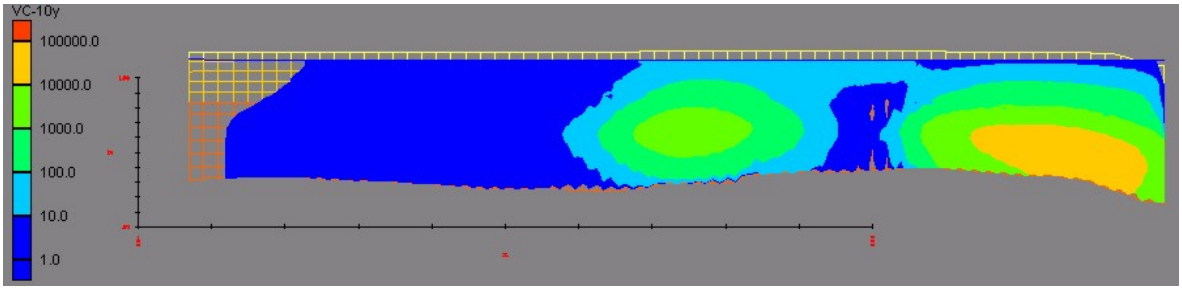

Figure 1.115. VC concentration (ppb) profile 10 years after the deep treatment, and approximately approximately 120 feet east of section A-A' [I=79]

Comparison of Intermediate and Deep Treatments after 10 years (A-A')

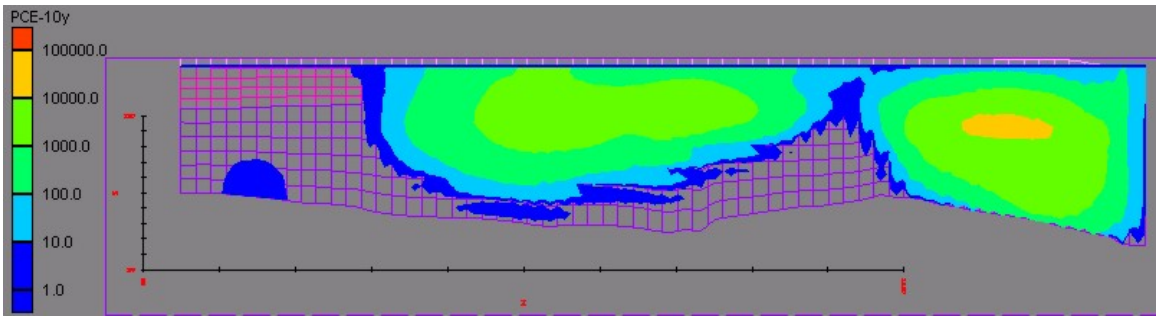

Figure 1.116. PCE concentration profile (ppb) 10 years after intermediate-depth treatment of plume core.

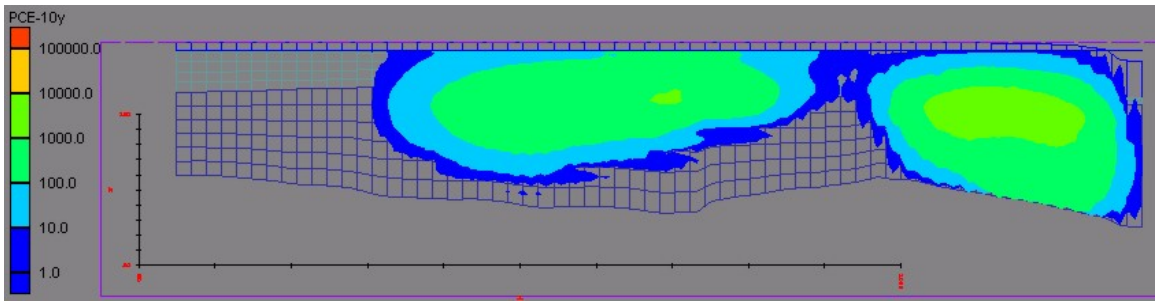

Figure 1.117. PCE concentration profile (ppb) 10 years after complete, intermediate-depth treatment A-A' [I=73] (Figure 1.111). Clearly, concentrations at the water table are lower than Fig. 1.109.

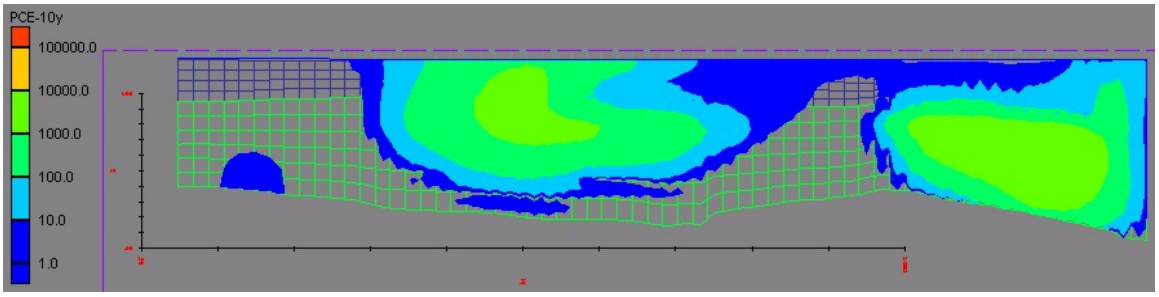

Figure 1.118. PCE profile 10 years after deep treatment of plume cores. [I=73]

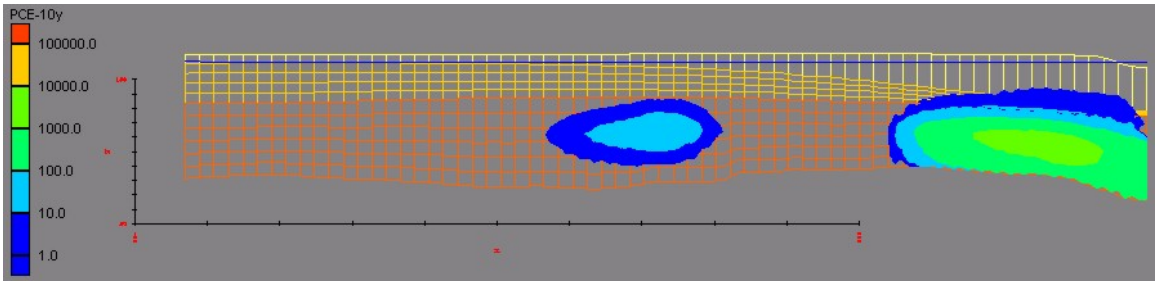

Figure 1.119. PCE concentration profile (ppb) 10 years after complete, deep treatment along profile near A-A' [I=79] showing the highest concentrations present. Clearly, deep and complete treatment is preferable to avoid contaminant rebound.

Task-2. ASSESS NATURAL ATTENUATION OF SOLVENTS

2.1 PROBLEM SUMMARY

Extensive contamination of groundwater by chlorinated solvents has been detected at the Stratford Army Engine Plant (SAEP). The contaminants include PCE, TCE, TCA, and their degradation products. Full or partial cleanup of three major hot spots (Figure 1.2) or land use alteration (perhaps with capping) would leave in place some level of residual solvents. Monitored natural attenuation (MNA) is under consideration as an alternative or supplement to engineered remediation.

The chlorinated aliphatic/aromatic hydrocarbons (**CAH**s) detected in SAEP groundwater appear to have resulted from the uncontrolled release of industrial solvents to the subsurface as dense non-aqueous phase liquids (**DNAPL**s). Being more dense than and immiscible with water (see **Table 2.1**), DNAPLs can percolate along highly irregular pathways deep into the subsurface, as long as there is sufficient mass to displace water from pore spaces. The low solubility of DNAPL components assures that it may act as a long-lived source of groundwater contamination. The presence of DNAPL at SAEP, though not confirmed by direct recovery, is indicated by observed high concentrations of chlorinated solvents (TCE, PCE, TCA). The presence of a DNAPL could have a significant influence on the design and duration of MNA.

2.2 APPROACH

The primary questions addressed here are whether MNA alone is a viable option for the cleanup of solvents detected at SAEP. Task 2 includes two independent sub-tasks: (a) PCE/TCE predictions, and (b) TCA predictions.

Uncertainty remains as to whether a DNAPL containing PCE, TCE, and/or TCA is present at SAEP. Simulating the presence of a DNAPL could have a strong influence on model predictions of the duration and efficacy of MNA. In the absence of unequivocal evidence supporting or dismissing the presence of a DNAPL, two end-member scenarios are considered: (1) no DNAPL, *i.e.*, that the initial solute concentrations define the only contaminant source, and (2) with a DNAPL of limited spatial extent to act as a persistent, internal source.

As discussed in section 0.6, FEMWATER simulations suggest that only minor changes in the distribution of head or flow velocities would result from the hypothetical removal of SAEP buildings. Therefore, consideration of the effect of altered recharge on solvent MNA was deemed unnecessary.

The numerical grid used here for MODFLOW and RT3D (**Figures 2.1** and **2.2**) is derived from the calibrated FEMWATER flow model developed in a previous study. Additional calibration of the MODFLOW model was conducted.

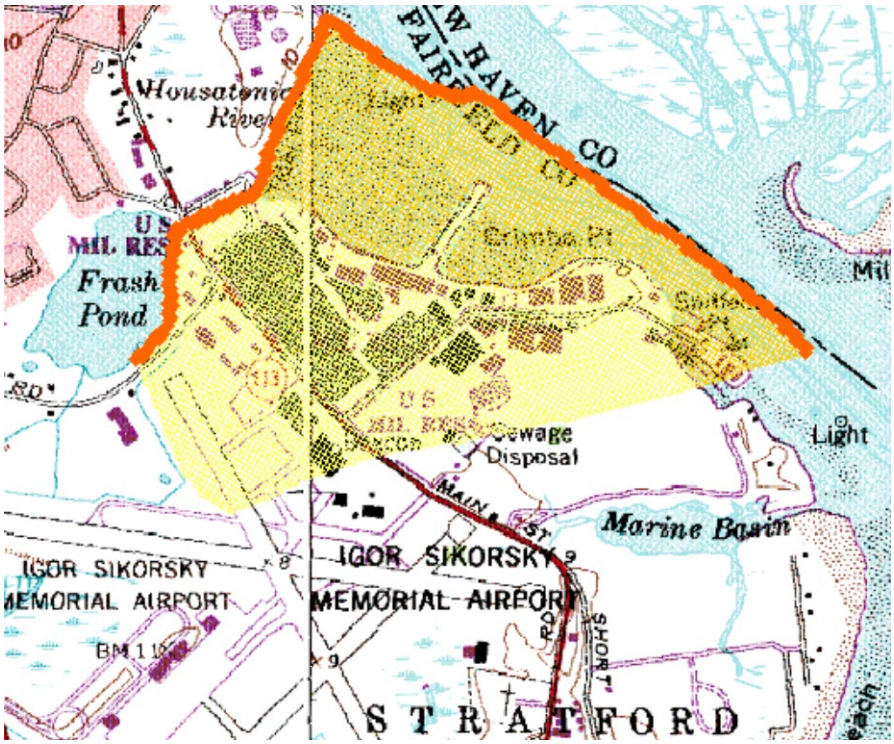

Figure 2.1. Numerical domain (yellow) used in Task-2 and -3 simulations. The thick red line indicates constant head MODFLOW boundaries.

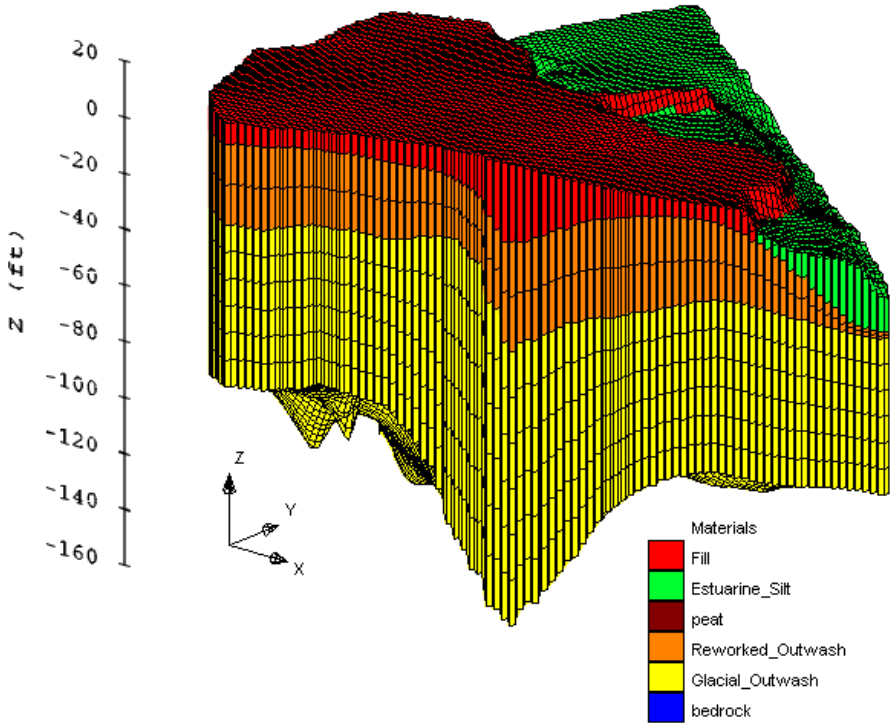

Figure 2.2. Three-dimensional representation of the MODFLOW-RT3D-MT3D grid used in Tasks 2 and 3.

Table 2.1. Summary of liquid densities and aqueous solubilities of key solvents.			
Chlorinated Solvents	Liquid Density (g/cm^3; 20 C)	Aqueous Solubility (ppb; 20 C)	Maximum 1999 Concentration (ppb or µg/L) and % of Solubility
Tetrachloroethene (PCE)	1.63	200,000	100,000 ≈ 50 %
Trichloroethene (TCE)	1.46	1,100,000	830,000 ≈ 75 %
Dichloroethene (DCE)	1.20	2,500,000	9,458 ≈ 0.38%
Vinyl Chloride (VC)	0.9106	2,700,000	100,000 ≈ 3.7 %
1,1,2,2-Tetrachloroethane (PCA)	1.60	2,952,000	—
1,1,1-Trichloroethane (TCA)	1.35	4,400,000	280,000 ≈ 6.4%
1,1,2-Trichloroethane	1.44	4,626,000	—
1,1-Dichloroethane (DCA)	1.175	5,075.000	15,000 ≈ 0.30%
1,2-Dichloroethane	1.256	8,700,000	—
Chloroethane (CA)	0.9214	5,740,000	3,800 ≈ 0.07%

RT3D-GMS

RT3D – Reactive Transport in 3-Dimensions (version 2; Clement and Jones 1998) – was applied to all PCE/TCE and TCA simulations. RT3D describes advective-dispersive transport and sorption, and includes several options for pre-set or user-developed reaction packages. Flow velocities are calculated based on local head gradients provided by a flow model, MODFLOW in this case. Flow velocities are used to calculate advective-dispersive transport. Modifications of the "sequential anaerobic degradation" package were utilized here. The graphical interface to RT3D incorporated into the DoD Groundwater Modeling System (GMS) version 3.1 was utilized in the definition of initial conditions, setting model parameters, and visualizing results.

RT3D solves the coupled partial differential equations describing the three-dimensional, reactive transport of multiple species in saturated groundwater systems. The code utilizes a reaction operator-split (OS) numerical strategy to solve any number of coupled transport equations.

Transport Processes

Natural attenuation may be defined as the reduction of contaminant toxicity, mobility, or volume to levels that are protective of human health and the ecosystem (US EPA 1999). The processes that may contribute to natural attenuation include advection, dispersion, dilution, sorption, volatilization, abiotic (chemical) transformation, and biodegradation. Among these coupled processes, the biogeochemical reactions that affect any irreversible transformation or immobilization of contaminants to innocuous products are of greatest interest.

Hydrodynamic Dispersion. Variations in flow velocity in all intrinsically heterogeneous porous media act to disperse solutes along the transport path. This dispersive process is typically most evident along the primary flow direction (longitudinal dispersivity), but lateral dispersion also occurs. For the RT3D-MT3D simulations presented here, longitudinal dispersivity was set between 10 to 30 feet. Transverse dispersivity was taken to be 10 to 30 percent of the longitudinal dispersivity and vertical dispersivity was defined as 10 to 20 percent of the longitudinal dispersivity.

Adsorption. The retardation of organic solute transport resulting from adsorption may be an important consideration in simulating the effects of natural attenuation. Partitioning of a solute to the aquifer matrix removes it from solution and, depending on the reaction mechanism, sequesters it from biotransformation. The pseudo first-order kinetic model used here for degradation applies only to the dissolved concentration, upon which the rate is dependent.

SAEP site-specific characterization of CAH partitioning is unavailable. However, some limited organic carbon content data were available. As a reasonable approximation, a hydrophobic partitioning model, conditioned on site measurements of organic carbon content, is adopted to estimate partitioning coefficients (K_d's). Karickhoff *et al.* (1979) defined a linear relation between the organic carbon partitioning coefficient (K_{oc}; L/kg) and the more readily available octanol/water partitioning coefficient ($K_{o/w}$) for aromatic and chlorinated hydrocarbons (equation 2.1a). They further suggested that the K_d could be estimated as the product of the K_{oc} and the mass fraction of organic carbon (f_{oc}) in the sediment (equation 2.1b):

$$K_{oc} = 0.63\, K_{o/w} \quad \text{(a)} \qquad (2.1)$$

$$K_d = f_{oc}\, K_{oc} \quad \text{(b)} .$$

The K_d model describes a linear isotherm, with the implicit assumptions of equilibrium and reversibility. The K_{oc}, and K_d values for SAEP solvents are summarized in Table 2.2 (source: RI Report). Media bulk density, which factors into the treatment of adsorption, is taken to be 1.45 g/cm^3 in all SAEP media (Durgin, NAE, personal communication 2001).

Table 2.2. Adsorption parameters of selected CAH

Compound	K_{oc} (L/kg)	f_{oc}	K_d (L/kg)
PCE	303.	0.005 for all SAEP media	1.515
TCE	152.		0.76
1,1-DCE	217.		1.085
VC	2.5		0.013
TCA	70.7		0.353
DCA	18.6		0.093
CA	17.0		0.085

Reductive Dechlorination Reactions. The conceptual model for the reactive transport processes active at SAEP was developed conditioned on the available monitoring data.

All of the components modeled are observed at SAEP and the general dechlorination pathway is a commonly used one at such sites. All three isomers of DCE (1,1-, cis-1,2- and trans-1,2-) are detected, but, to avoid unnecessary complication of the model, we chose not to differentiate the isomers. Since the 1,1-DCE is the most commonly reported and with the highest concentrations, we refer to the lumped DCE product as 1,1-DCE throughout this report. The DCE concentrations reported should be interpreted implicitly as inclusive of the three isomers, predominated by 1,1-DCE. If deemed useful, the other isomers could be modeled explicitly, but it would require development and testing of a new RT3D reaction module, which was well beyond the scope of this project.

The RT3D reaction packages employed here assume a first-order kinetic model for each transformation of the CAHs of interest (Table 2.3) as well as ethene, ethane, and chloride. Application of such a lumped kinetic model does not differentiate between abiotic and microbially mediated processes. Both processes are presumed to be active at SAEP, *albeit* at low rates.

Initial reaction rate estimates were based on typical values reported in the technical literature. Most of these data were estimated for similarly aerobic groundwater. Adjustments were made subsequently to better capture general trends in the SAEP data (Table 2.3). However, proper calibration was precluded by the lack of multiple, discrete, complete "snapshots" of contaminant distribution. Only the 1999 data set, which is used to define all initial conditions in this study, was reasonably complete in terms of analytes and spatial coverage. A second, full sampling of contaminant distribution, currently in progress, should provide data with which to calibrate the reaction rates more effectively.

The PCE/TCE reaction package utilized here describes the sequential dechlorination of PCE to TCE to DCE to VC to ethene using a first-order decay model. The coupled effects of advective-dispersive transport, adsorption, and these reactions are summarized in the following set of partial differential equations:

$$
\begin{aligned}
R_P \frac{\partial [PCE]}{\partial t} &= \frac{\partial}{\partial x_i}\left(D_{ij} \frac{\partial [PCE]}{\partial x_i} \right) - \frac{\partial (v_i [PCE])}{\partial x_i} + \frac{q_s}{\phi}[PCE]_s - K_P [PCE] \\
R_T \frac{\partial [TCE]}{\partial t} &= \frac{\partial}{\partial x_i}\left(D_{ij} \frac{\partial [TCE]}{\partial x_i} \right) - \frac{\partial (v_i [TCE])}{\partial x_i} + \frac{q_s}{\phi}[TCE]_s - K_T [TCE] + Y_{TCE/PCE} K_P [PCE] \\
R_D \frac{\partial [DCE]}{\partial t} &= \frac{\partial}{\partial x_i}\left(D_{ij} \frac{\partial [DCE]}{\partial x_i} \right) - \frac{\partial (v_i [DCE])}{\partial x_i} + \frac{q_s}{\phi}[DCE]_s - K_D [DCE] + Y_{DCE/TCE} K_T [TCE] \\
R_V \frac{\partial [VC]}{\partial t} &= \frac{\partial}{\partial x_i}\left(D_{ij} \frac{\partial [VC]}{\partial x_i} \right) - \frac{\partial (v_i [VC])}{\partial x_i} + \frac{q_s}{\phi}[VC]_s - K_V [VC] + Y_{VC/DCE} K_D [DCE]
\end{aligned}
\qquad (2.2)
$$

where [PCE], [TCE], [DCE], and [VC] are the concentrations of the respective contaminants; K_P, K_T, K_D, and K_V are first-order degradation rates, R_P, R_T, R_D, R_V are retardation coefficients; and $Y_{TCE/PCE}$, $Y_{DCE/TCE}$, and $Y_{VC/DCE}$ are yield coefficients (stoichiometric ratios of product to reactant molecular mass). A similar set of equations describes the sequential dechlorination of TCA to DCA to CA to ethane. The reaction rates and yield coefficients are summarized in Table 2.3.

Table 2.3. Estimated decay rates			
Transformation Step			Rate ($year^{-1}$)	Yield Coeff.
Chlorinated Ethenes				
PCE	→	TCE	4.415	0.79
TCE	→	DCE	0.230	0.74
DCE	→	VC	1.121	0.64
VC	→	Ethene	0.391	0.46
Chlorinated Ethanes				
TCA	→	DCA	1.030	0.742
DCA	→	CA	0.916	0.652
CA	→	Ethane	1.427	0.466

The second phase of Task-2 is an assessment of the natural attenuation of trichloroethane (TCA). Research on the environmental degradation pathways and reaction rates affecting chlorinated ethanes, such as TCA, is not as extensive as that for the chlorinated ethenes (PCE, TCE, *etc.*). Sequential dechlorination, similar to that observed with ethenes, is one common reaction pathway and the one employed here.

All elevated concentrations of TCA detected in SAEP are for the 1,1,1-TCA isomer. PCA (1,1,1,2 or 1,1,2,2-tetrachloroethane) and 1,1,2-TCA are among the analytes, but only minor, irregular, and equivocal detections are reported (apparent detection limits). The DCA reported is dominated by the 1,1-DCA isomer with concentrations up to ~9 ppm. The 1,2-DCA concentrations reported appear to be predominantly detection limits, with the highest being 0.5 ppm. These observations support the choice of a sequential dehalogenation model and the neglect of pathways such as the halo-ethane to halo-ethene pathway.

Effective Porosity. An average effective porosity of 0.24 reported in the site SAEP RI Report was used for all SAEP hydrogeologic units. The effective porosity influences the relative speed of advective and diffusive transport.

Initial and Boundary Conditions for Transport

For all three modeling tasks, initial chemical concentrations are based on data collected in 1999. The 1999 data set was the most complete in terms of analytes and spatial coverage, including delineation of the three solvent hot spots. The data reduction process for use in the GMS is described in Section 1.2

The model boundaries were located such that the conditions imposed on those boundaries would not affect the predicted concentration fields in the areas of interest. The default boundary conditions in the RT3D (zero concentration) were applied to all boundaries.

Thus, contaminants potentially originating outside the SAEP model region, *e.g.*, from sources up gradient, are not considered beyond definition of initial conditions.

DNAPL Simulations

The presence of DNAPL at SAEP is unconfirmed by direct observation, *e.g.*, free product recovery. Unless the DNAPL pools at a permeability interface, direct encounter with one of the commonly irregular flow paths would be fortuitous. The effect of a PCE and a TCA DNAPL are treated separately.

For the PCE DNAPL simulations, the initial concentration of PCE was maintained at 100,000 ppb throughout the simulation in the grid cells representing the –20 and –30 foot elevation samples from well WP-99-45. This sample location is associated with hot spot #2 (see Figure 1.2). In the consideration of a TCA DNAPL, the initial concentration was fixed in the grid block at –25 feet elevation sample point associated with CP-99-08 within hot spot #3. These points were selected because they represent the highest PCE/TCA concentrations in the 1999 observations. The constant concentration points approximate a DNAPL source, assuming persistent of the same dissolution conditions that created the 1999 concentrations. In the absence of site data regarding the mass and distribution of DNAPL, this approach represents a conservative treatment of an internal source. The two other hot spots may be expected to follow the same trend, though at lower concentrations.

2.3 RESULTS FOR PCE/TCE

An arbitrary 20-year simulation period was selected for MNA predictions. The results of reactive transport simulations are presented below in figures for each CAH constituent. Two figures are presented for each chemical – one representing the initial plume distribution (1999) and the second presenting the predicted distribution after 20 years of reactive transport.

Figures 2.3 through 2.18 illustrate PCE/TCE simulations for scenarios without DNAPL, *i.e.*, the initial contaminant distribution as the only source. Figures 2.19 through 2.16 illustrate the simulations that include a continuous source of PCE at a hot spot. Note that the concentration scales are consistent for any particular species, but vary between species.

The contour plots presented here indicate a general reduction trend of contaminants. Low levels of transformation products encroach on the mudflat region (see Figure 2.6 and 2.10) after 20 years. The presence of DNAPL extends the persistence of the plume but has only a minor effect on the downstream extent.

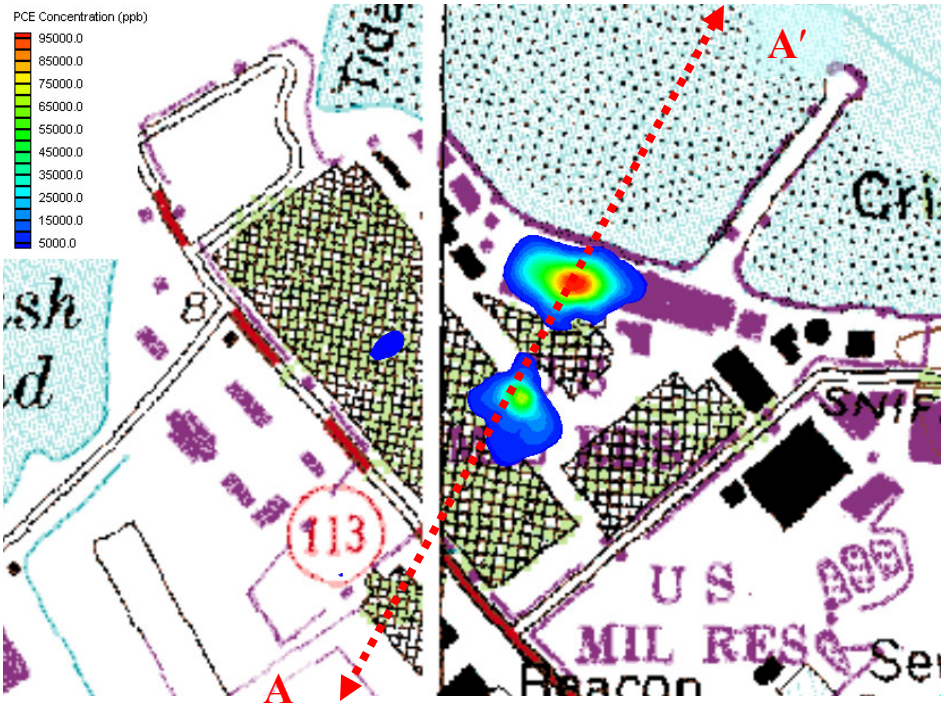

Figure 2.3. Initial PCE distribution (1999) in the lower reworked glacial sediments (grid layer 3) in which some of the higher concentrations are observed. The A-A' arrow indicates the trace of all PCE-related profiles through hot spots #1 and #2.

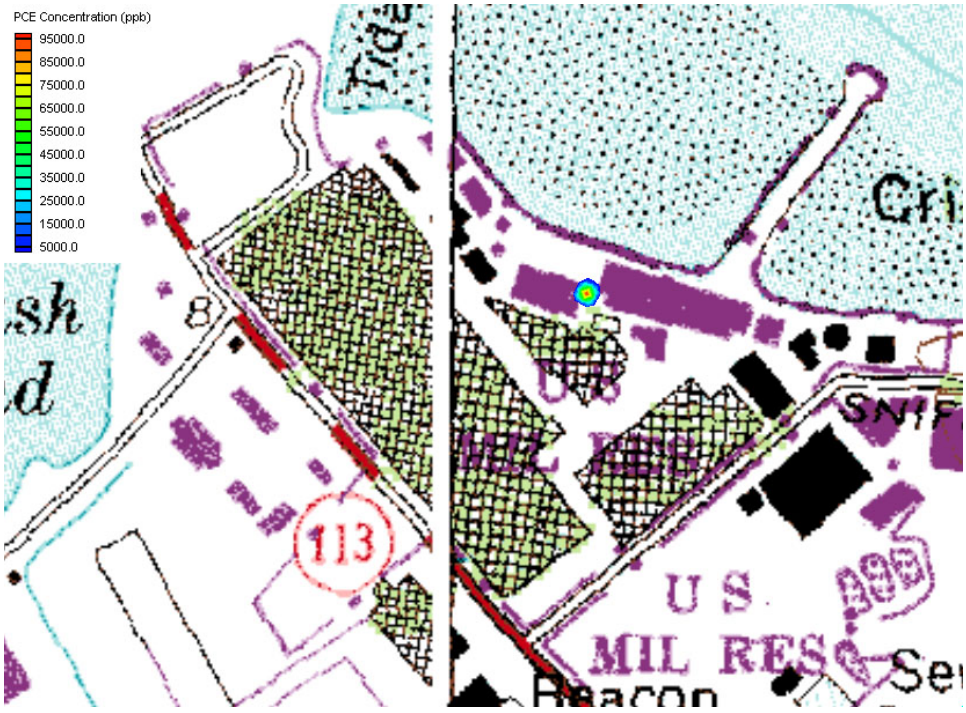

Figure 2.4. Predicted PCE distribution in the lower reworked glacial sediments (grid layer 3), after 20 of reactive transport.

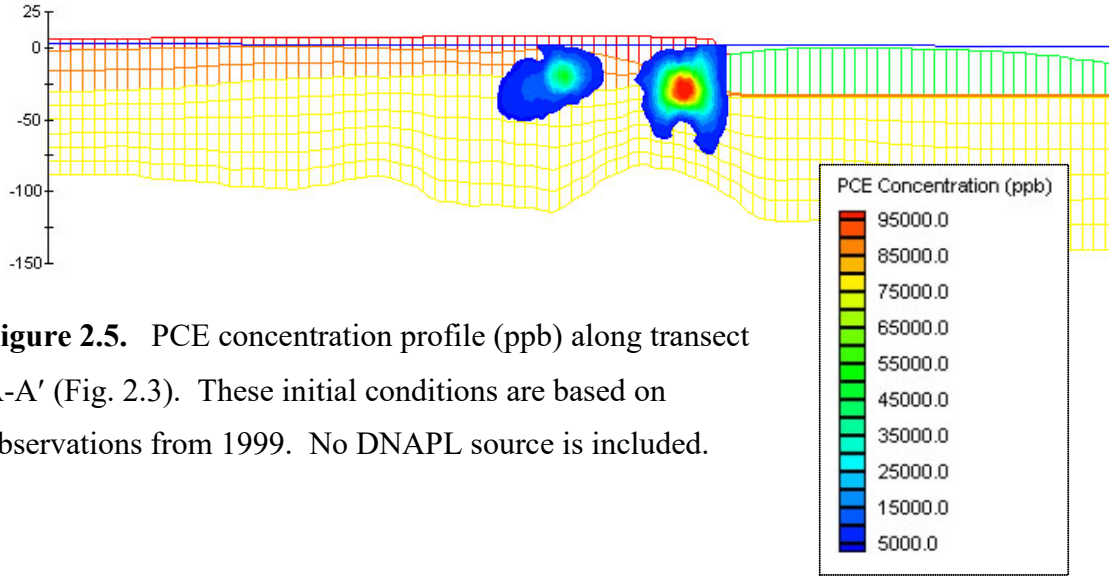

Figure 2.5. PCE concentration profile (ppb) along transect A-A′ (Fig. 2.3). These initial conditions are based on observations from 1999. No DNAPL source is included.

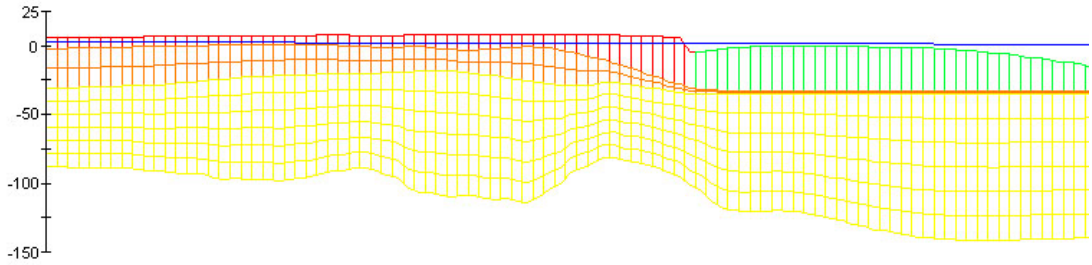

Figure 2.6. PCE concentration profile at A-A′ (Fig. 2.3). No DNAPL.

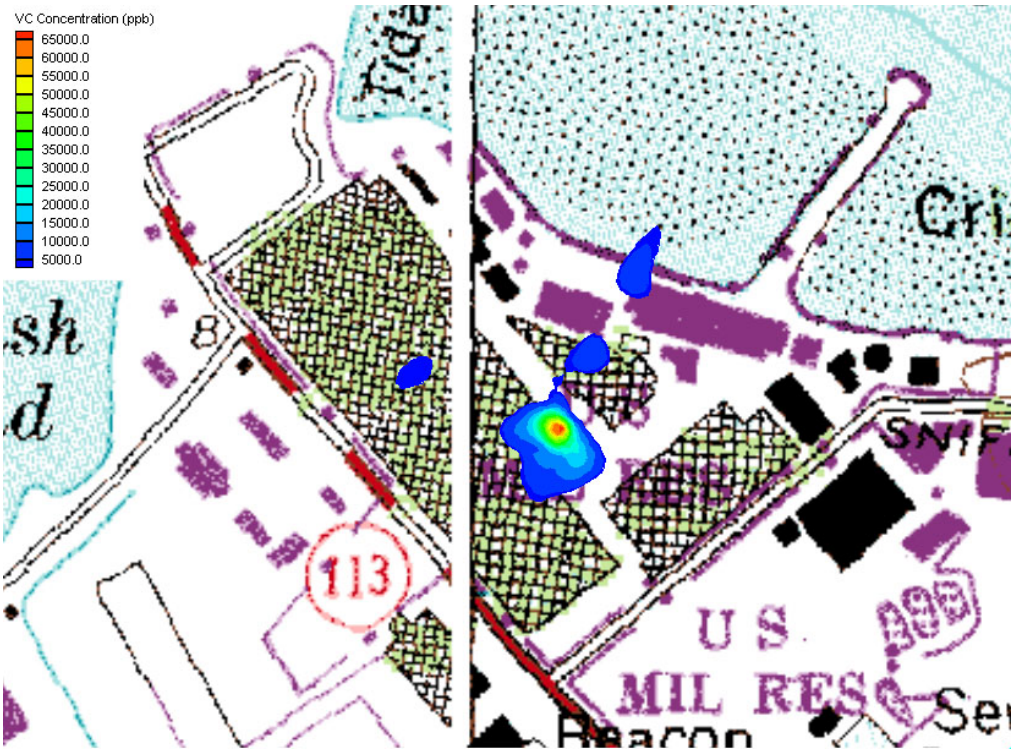

Figure 2.7. Initial TCE distribution (1999) in grid layer 3 (lower reworked glacial).

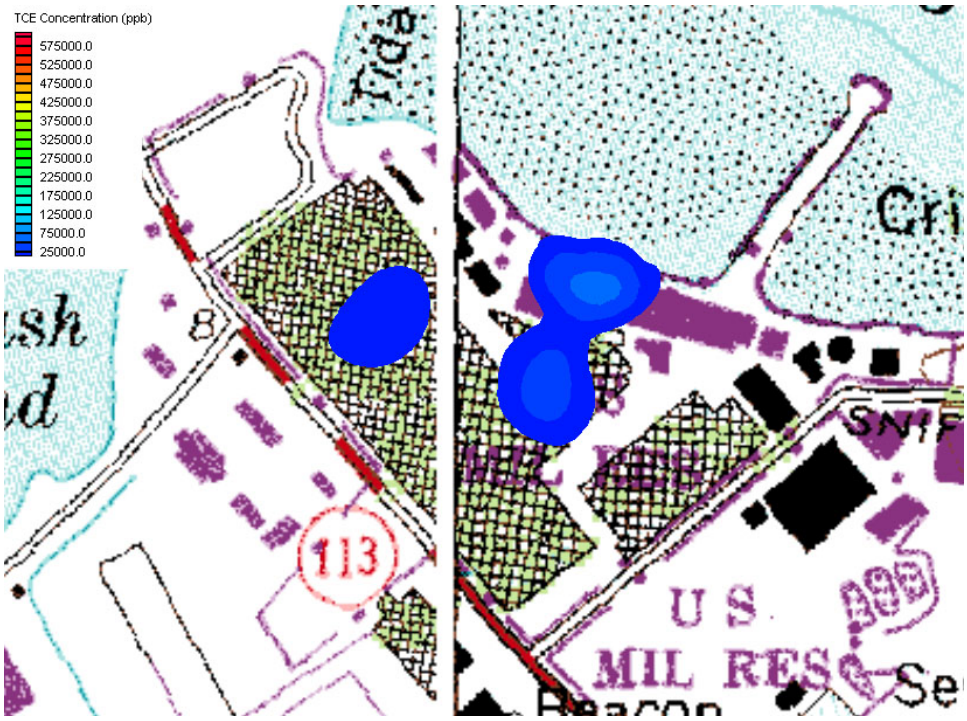

Figure 2.8. Predicted TCE distribution after 20 years (grid layer 3). The peak concentration decreases by nearly one order of magnitude.

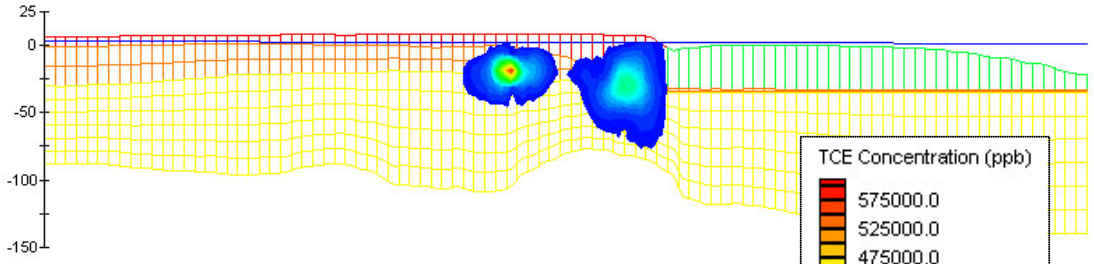

Figure 2.9. Initial TCE profile at A-A′ (Fig. 2.3); no DNAPL.

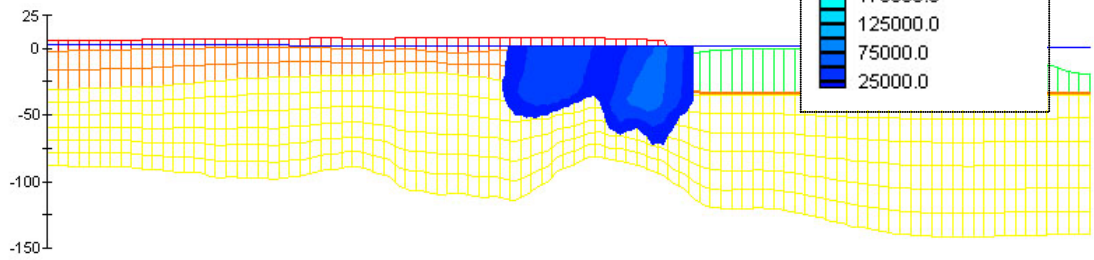

Figure 2.10. Predicted TCE profile at A-A′ after 20 years; no DNAPL source.

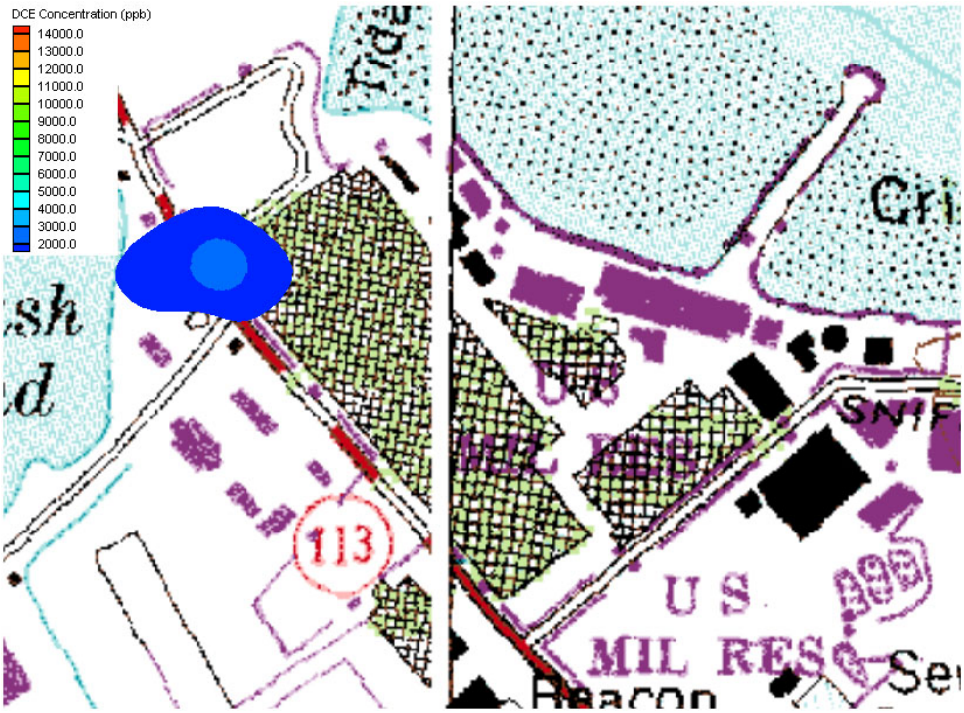

Figure 2.11. Initial DCE distribution; no DNAPL

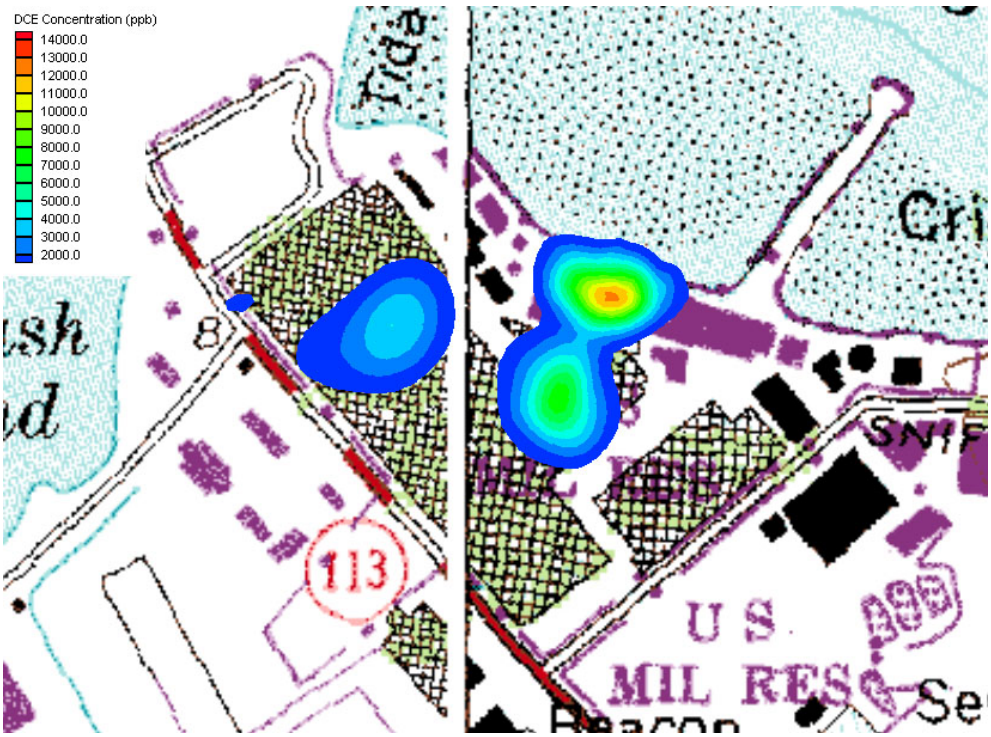

Figure 2.12. Predicted DCE after 20 years; no DNAPL

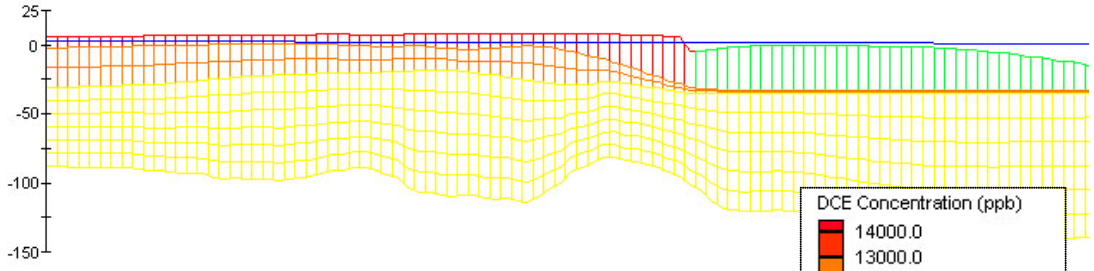

Figure 2.13 DCE initial conditions along A-A′ (Fig. 2.3); only low concentrations in this section.

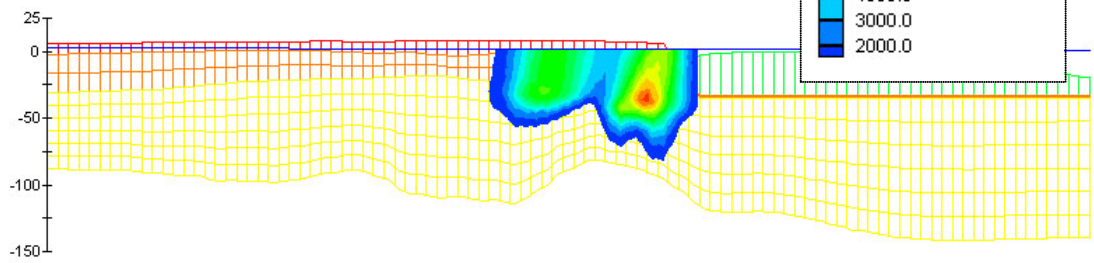

Figure 2.14. Predicted DCE profile at A-A′ after 20 years; no DNAPL.

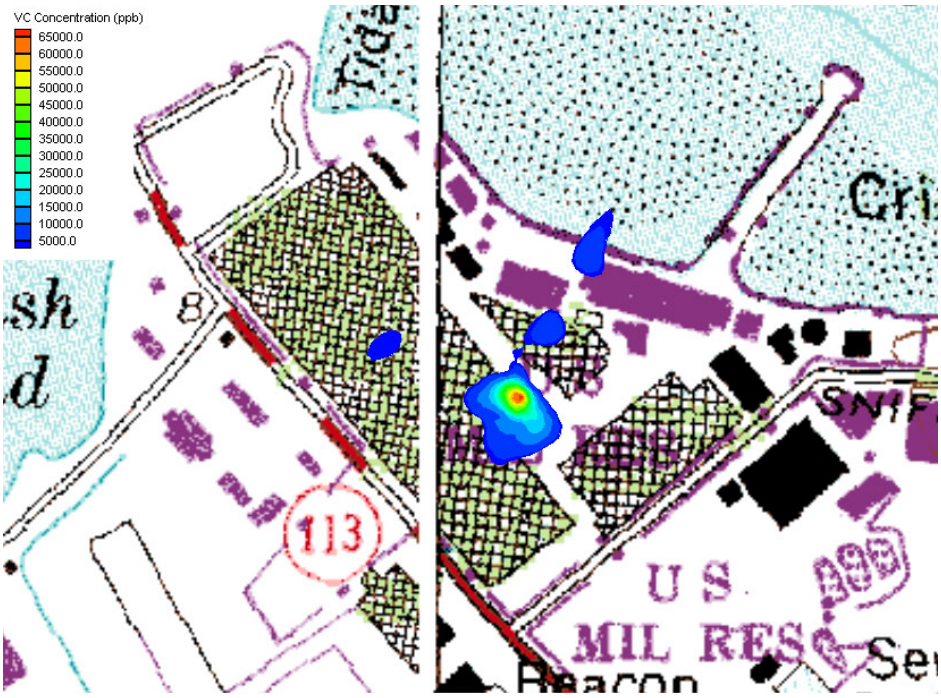

Figure 2.15. Initial VC (ppb) distribution (1999) in grid layer 3 (lower reworked glacial sediments)

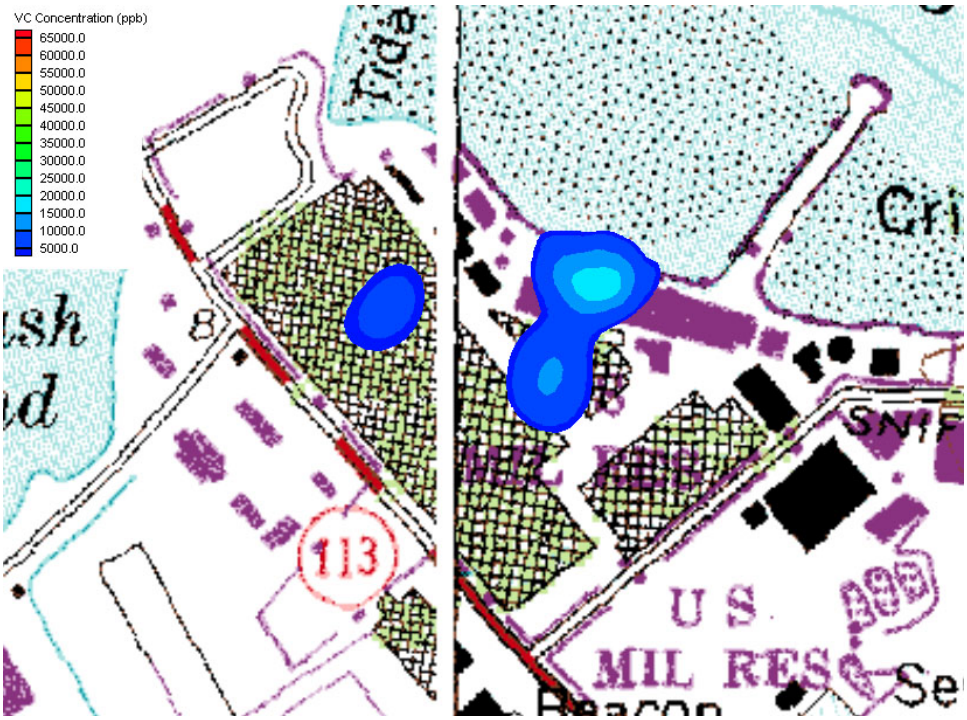

Figure 2.16. Predicted VC (ppb) distribution in grid layer 3 (lower reworked glacial sediments) after 20 years; no DNAPL.

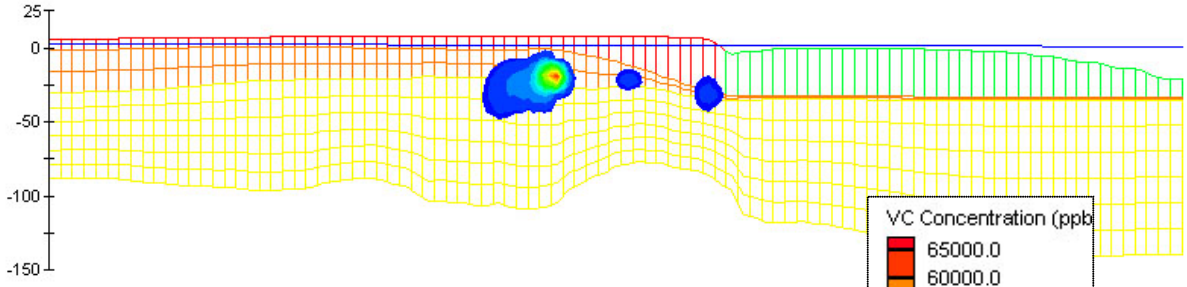

Figure 2.17. Initial VC profile along A-A′ (Fig. 2.3); no PCE DNAPL.

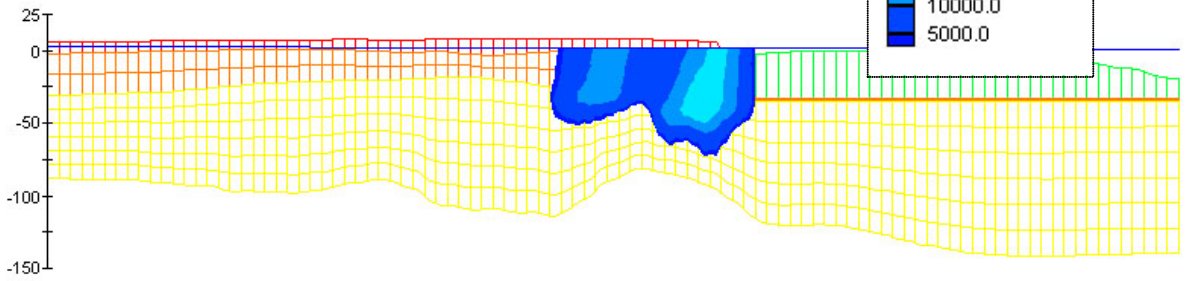

Figure 2.18. Predicted VC profile at A-A′ after 20 years; no DNAPL.

Simulations Including a PCE DNAPL

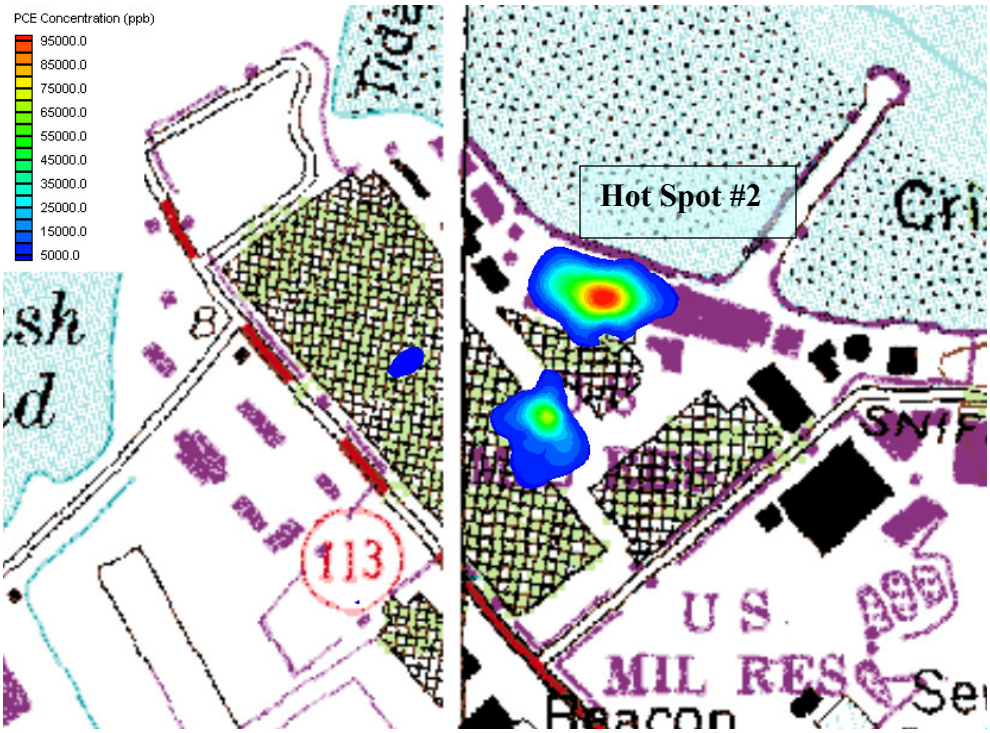

Figure 2.19. Initial PCE distribution with DNAPL source.

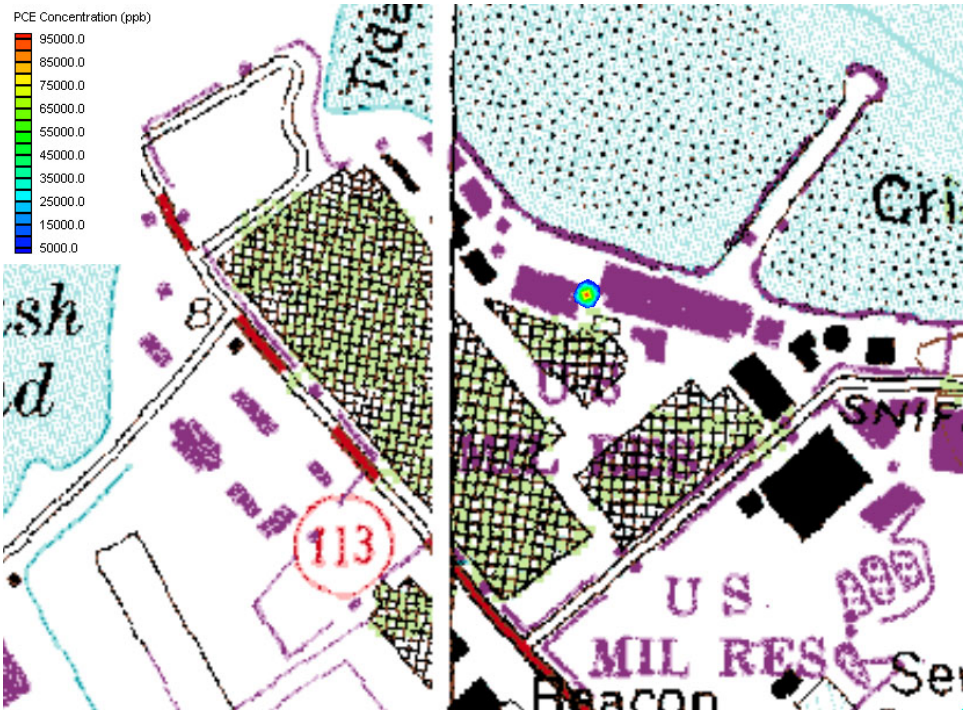

Figure 2.20. Predicted PCE distribution after 20 years; DNAPL source imposed in hot spot #2, within reworked glacial sediments (grid layer 3).

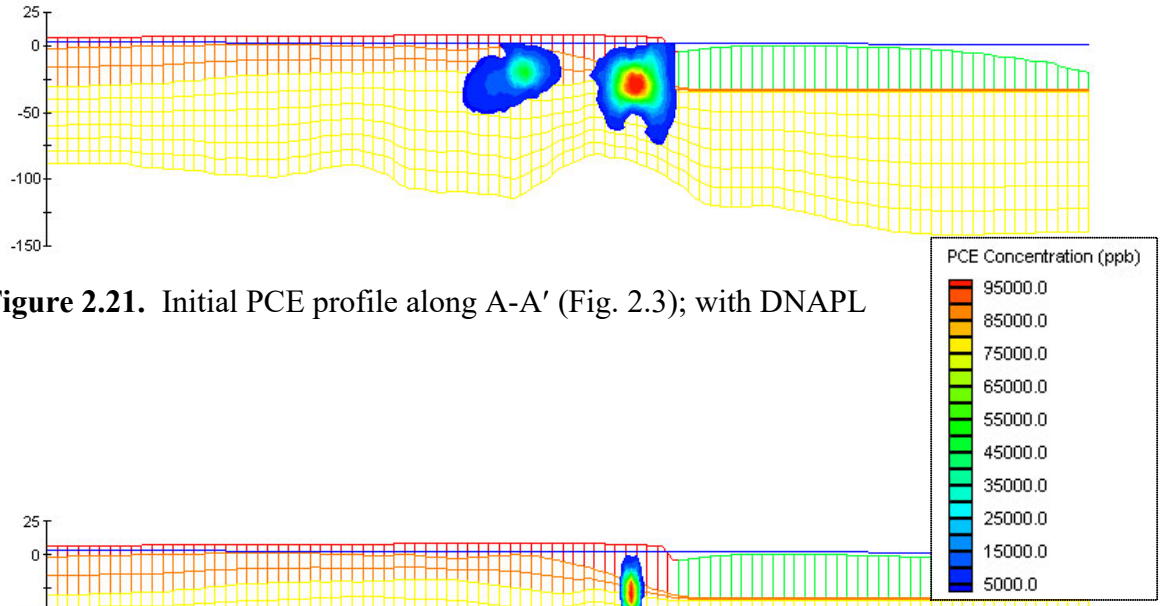

Figure 2.21. Initial PCE profile along A-A′ (Fig. 2.3); with DNAPL

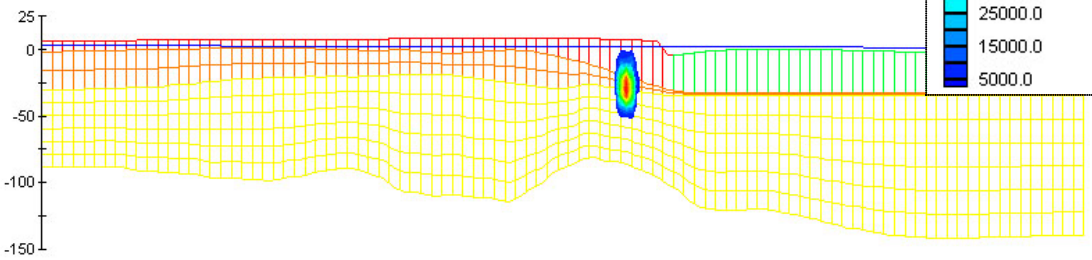

Figure 2.22. Predicted PCE distribution on A-A′ after 20 years; PCE DNAPL source maintained.

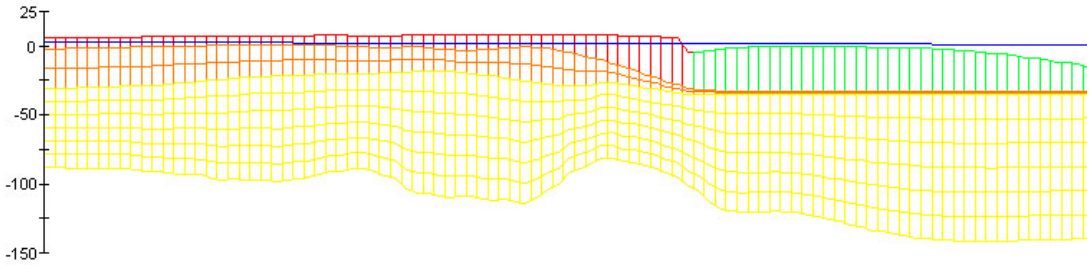

Figure 2.23. For comparison, PCE distribution on A-A′ after 20 years without the PCE source.

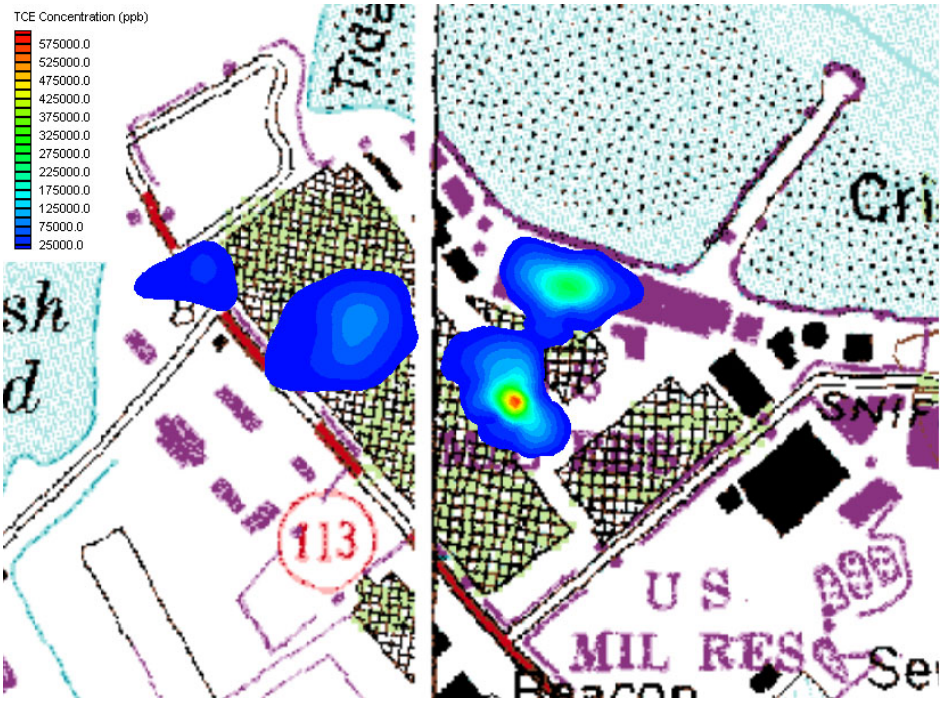

Figure 2.24. Initial TCE distribution with PCE DNAPL.

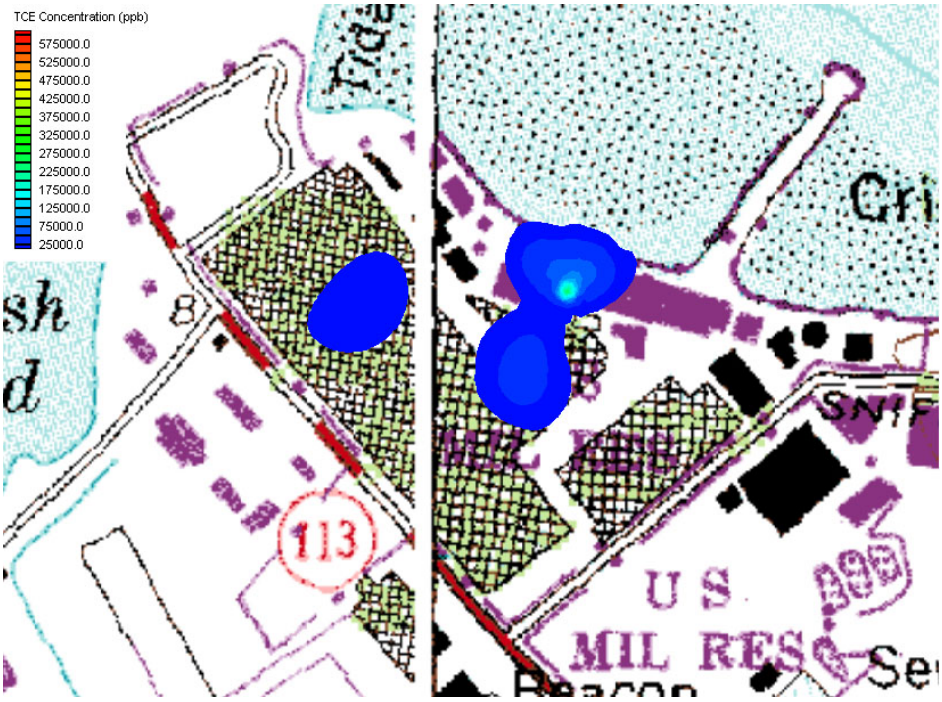

Figure 2.25. Predicted TCE distribution after 20 years; PCE DNAPL source maintained within hot spot #2.

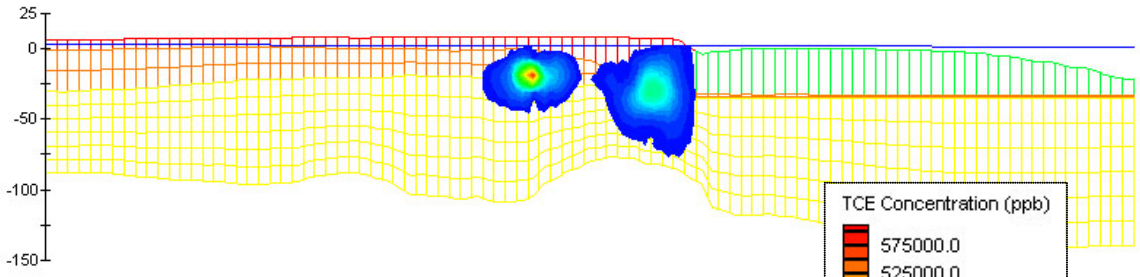

Figure 2.26. Initial TCE profile along A-A′ (Fig. 2.3); with PCE DNAPL source.

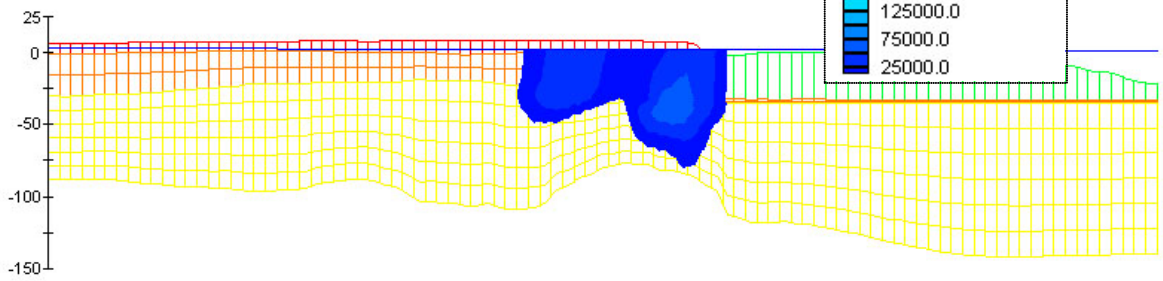

Figure 2.27. Predicted TCE profile at A-A′ after 20 years with PCE DNAPL source maintained within hot spot #2.

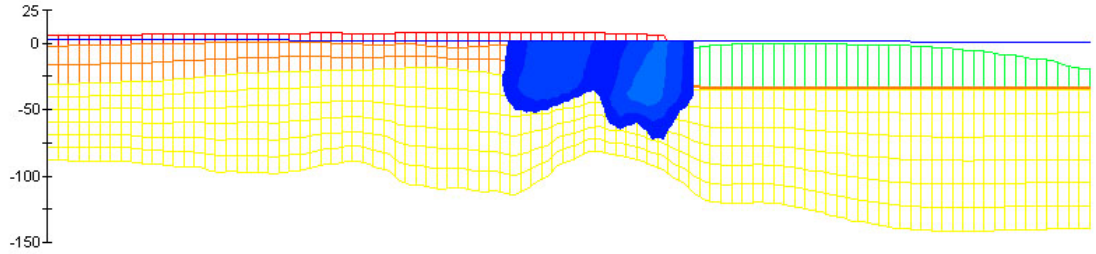

Figure 2.28. For comparison, TCE profile after 20 years without PCE source.

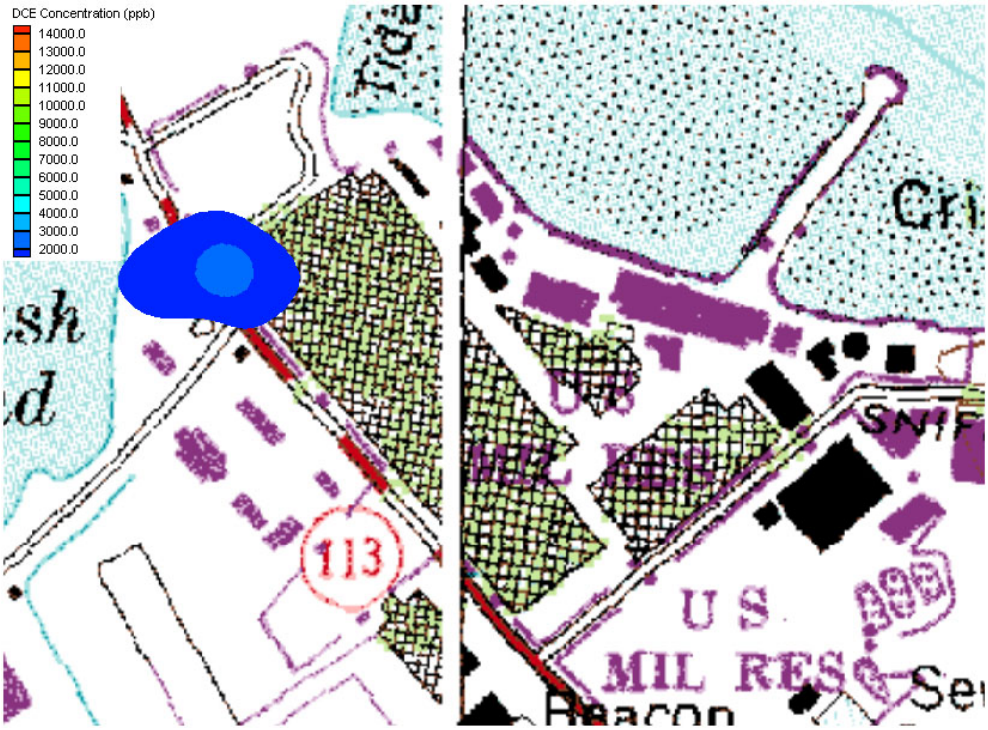

Figure 2.29. Initial DCE distribution with DNAPL (PCE).

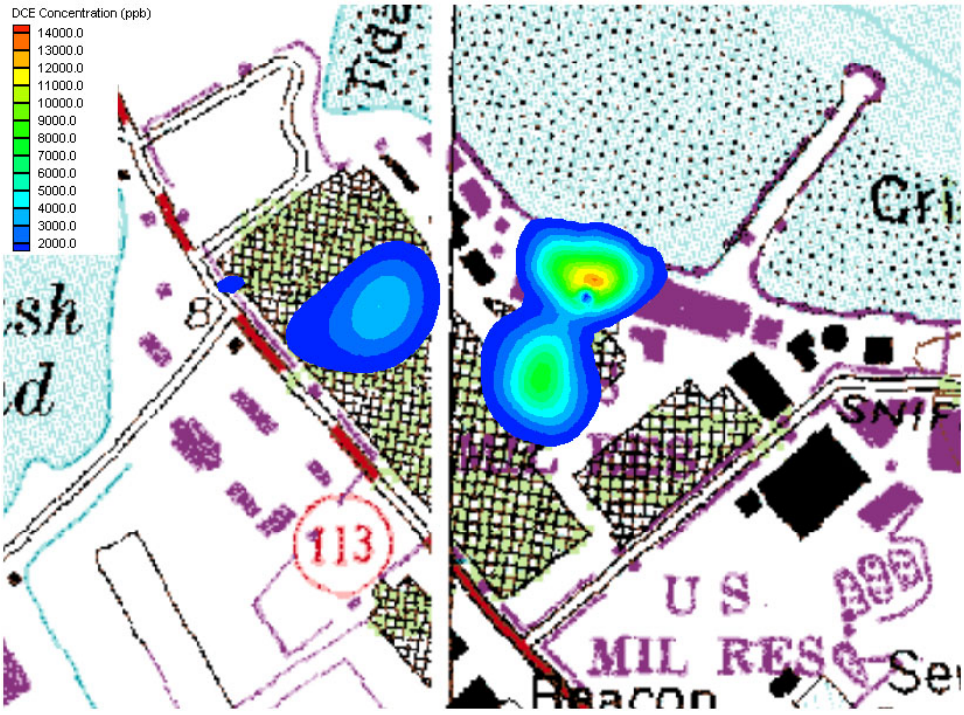

Figure 2.30. Predicted DCE distribution after 20 years; PCE source (DNAPL) is maintained within hot spot #2.

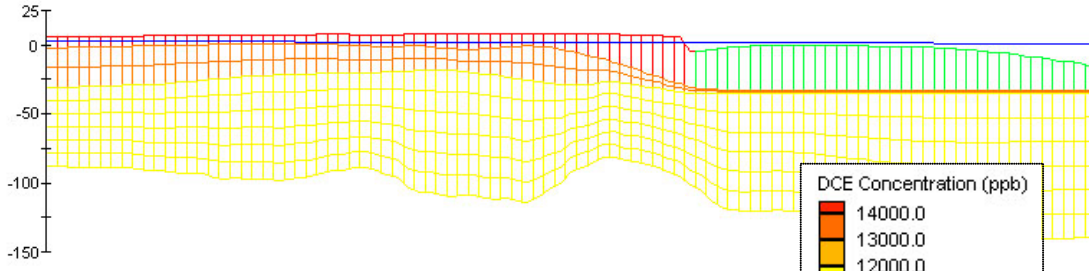

Figure 2.31 DCE initial profile at section A-A′ (Fig. 2.3); Only low concentrations are detected in this section.

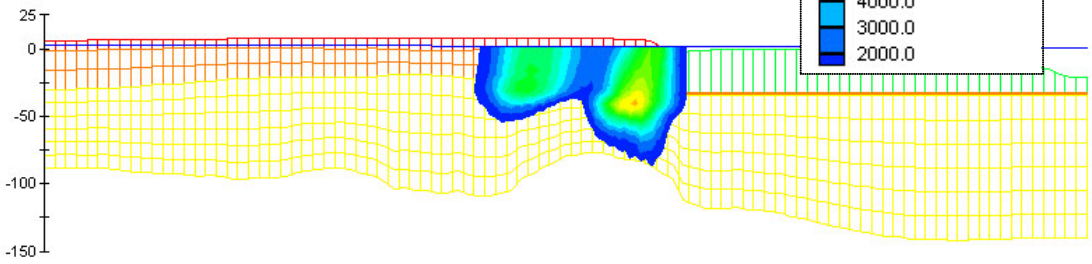

Figure 2.32. Predicted DCE profile on A-A′ after 20 years with PCE source.

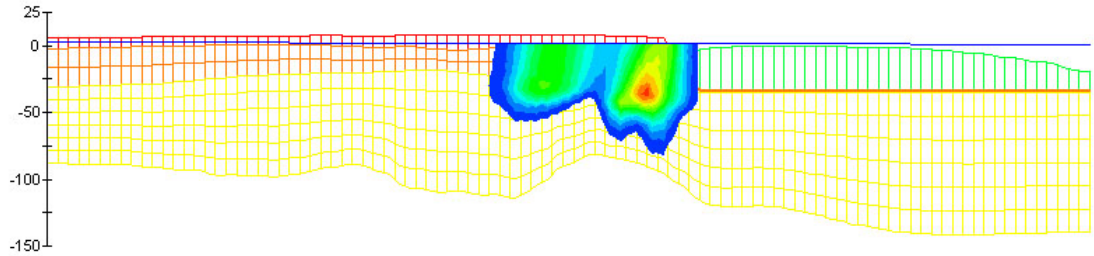

Figure 2.33. For comparison, DCE profile on A-A′ after 20 years without the PCE source.

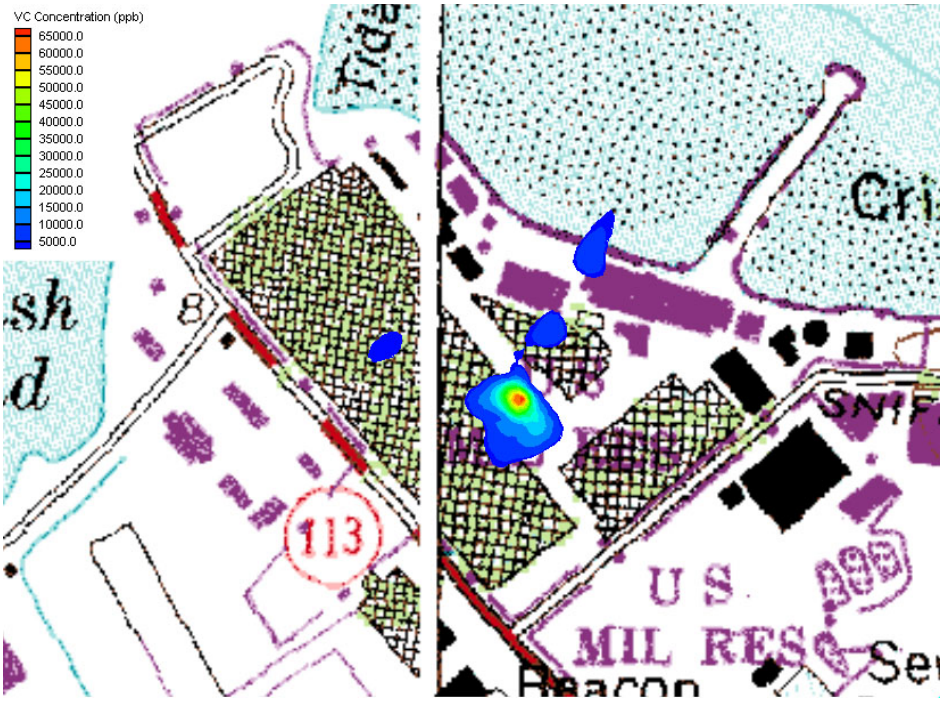

Figure 2.34. Initial VC concentration in the upper layer; with DNAPL.

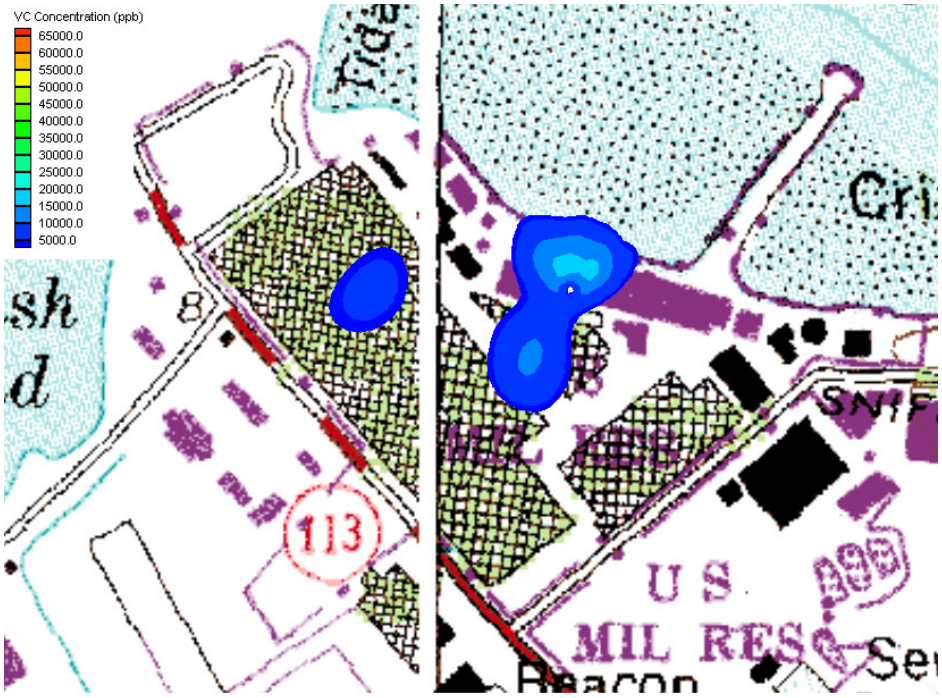

Figure 2.35. Predicted VC plumes in the upper layer after 20 years with PCE source DNAPL.

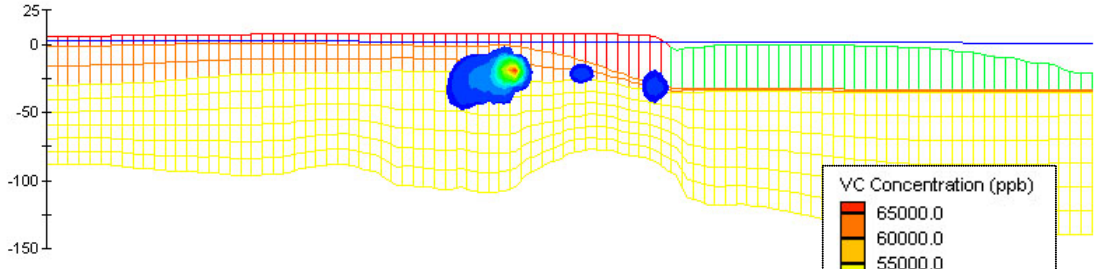

Figure 2.36. Initial VC profile along section A-A′ (Fig. 2.3); with PCE DNAPL source.

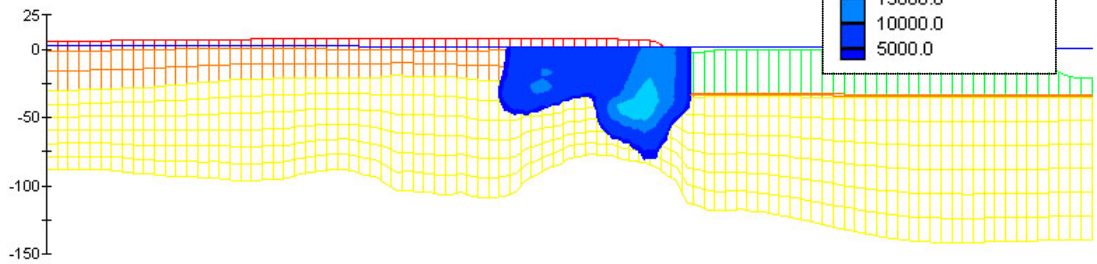

Figure 2.37. Predicted VC profile on A-A′after 20 years, PCE maintained within hot spot #2.

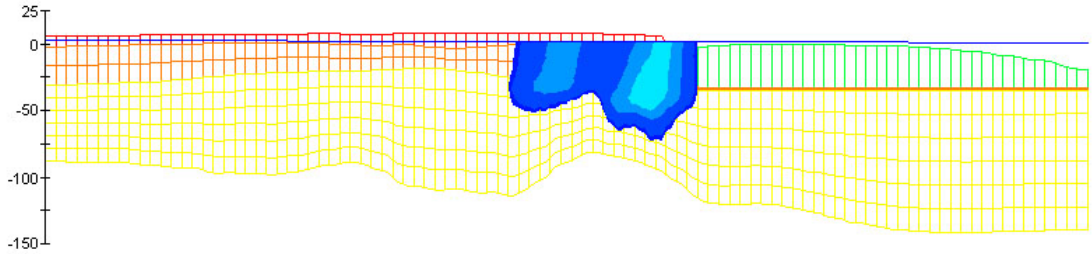

Figure 2.38. For comparison, VC profile after 20 years without PCE source.

2.4 RESULTS FOR TCA

Figures 2.17 to 2.22 summarize the simulations of TCA attenuation in the absence of a TCA DNAPL. For each constituent (TCA, DCA, CA), the initial condition (1999) and 20-year simulation results are presented. All contaminant transport is slow due to low flow velocities and retardation due to adsorption. For each reactant, the temporal trend is toward lower concentrations, with little if any contaminant reaching the Housatonic River.

Figures 2.23 to 2.28 demonstrate the influence of a localized occurrence of TCA DNAPL. The hot spot remains throughout the simulation, of course, set as a boundary condition. However, the extent of the plume is not greatly extended relative to non-DNAPL plumes, consistent with the slow rates of advective transport and the modest decay rates.

TCA Simulations from 1999 Initial Conditions (no DNAPL)

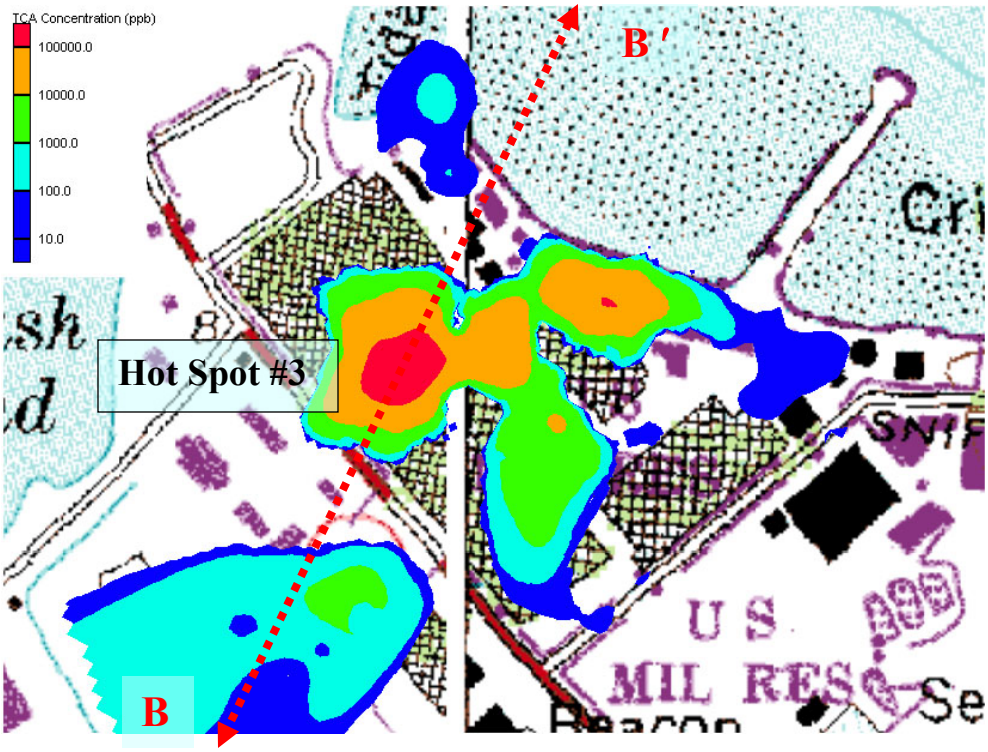

Figure 2.39. Initial (1999) distribution of TCA plume in the upper layers. The red B-B' arrow indicates the trace of all TCA-related profiles.

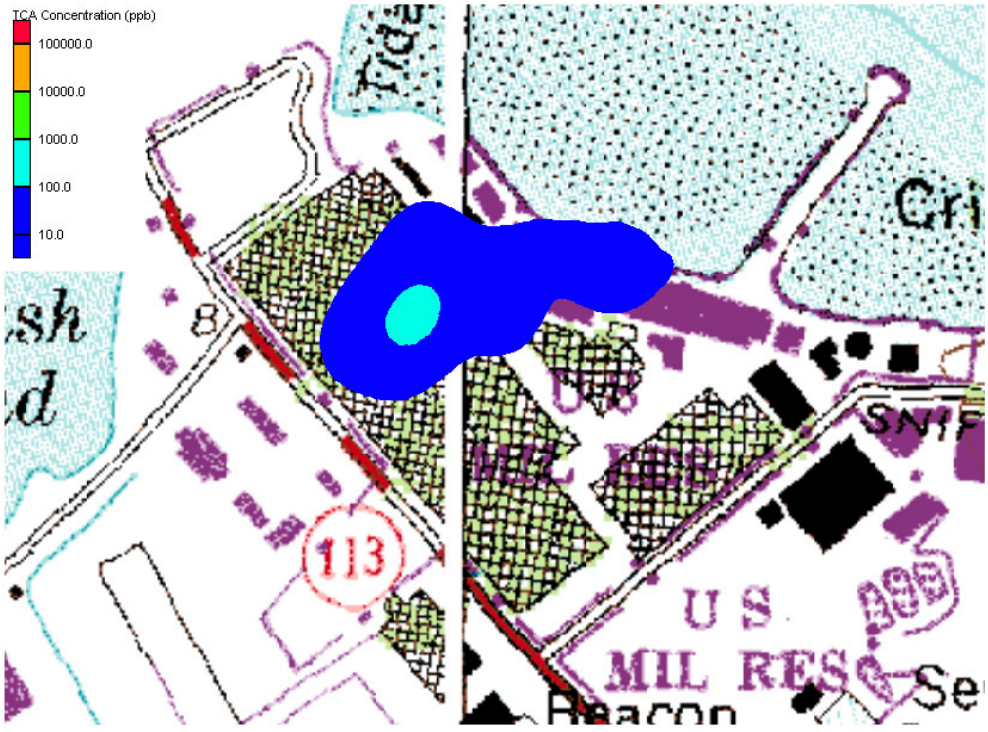

Figure 2.40. Predicted TCA distribution in the upper layers after 20 years.

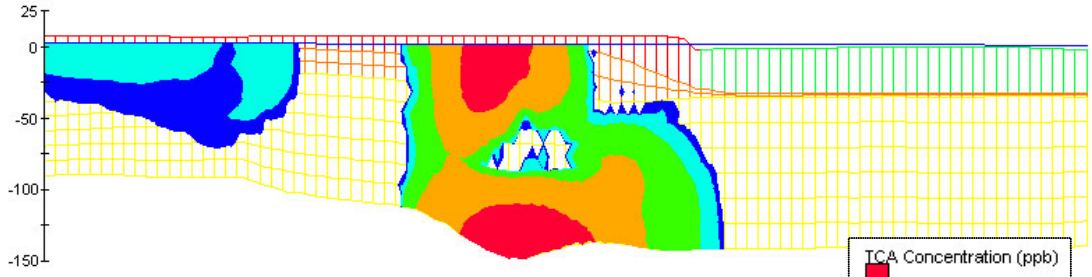

Figure 2.41. TCA profile along section B-B′ (Fig. 2.29); no TCA DNAPL.

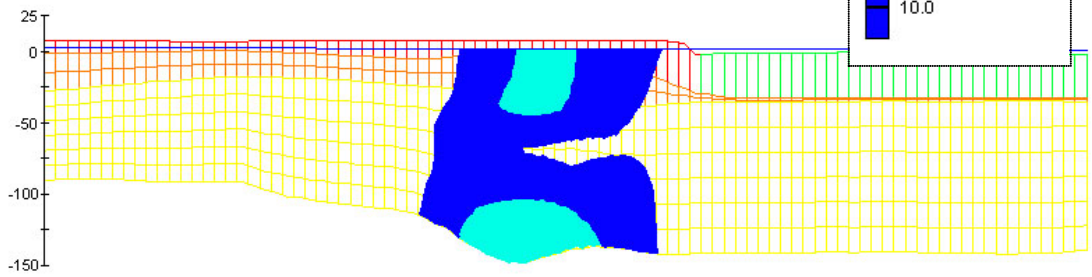

Figure 2.42. Predicted TCA profile at B-B′ after 20 years; no TCA DNAPL source.

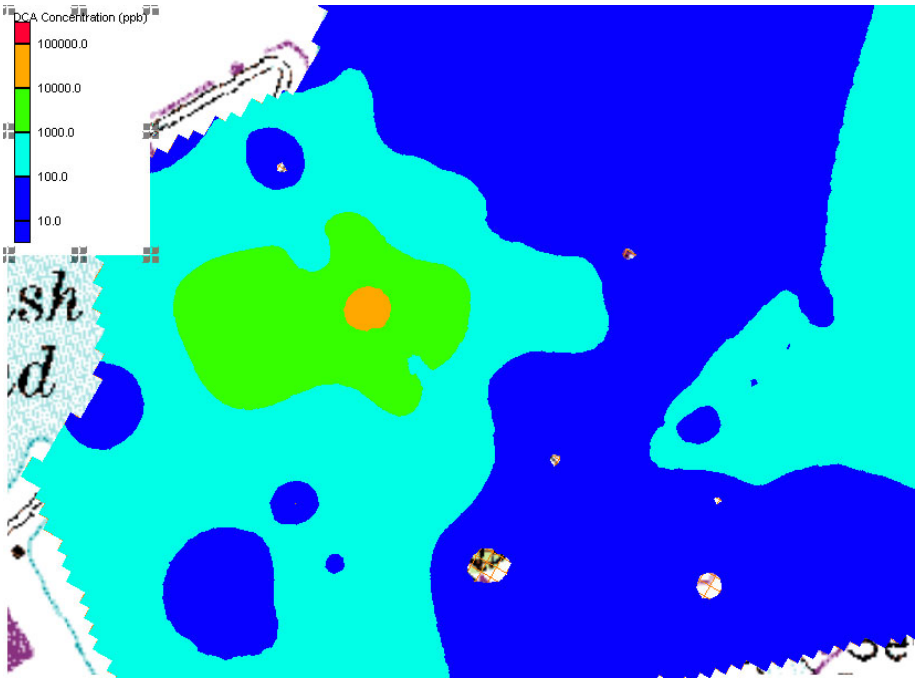

Figure 2.43. Initial (1999) distribution of DCA in the upper layers

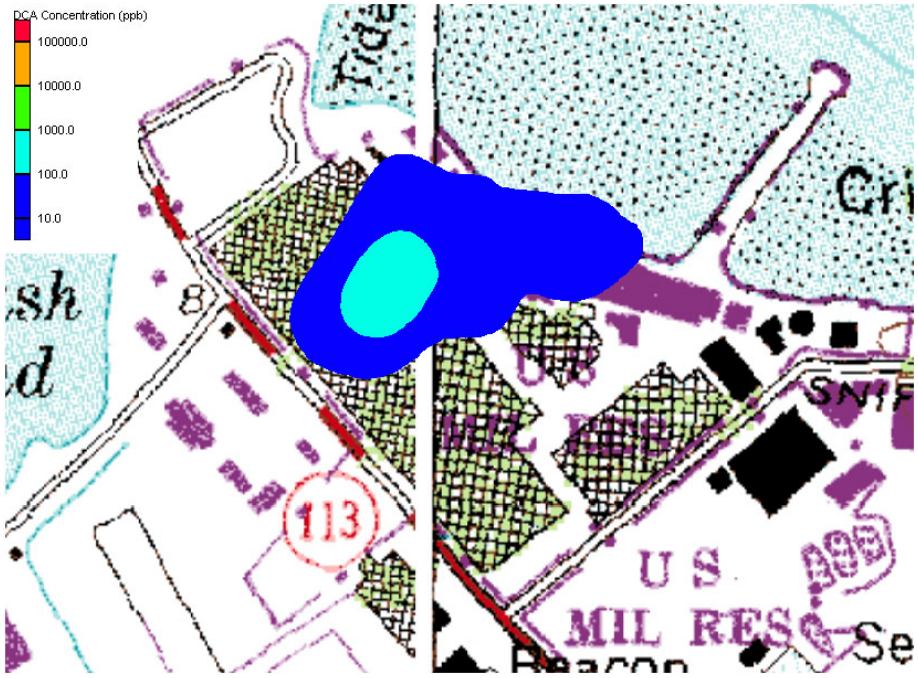

Figure 2.44. Predicted distribution of DCA plume after 20 years

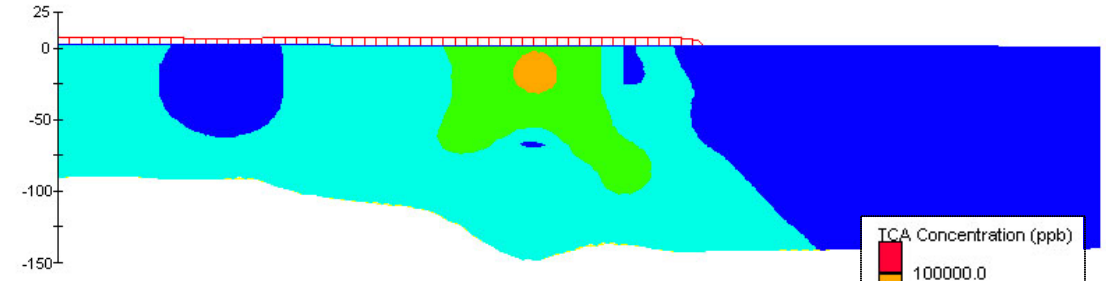

Figure 2.45. Initial DCA profile along section B-B′ (Fig. 2.29); no TCA DNAPL.

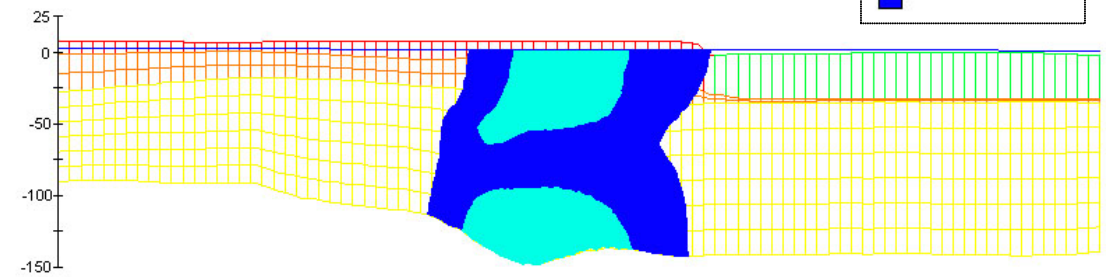

Figure 2.46. Predicted DCA profile at B-B′ after 20 years; no TCA DNAPL source.

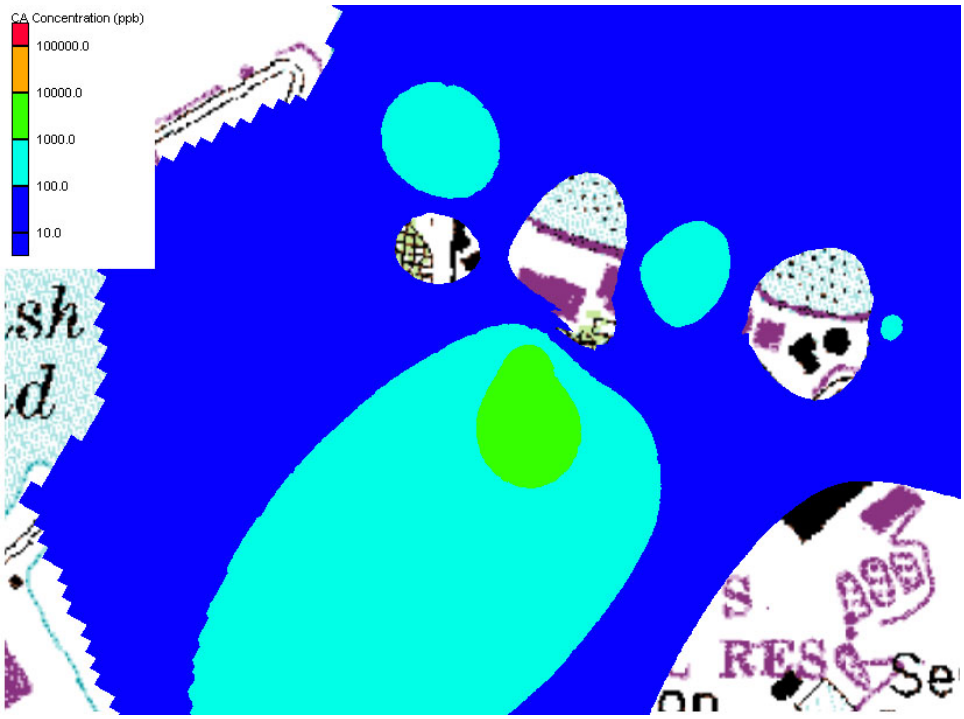

Figure 2.47. Initial (1999) distribution of CA plume in the upper layers

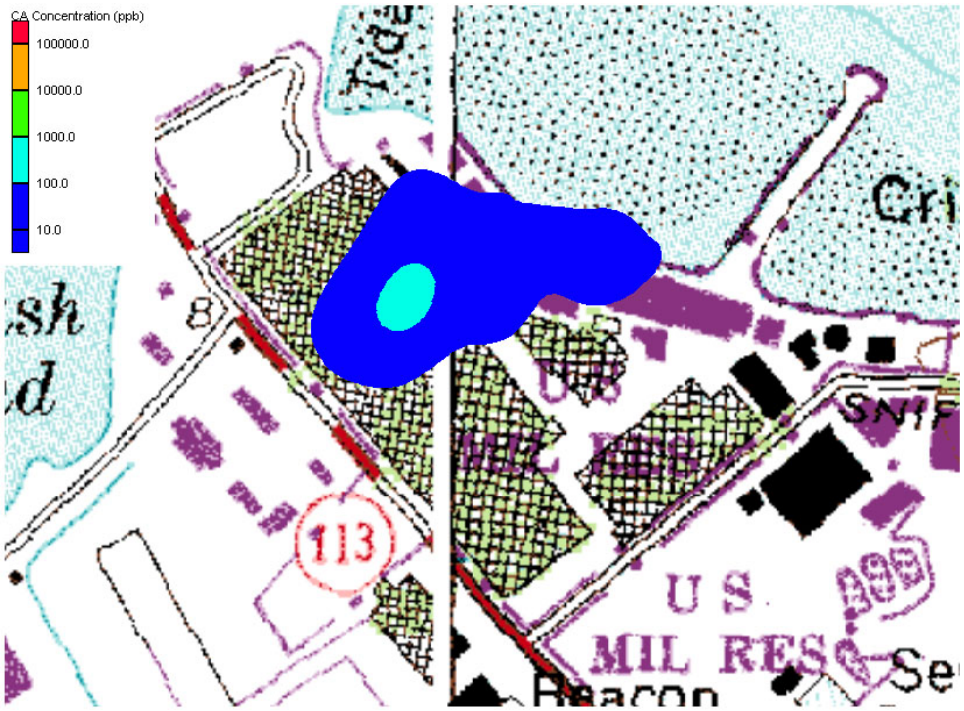

Figure 2.48. Predicted CA plume after 20 years in the upper layers

Figure 2.49. Initial CA profile along section B-B′ (Fig. 2.29); no TCA DNAPL

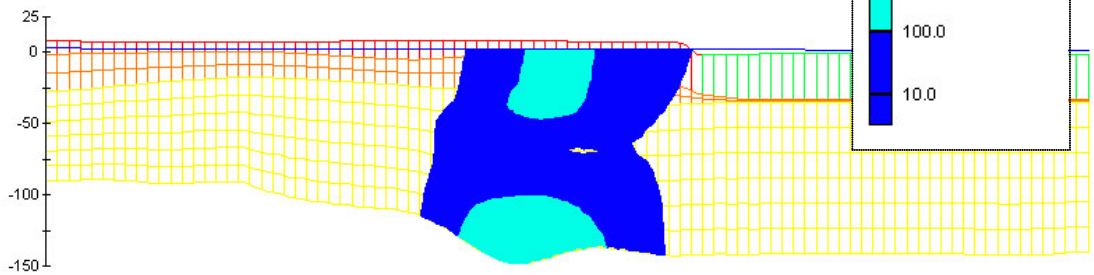

Figure 2.50. Predicted CA profile at B-B′ after 20 years; no TCA DNAPL source.

TCA Simulations with DNAPL Source

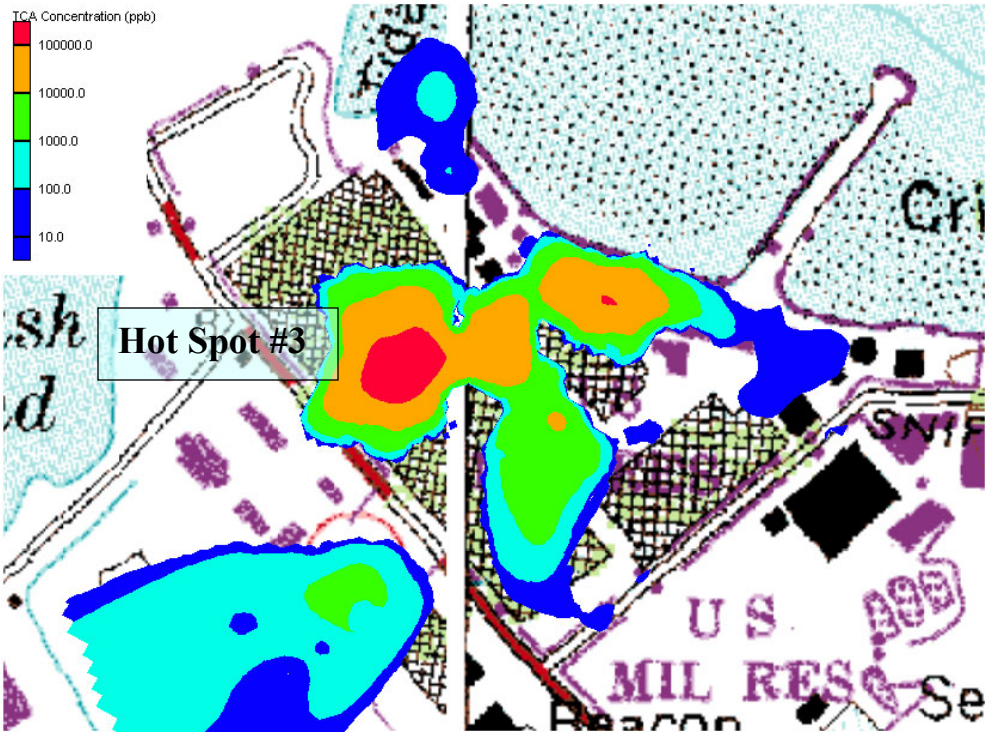

Figure 2.51. Initial (1999) TCA plume distribution in the upper layer. Constant TCA concentration imposed at maximum observed value (center of image).

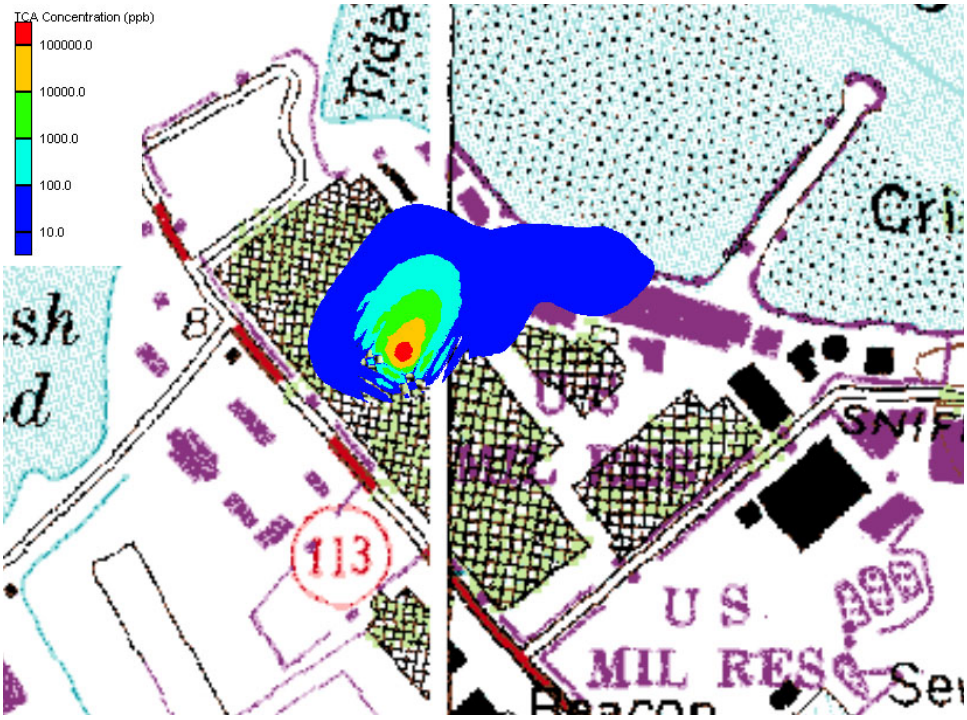

Figure 2.52. Predicted TCA distribution in the upper layer after 20-years.

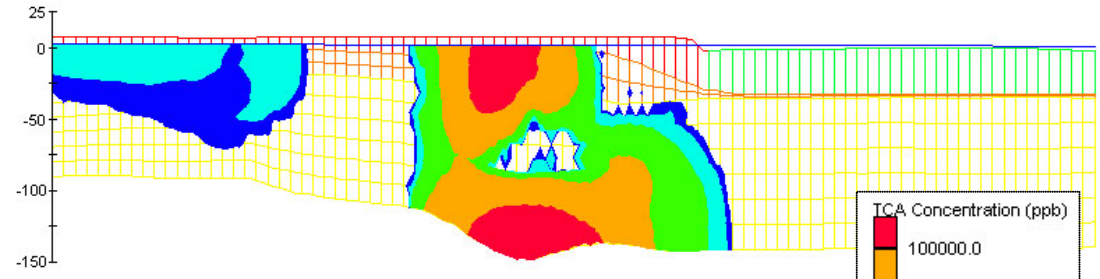

Figure 2.53. Initial TCA profile along section B-B′ (Fig. 2.29); with TCA DNAPL source within hot spot #3.

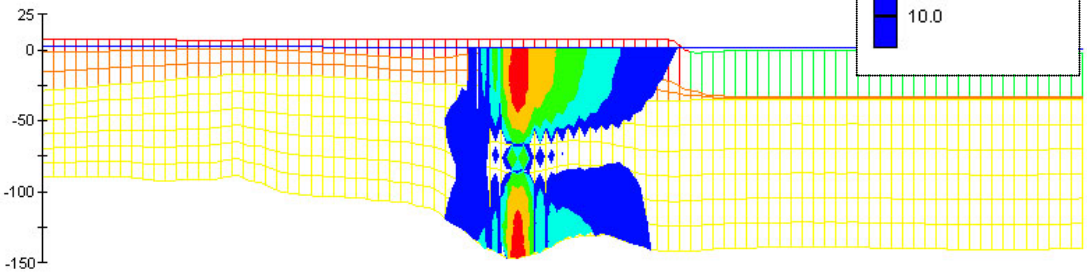

Figure 2.54. Predicted TCA profile at B-B′ after 20 years; with TCA DNAPL source.

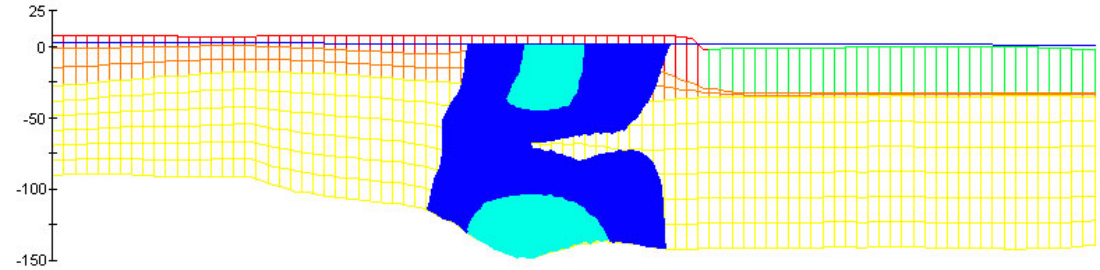

Figure 2.55. For comparison, the predicted TCA after 20 years without a TCE source DNAPL.

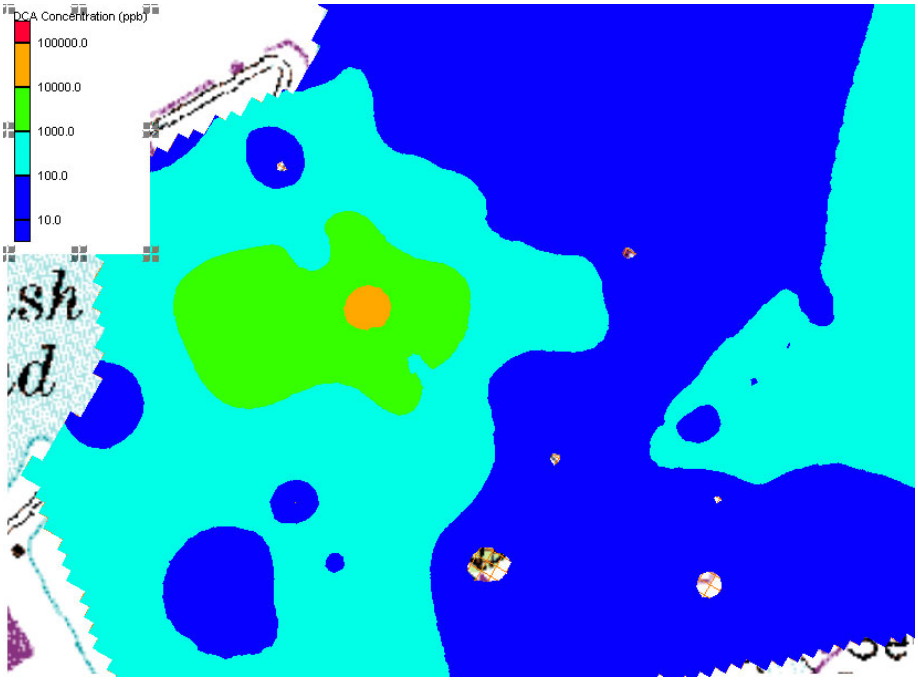

Figure 2.56. Initial (1999) DCA plume distribution in the upper layer

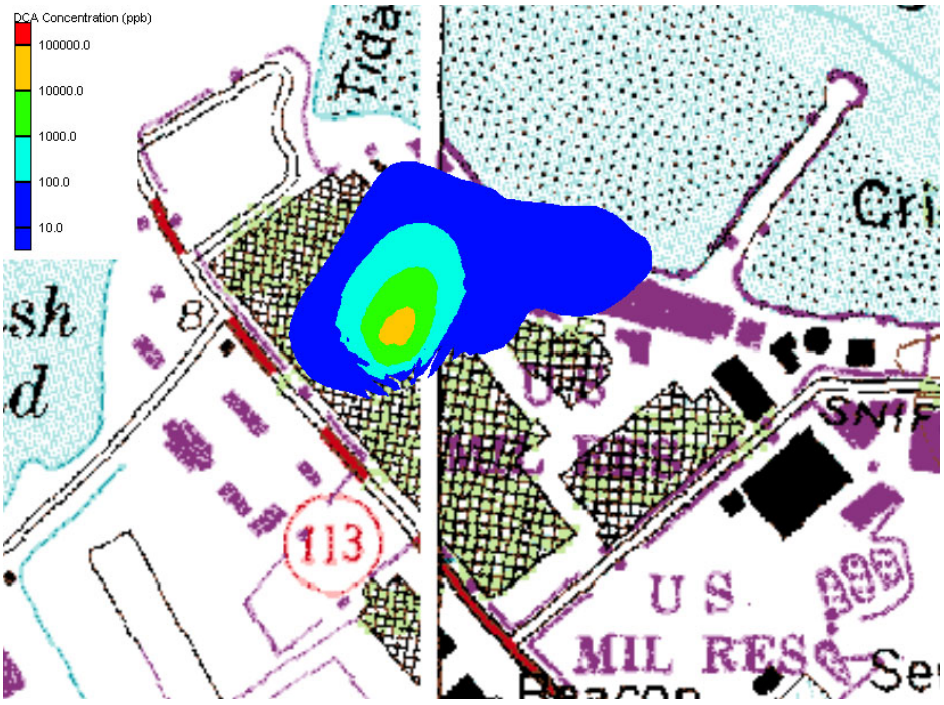

Figure 2.57. Predicted DCA distribution after 20-years with TCA source in the upper layer.

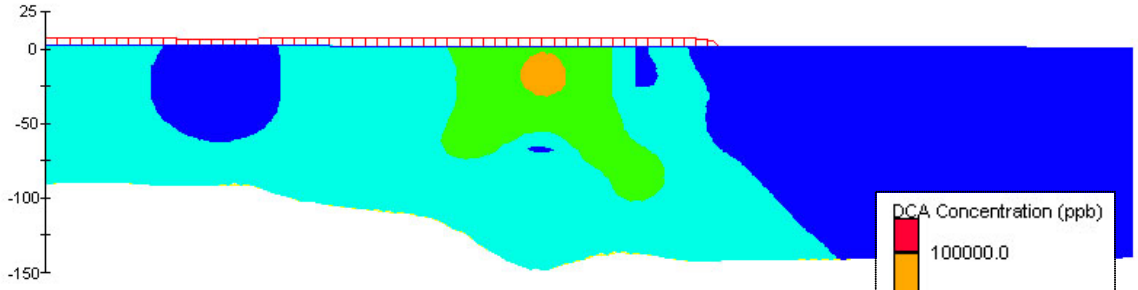

Figure 2.58. Initial DCA profile along section B-B′ (Fig. 2.29); a TCA DNAPL source established within hot spot #3.

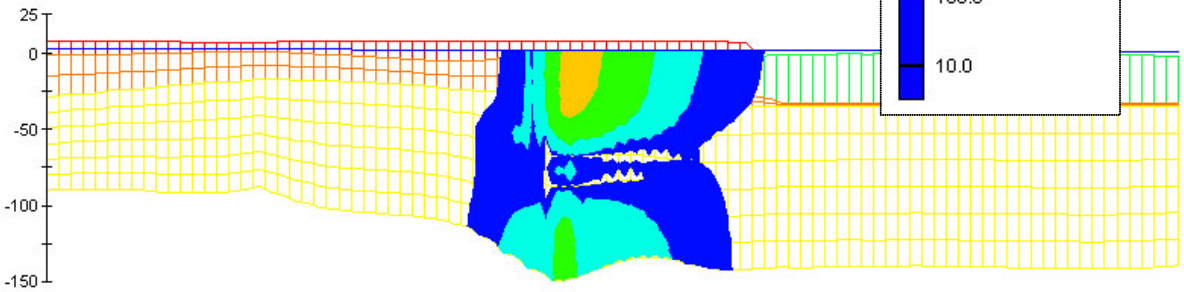

Figure 2.59. Predicted DCA profile at B-B′ after 20 years; with TCA DNAPL source.

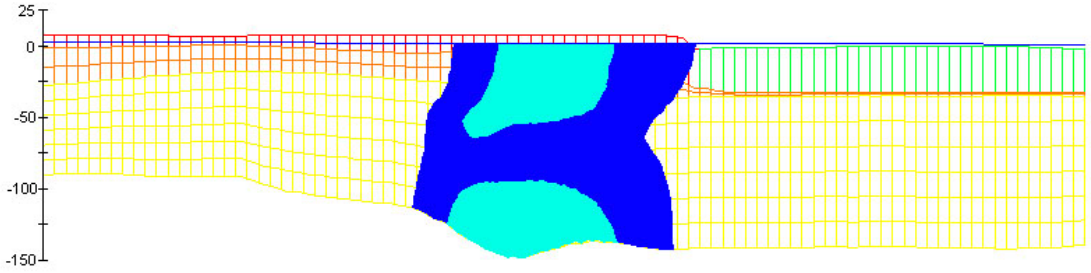

Figure 2.60. For comparison, the predicted DCA profile after 20 years without the TCA source.

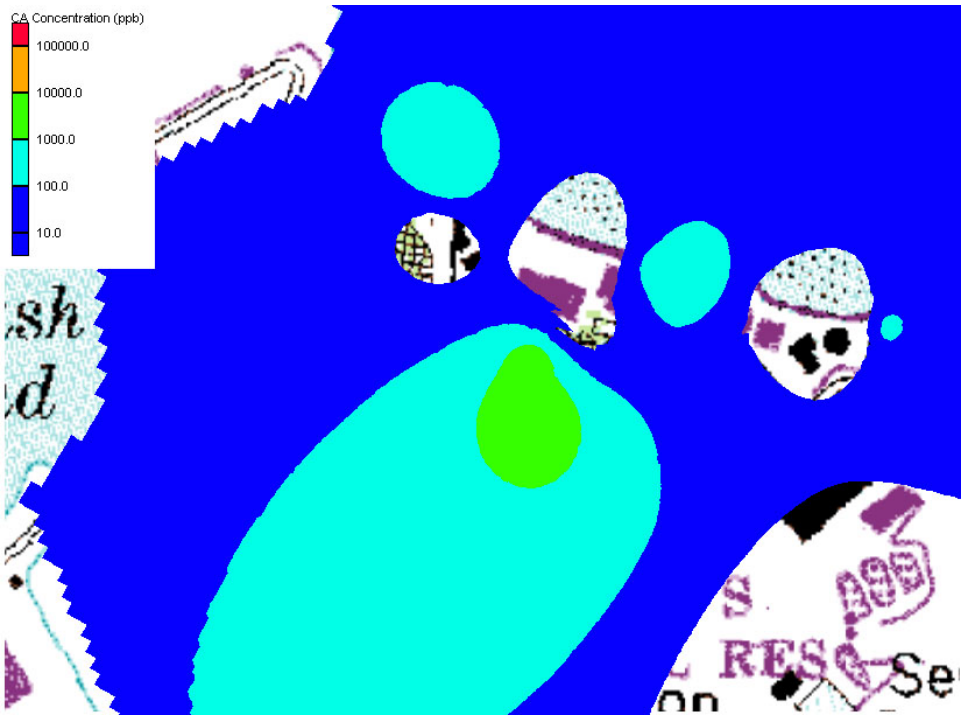

Figure 2.61. Initial (1999) CA plume distribution in the upper layer.

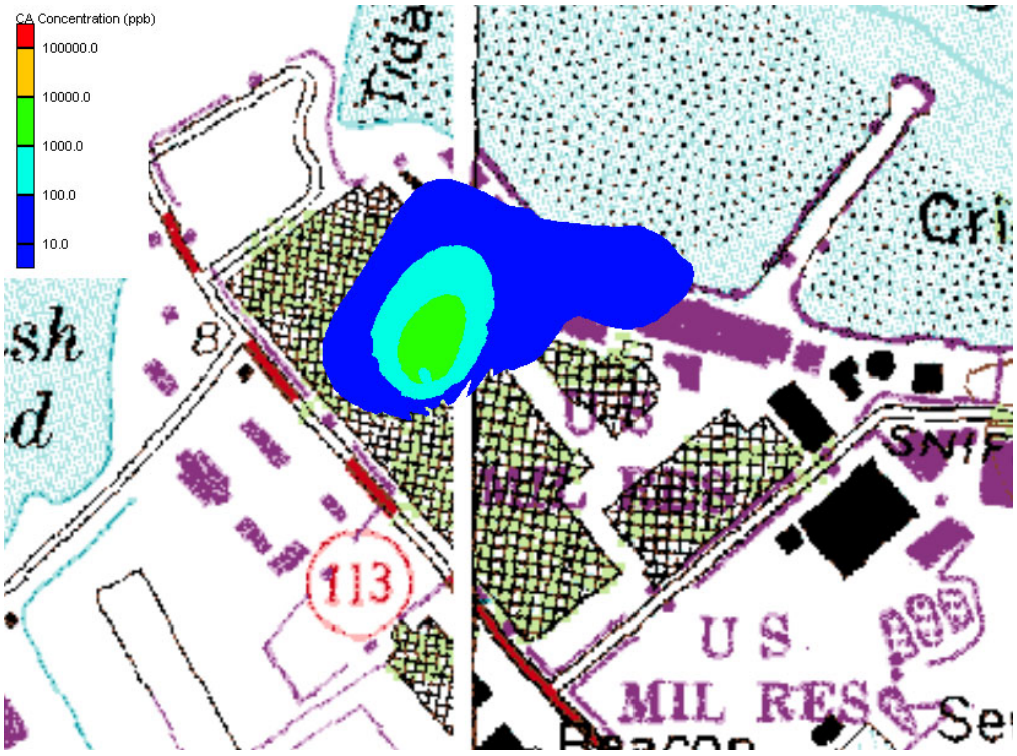

Figure 2.62. Predicted CA distribution after 20-years with TCE DNAPL source.

Figure 2.63. Initial CA profile along section B-B′ (Fig. 2.29); with TCA DNAPL source within hot spot #3.

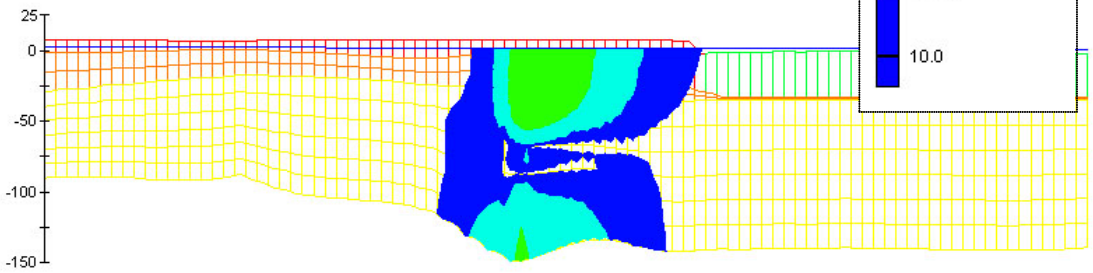

Figure 2.64. Predicted CA profile at B-B′ after 20 years; with TCA DNAPL source.

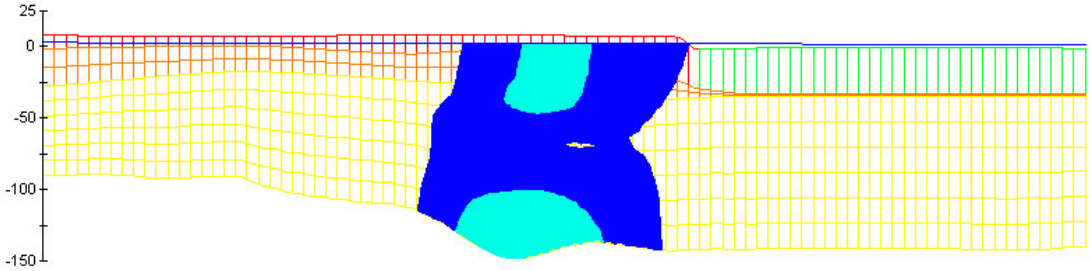

Figure 2.65. For comparison, CA after 20 years with no TCA source term.

Conclusions

The RT3D-GMS simulations of PCE/TCE and TCA natural attenuation suggest that the solvents at Stratford will be degraded and attenuated during their slow transport toward the Housatonic River. Adsorption and low flow rates contribute to the slow rates of transport. The reaction rates utilized here should be considered tentative due to data limitations. Results of a new, thorough sampling round (late 2001) are expected to provide data to support more thorough model calibration.

TASK-3. ASSESS NATURAL ATTENUATION OF CHROMIUM

3.1 PROBLEM SUMMARY

Hexavalent chromium (Cr[VI]), has been detected in groundwater at the Stratford Army Engine Plant (SAEP) in excess of its MCL (5 mgL^{-1}). The major Cr hot spot, with 1999 concentrations as high as 950 mgL^{-1}, is associated with the solvent hot spot number 1, beneath the "Chromium Plating Facility" in Building B-2. Minor, isolated hits of Cr are reported elsewhere at SAEP, but the major plume is the focus of this investigation. As with the solvents, the chromium plume appears to be moving very slowly toward a zone of anoxic, tidal mudflat sediments.

Monitored natural attenuation (MNA) may be an attractive, cost-effective, cleanup alternative for chromium at SAEP. The most encouraging conditions promoting the possible MNA of Cr include the following: (1) the reducing conditions in the estuarine, tidal mudflat sediments located between the source and the river may act as a natural permeable reactive barrier (PRB); (2) the slow rates of advective transport provide sufficient time for MNA, though Cr reduction reactions tend to be quite rapid; (3) there are no human receptors in the path of the plume. Conversely, MNA may not be a viable alternative if: (1) reducing conditions in the tidal flat sediments are not effective in reducing and immobilizing Cr, and/or (2) if part of the plume manages to circumvent the tidal flat sediments.

3.2 APPROACH

Chromium Chemistry
Under typically environmental conditions – aerobic and circumneutral pH – the predominant aqueous form of chromium as chromate (CrO_4^{-2}) or perhaps dichromate ($Cr_2O_7^{-2}$). The high toxicity of hexavalent chromium (*vs*. trivalent) is due to its strength as an oxidizing agent. Reduction in Eh and/or pH conditions can induce transformation to the trivalent form, Cr[III], which is sparingly soluble. One possible oxidation-reduction reaction using ferrous iron as the electron donor may be:

$$CrO_4^{-2} + 3\,Fe^{+2} + 8\,H^{+} \Rightarrow Cr^{+3} + 3\,Fe^{+3} + 4\,H_2O$$

Other possible electron donors could include sulfide or any reduced valence metal. Modestly reducing conditions (reduction potentials < 750 mV) are required to affect the reduction of Cr[VI] to (Cr[III]) (Stumm and Morgan 1995). See **Figure 3.1** for an example Eh-pH diagram for a simple Cr-Fe-SO_4 system [prepared using Geochemist's Workbench (Bethke 2001)]. Precipitation of the trivalent chromium as $Cr(OH)_3$., for example:

$$Cr^{+3} + 3\,OH^{-} \Rightarrow Cr(OH)_3\,(s)$$

also tends to be a relatively rapid reaction, whereas the reverse oxidation reaction is very slow. Other Cr[III] precipitates are possible, depending on water chemistry, as suggested in Figure 3.1. These reactions may serve to immobilize Cr in the tidal flat muds in a fashion analogous to the use of zero-valent iron (ZVI; metallic iron) in permeable reaction barriers (PRBs). ZVI PRBs are being employed for the in-situ treatment of chromium, solvents, and other contaminants (Puls *et al.* 1999). Although strongly reducing conditions have been observed in the tidal flat

sediments (Durgin 2001, personal communication; **Figure 3.2**), additional sampling or a feasibility study would be useful to verify that the sediments are sufficiently reducing to affect the target reduction reactions.

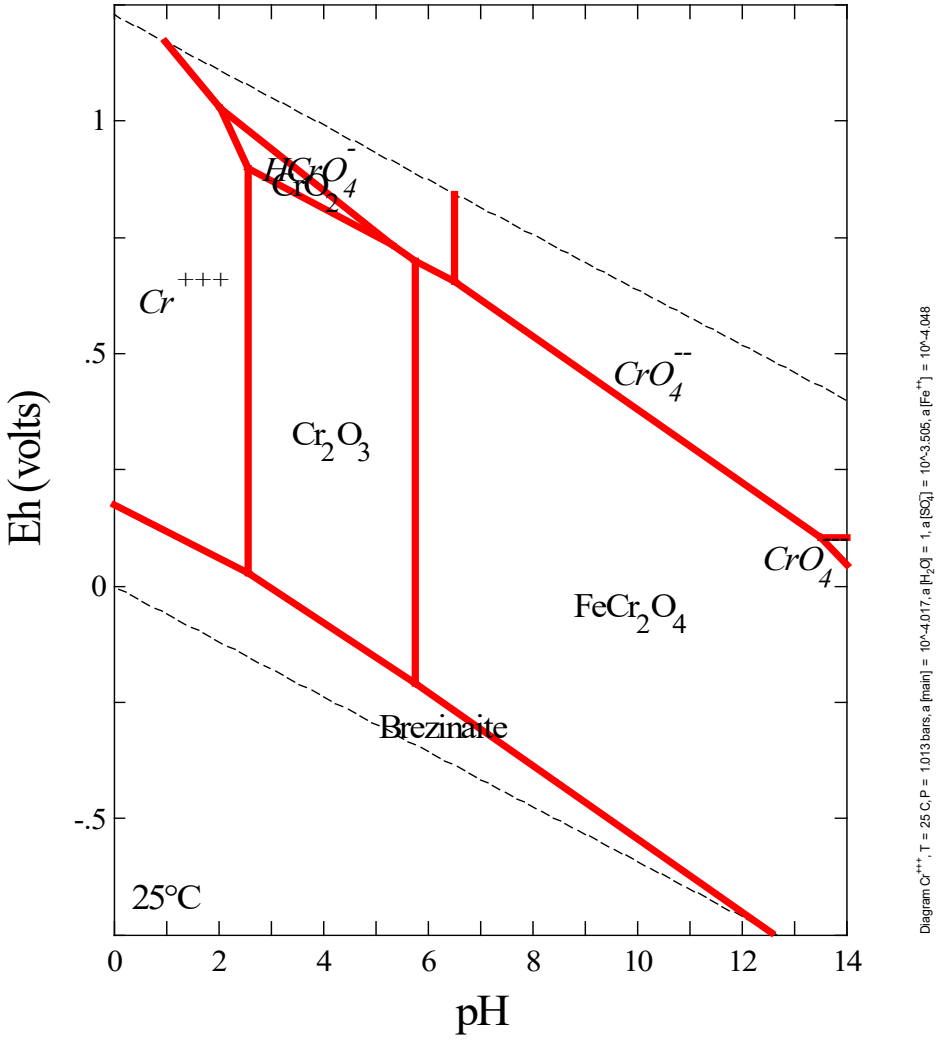

Figure 3.1. Predominant chromium species as a function of Eh and pH for an aqueous system of approximately 5 ppm Cr, 5 ppm Fe, and 30 ppm $SO_4^{=}$. This diagram is intended only to indicate the relatively limited extent of hexavalent chromium stability (high Eh ranges).

Chromate is an anion, which tend to adsorb to a lesser degree than cationic metal species. Yet, modest to significant partitioning coefficients (K_ds) are observed for chromate depending strongly upon system pH and the type and concentration of competing anions (particularly sulfate, $SO_4^{=}$), which tends to reduce Cr adsorption (EPA 1999b). The pH of groundwater at SAEP is largely circum-neutral (6-7) with numerous observations in the 3 to 6 range.

Figure 3.2. Black mud from beneath the tidal flat surface, consistent with the strongly reducing conditions indicated by low Eh and dissolved oxygen observations. (Durgin, 9/24/01).

Figure 3.3. Extensive mudflats exposed at low tide. These sediments may be covered at high tide. (Durgin 9/24/01)

Sulfate at SAEP is generally below 100 ppm but many observations up to 600 ppm and higher are reported. For sulfate and pH in these ranges, typical K_d's are on the order of 1 to 5 L kg^{-1} (EPA 1999b). Conditioned on the characterizations by EPA (1999b), a median value of approximately 3 L kg^{-1} was selected as a representative K_d for non-mudflat SAEP media. Decreases in pH would tend to increase Cr partitioning. This K_d range also assumes low extractable iron (<0.25 mmol/g); higher levels of iron would increase partitioning.

MT3DMS Modeling

The reactive transport model MT3DMS (Zheng 1999) is utilized to simulate chromium transport at SAEP. Flow conditions were defined with MODFLOW, using the larger numerical grid, which extends into the mudflat sediments (as in Task-2). MT3DMS describes advective-dispersive transport, equilibrium adsorption, and first-order decay of independent constituents. This relatively simple modeling approach was adopted to make long-term simulations (up to 50 years) more practical.

The reduction and precipitation, conceptual model described above is approximated by a simple advective-dispersive transport scheme with spatially variable partitioning. Cr adsorption is modeled with a linear isotherm model. A modest adsorption K_d of 0.5 to 3 L kg^{-1} is assigned to all geologic media other than the tidal mudflats. The rapid reduction and precipitation reactions are approximated by very strong adsorption of Cr to the tidal flat sediments, which were assigned a K_d on the order of 50 to 3500 L kg^{-1}. The net effect of Cr immobilization is the same.

Initial chromium distribution was conditioned on field observations from 1999. As described in Section 1, some subjectivity was involved in reducing multiple data entries for the same point at the same or a proximal date. An averaged or higher value was assigned in the case of multiple 1999 entries. Interpolation of the reduced dataset onto the numerical grid defined the initial conditions (**Figure 3.4** and **3.6**). Several artificial, background level data points were introduced in uncharacterized, peripheral areas to constrain extrapolated estimates of unjustifiably high concentrations in these areas.

Predictive simulation of Cr reduction and precipitation would require a more sophisticated geochemical model than could be considered in this project. Several appropriate, geochemical reactive transport models are available (*e.g.*, PHT3D, CRUNCH) to describe the redox and precipitation reactions more explicitly. However, such models are computationally highly demanding and were not considered practical given the abbreviated duration of this project. Given the lack of characterization of the tidal mudflat sediments or the presence of contaminants within them, application of a complex geochemical model would be unjustified at this time.

3.3 RESULTS

MT3DMS-GMS simulations indicate that chromium transport toward the Housatonic River is very slow. Assuming a modest partition coefficient of 3 L/kg, the Cr has moved little after 50

years. Assuming an even lower partition coefficient of 0.5 L/kg, the Cr plume can reach the mudflat sediments, where it is immobilized by strong adsorption (as a surrogate for chemical reduction and precipitation). Pump-and-treat to affect a partial reduction of Cr concentrations in the hot spot, which is under consideration, would reduce the plume concentrations but not change the net behavior predicted for the untreated plume.

Figures 3.4 to 3.7 illustrate Cr transport using the modest K_d value of 3 L kg^{-1}, consistent with site geochemical conditions. Cr transport is minimal during the 40 years simulation. Apparently, adsorption in combination with slow flow rates, are sufficient to significantly retard Cr transport.

Figures 3.8 to 3.9 illustrate the effect of reducing the K_d to 0.5 L kg^{-1} to permit transport into the mudflat. The simulations represented by Figures 3.6 and 3.7 use the same 1999 initial Cr distribution as in Figures 3.2 to 3.5. The Cr is immobilized quickly upon entry to the mudflat sediments.

Figures 3.10 to 3.15 depict the effect of partial cleanup of the chromium plume (all initial concentrations greater than 5 ppm were edited to 5 ppm). The lower K_d value (0.5 L kg^{-1}) is retained for the non-mudflat media and a higher K_d (50 L kg^{-1}) is assigned to the mudflat sediments. The same effect of immobilization in the mudflat sediments is observed.

3.4 CONCLUSIONS

Geochemical and hydrogeologic conditions appear to be amenable to the natural attenuation of hexavalent chromium by sequestration in the tidal mudflat facies. A reasonable estimate of a linear adsorption coefficient ($\leq$ 3 L/kg), conditioned on site water quality, and the low flow rates effectively inhibits Cr migration toward the river. If a lower K_d is considered (0.5 L/kg), the plume reaches the reducing mudflat sediments, where it is estimated that it will be immobilized by chemical reduction and precipitation. A more thorough characterization of the extent and chemistry of the mudflat facies is warranted. If the mudflat facies extends inland beneath the fill material (Durgin 2001, personal communication), Cr immobilization may occur further inland.

The strongly anaerobic mudflat facies located between the plume and the river may act as a natural, permeable reactive barrier to induce chemical reduction to trivalent chromium and precipitation of sparingly soluble mineral phases, effectively immobilizing chromium. Though this hypothesis requires more field documentation and feasibility analysis, the modeling conducted here suggests no impediment to its potential success.

Chromium Transport with Modest Sorption Outside Mudflat Sediments

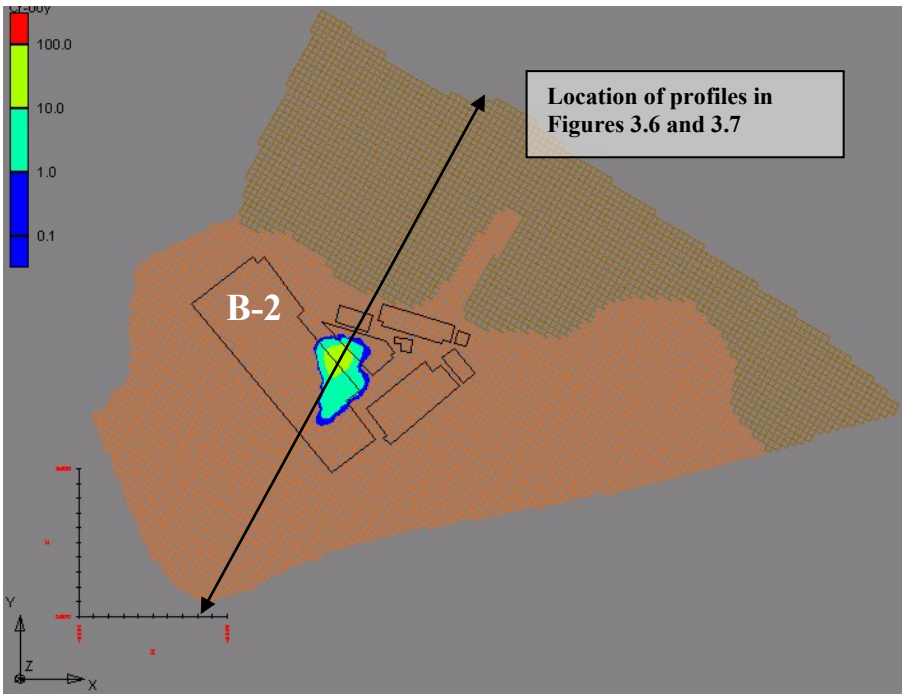

Figure 3.4. Chromium distribution (ppm) at water table (grid layer 1) in 1999. [Note: log scale for concentration; 100–foot increments on 1000-foot spatial axes.]

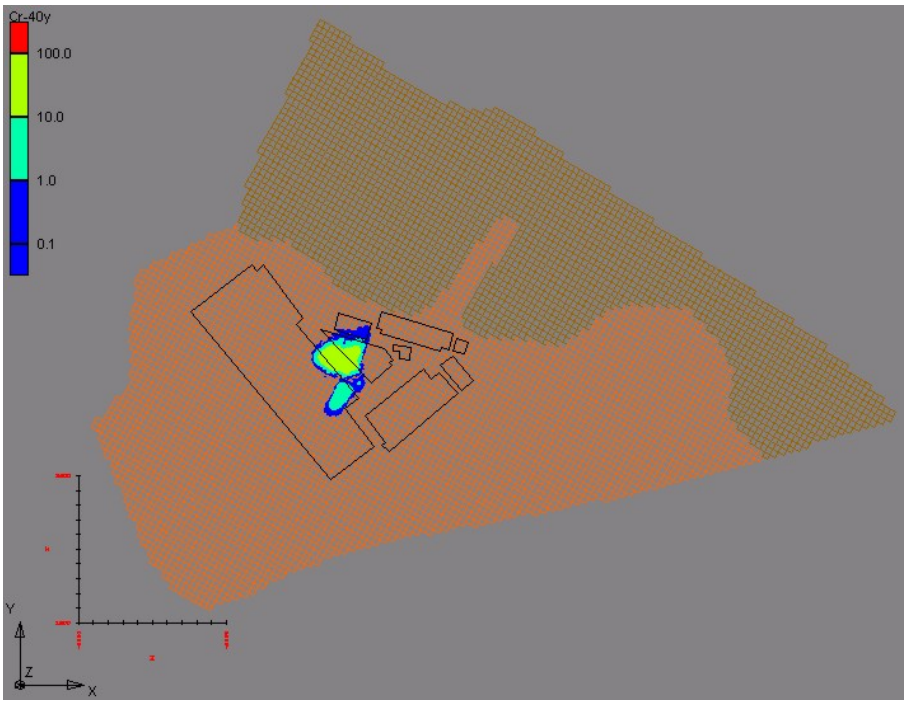

Figure 3.5. Chromium distribution (ppm) at water table after 40 years of transport through modest K_d media (~3 L/kg). Very little movement is predicted.

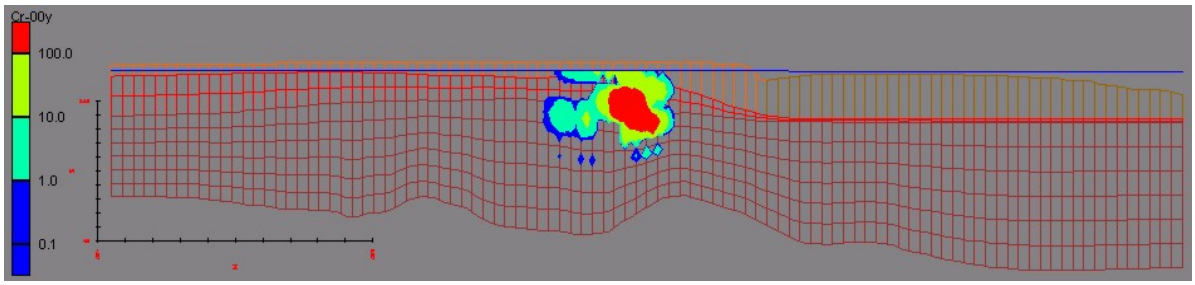

Figure 3.6. Chromium concentration (ppm) profile along the transect indicated in Figure 3.4; conditioned on 1999 data. Vertical exaggeration is 5X. [i = 38]

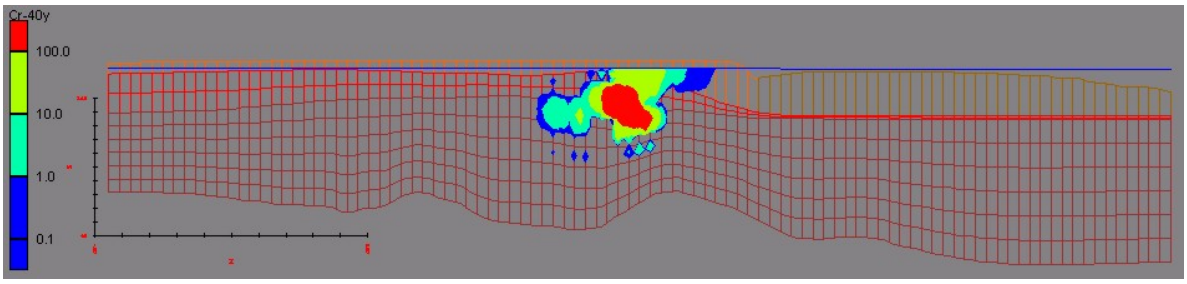

Figure 3.7. Chromium concentration (ppm) profile after 40 years of transport through SAEP subsurface assigned a modest K_d (~3 L/kg). Chromium does not reach the mudflat sediments in this scenario. [i = 38]

Chromium Transport with Lesser Sorption Outside Mudflat Sediments

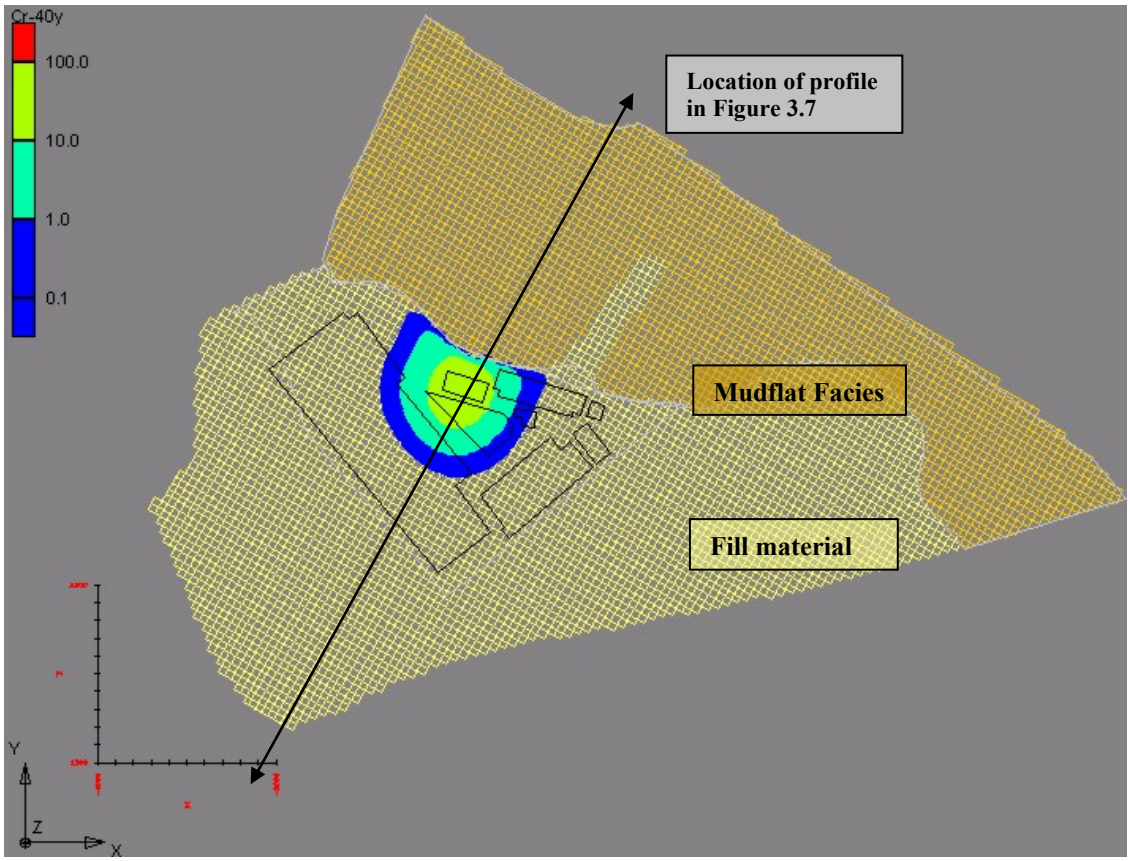

Figure 3.8. Chromium distribution at water table (grid layer 1) after 50 years transport through low K_d media (0.5 L/kg). Lesser retardation (*vs*. 3 L/kg in Figure 3.4) permits transport into mudflat sediments (darker brown color) where Cr is immobilized.

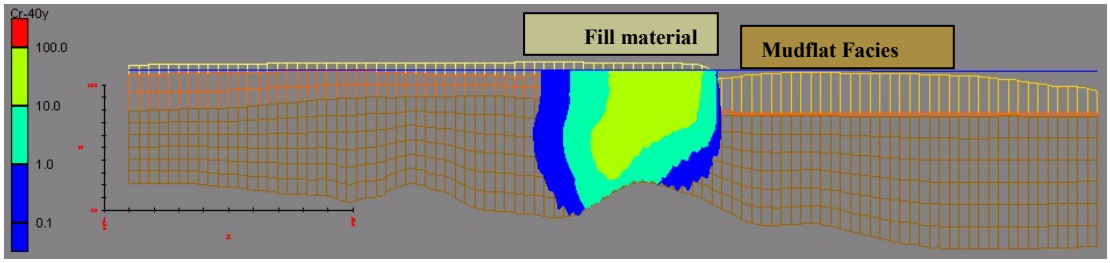

Figure 3.9. Chromium concentration profile after 40 years transport through with a low K_d media (0.5 L/kg) to be immobilized in mudflat sediments (K_d = 50 L/kg). Bypassing mudflat sediments does not appear to be significant due to low flow velocities at depth. [i=38]

Chromium Transport After Partial Source Removal (≤ 5 ppm)

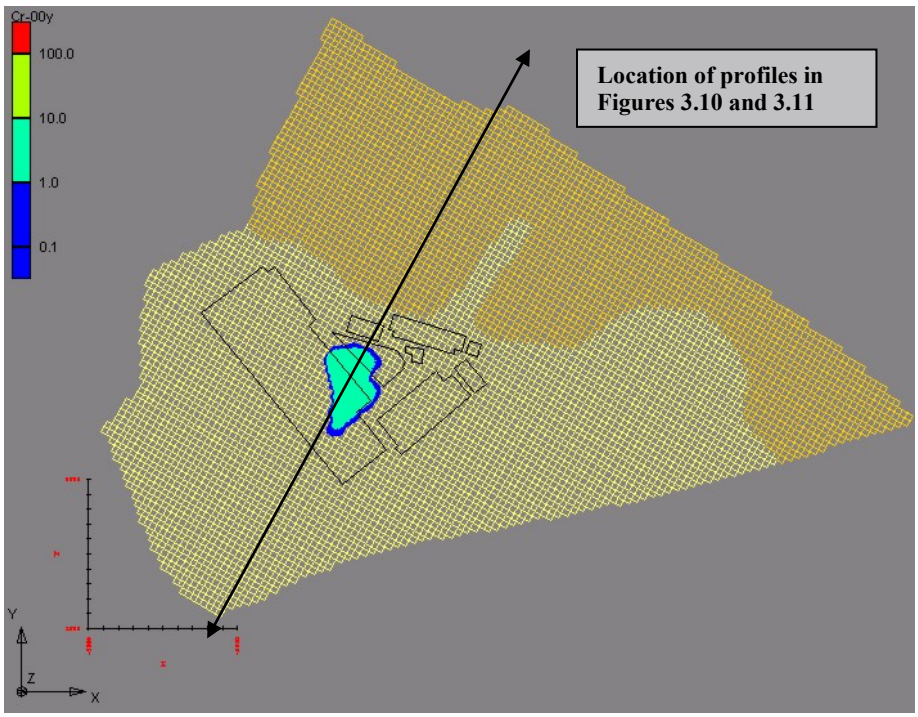

Figure 3.10. Chromium distribution at water table after source reduction (all points in excess of 5 ppm reduced to 5 ppm).

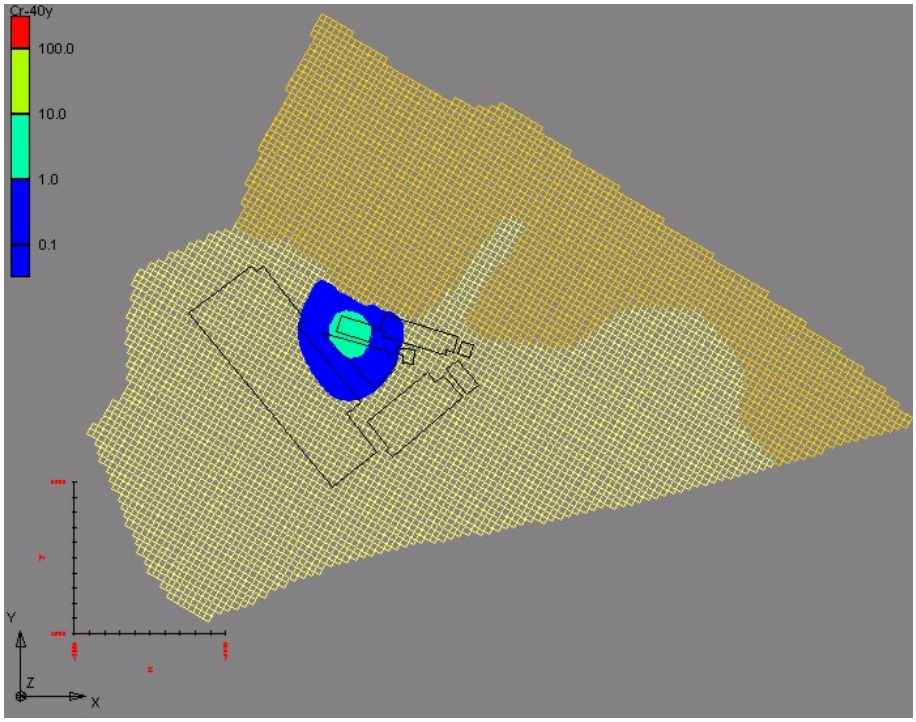

Figure 3.11. Chromium distribution at the water table 40 years after source reduction.

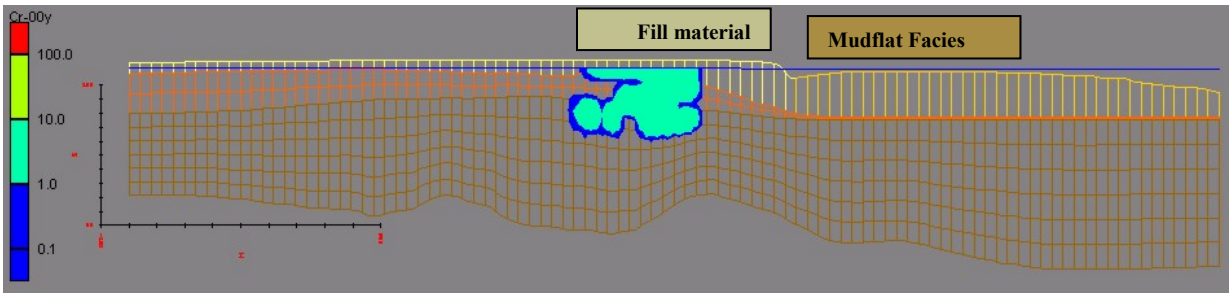

Figure 3.12. Chromium distribution after partial source reduction (all points en excess of 5 ppm reduced to 5 ppm).

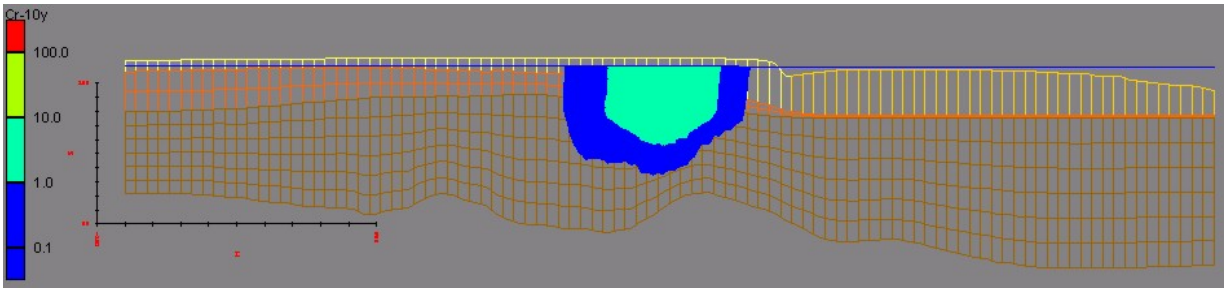

Figure 3.13. Chromium distribution 10 years after conditions in Figure 3.12.

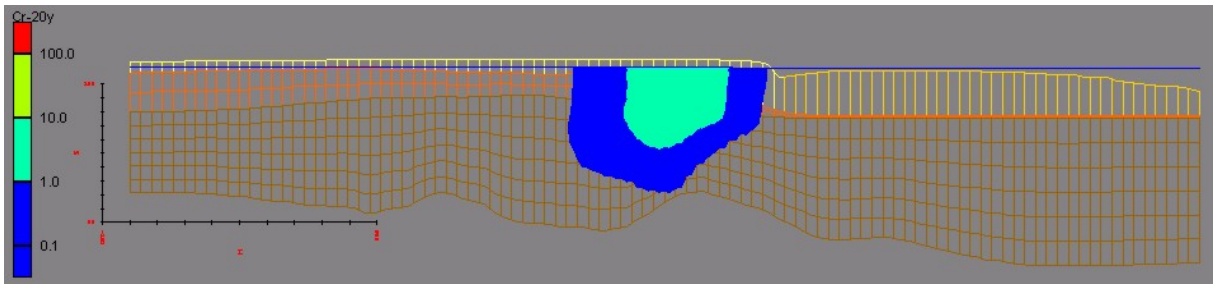

Figure 3.14. Chromium distribution 20 years after conditions in Figure 3.12.

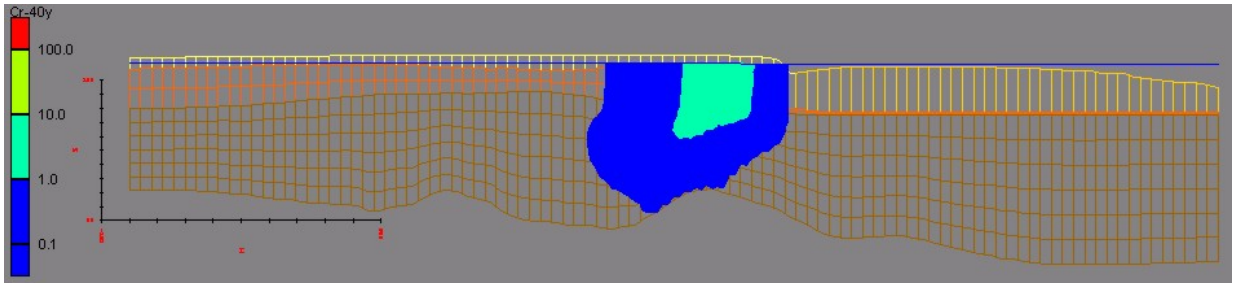

Figure 3.15 . Chromium distribution 40 years after conditions in Figure 3.12.

4.0 CONCLUSIONS

This document describes the application of groundwater flow and reactive transport models in the quantitative assessment of several remediation alternatives proposed for the Stratford Army Engine Plant (SAEP). The contaminants of primary concern are chlorinated solvents (PCE, TCE, TCA and their transformation products) and hexavalent chromium. The SAEP is located on the west side of the Housatonic River, near it's terminus at Long Island Sound.

Groundwater flow simulations indicate low flow velocities beneath SAEP in the general direction of the Housatonic River. The low hydraulic gradient reflects the low topographic relief and low elevation of the area. Three-dimensional groundwater flow simulations using FEMWATER indicate that the alteration in recharge patterns associated with the removal of buildings and paved areas would not dramatically alter the groundwater flow paths or velocities. It is unlikely that land use conversion would have a significant effect on contaminant transport.

Assessment of the long-range efficacy of a stripping of the three "hot spots" (Task-1) indicates that stripping the entire lateral and vertical extent of the contaminant plumes to an elevation of –30 to –40 feet is necessary to minimize the likelihood of VOC rebound and re-contamination at the water table. Stripping to any significantly shallower depth increases the risk of recontamination of the treatment zone by upward contaminant migration. Any residual contaminant halo upgradient of the treated zone will migrate laterally into that zone. Thus, accurate delineation of the lateral and vertical extent of the contaminant plumes and full treatment of that area is required for the application of this remediation alternative.

Assessment of natural attenuation of the chlorinated solvents (Task-2) suggests that advective transport rates are sufficiently slow to allow slow rates of natural attenuation to degrade TCA- and PCE/TCE-related contaminants before seepage into the Housatonic. The possible presence of a DNAPL phase would extend the longevity of the contamination plume, but has a minimal effect on the longitudinal extent of the down-gradient plume.

Assessment of the natural attenuation of hexavalent chromium (Task 3) suggests that adsorption combined with the low rates of advective transport will retard the migration of chromium toward the Housatonic River. The anaerobic mudflat facies between the plume and the river may act as a natural permeable reactive barrier to induce chemical reduction to trivalent chromium and precipitation of sparingly soluble mineral phases, effectively immobilizing chromium. Though this hypothesis requires more field documentation and feasibility analysis, the modeling conducted here suggests no impediment to its potential success.

These conclusions are conditioned on the available water quality data from SAEP. The degradation rates are not well validated to site-specific conditions due to data limitations. The results of a new, thorough sampling round planned for the near future are expected to provide data to support more thorough model calibration/validation.

5.0 RECOMMENDATIONS

- Reaction rates should be re-evaluated when the new, complete, water quality data set is available.
- Quantitative documentation of reducing conditions in the mudflat facies would lend support to the MNA of both chromium and chlorinated solvents. Measurement of reduction potentials, or indications of sulfate reduction (sulfide generation), hydrogen production, or methanogenesis would strengthen the argument that conditions are sufficiently reducing to affect Cr [VI] reduction. Determination of labile organic matter content in the sediments along the predicted flow path could be useful in support of the modeling hypothesis that the medium contains an excess of reducing capacity. Increased microbial activity may also assist in mineralization of any remaining solvent products.
- Additional data on general water chemistry (*e.g.*, major cations and anions, TDS/salinity/conductivity) would be useful in determining the nature of Cr aqueous complexes, which, in turn, control transport behavior.
- Determination of the mass and distribution of any DNAPL should be a high priority, not only as input to predictive attenuation modeling, but as fundamental information needed in the design and successful implementation of any engineered remediation. The presence of extensive pools of DNAPL would pose an entirely different condition than the assumption that DNAPLs are limited to residual saturations directly beneath the source areas. Refinement of the hydrogeologic conceptual model would permit more accurate predictions of contaminant transport and the potential location of pooled DNAPL.

6.0 REFERENCES

Bethke, C.M. (2001). *The Geochemist's Workbench: A User's Guide to Rxn, Act2, Tact, React, and Gtplot, version 3.2*, University of Illinois.

Clement, T. P., and Jones, N. L. (1998). "RT3D Tutorials for GMS Users," *PNNL-11805*, Pacific Northwest National Laboratory, Richland, WA.

Clement, T. P., Hooker, B. S., and Skeen, R. S. (1996). "Numerical modeling of biologically reactive transport near a nutrient injection well," *ASCE Journal of Environ. Engineering*, 122(9), 833-839.

Durgin, Philip B., 2001. Personal communication. U.S. Army Corps of Engineers, New England District, Concord, MA (CENAE-EP-GE); Tele.: 978-318-8507; e-mail: Philip.B.Durgin@nae02.usace.army.mil

Karickhoff, S. W., Brown, D. S., and Brown, D. S., and Scott, T. A. (1979). "Sorption of hydrophobic pollutants on natural sediments," *Water Res.* 13:241-248.

McDonald, M.G., and Harbaugh, A.W. (1988). "MODFLOW, a modular three-dimensional finite difference ground-water flow model," U.S. Geological Survey, *Open-file Report 83-875*, Chapter A1.

Puls, R.W., Paul, C.J., and. Powell, R.M. (1999). "The application of in situ permeable reactive (zero-valent iron) barrier technology for the remediation of chromate-contaminated groundwater: a field test," *Applied Geochemistry*, 14(8): 989-1000.

Stumm, W., and Morgan, J.J (1995). *Aquatic Chemistry: Chemical Equilibria and Rates in Natural Waters*, 3rd edition. John Wiley & Sons, Inc.

U.S. Environmental Protection Agency (1986). "Background Document for the Ground-Water Screening Procedure to Support 40 CFR Part 269 - Land Disposal," *EPA/530-SW-86-047*, January 1986.

U.S. EPA (1999). "Use of Monitored Natural Attenuation at Superfund, RCRA Corrective Action, and Underground Storage Tank Sites," *Directive Number 9200.4-17P*, United States Environmental Protection Agency, Office of Solid Waste and Emergency Response, Washington, DC.

U.S. EPA (1999b). "Understanding Variations in Partition Coefficients, K_d, Values. Vol. II: Review of Available K_d Values for Cadmium , Cesium, Chromium, Lead, Plutonium, Radon, Strontium, Thorium, Tritium (^3H) and Uranium," *EPA 404-R-99-004B*.

Zheng, C., and Wang, P. Patrick. (1999). *A modular three-dimensional multispecies transport model for simulation of advection, dispersion and chemical reactions of contaminants in groundwater systems* (Release DoD_3.50.A), University of Alabama, Tuscaloosa, Alabama..